Università degli Studi di Napoli Federico II

Dottorato in Scienze Chimiche – XXI Ciclo

Amphiphilic Biostructures as Nanotechnological Devices in Cancer Diagnosis and Therapy

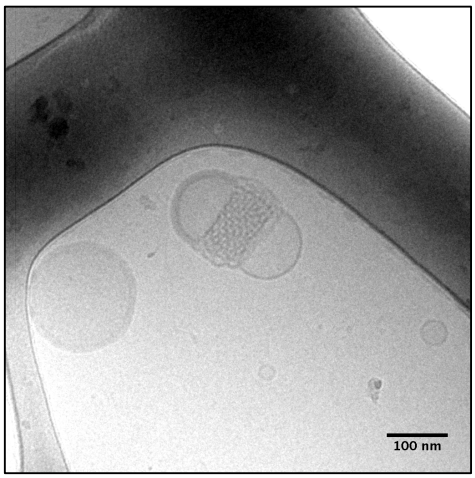

Relatore:
Ch.mo Prof. Martino Di Serio

Dottorando:
Mauro Vaccaro

Coordinatore:
Ch.mo Prof. Aldo Vitagliano

Tutore:
Ch.mo Prof. Luigi Paduano
Dott. Gerardino D'Errico

List of Papers

This thesis has been submitted as a part of the requirement for the degree of doctor of philosophy in Chemistry. The manuscript is based on different research papers that have been submitted during the PhD study period. Below a complete list of all the research papers submitted is reported.

1. Supramolecular Aggregates of Amphiphilic Gadolinium Complexes as Blood Pool MRI/MRA Contrast Agents: Physico-chemical characterization.

M. Vaccaro, A. Accardo, D.Tesauro, G. Mangiapia, D. Löf, K. Schillén, O. Söderman, G. Morelli, and L. Paduano.
Langmuir (2006) 22, 6635-6643.

2. High-Relaxivity Supramolecular Aggregates Containing Peptides and Gd Complexes as Contrast Agents in MRI.

A. Accardo, D. Tesauro, G. Morelli, E. Gianolio, S. Aime, M.Vaccaro, G. Mangiapia, K. Schillén, and L. Paduano.
Journal Biological Inorganic Chemistry (2007) 12, 267-276.

3. Peptides and Gd Complexes containing Colloidal Assemblies as Tumor Specific Contrast Agents in MRI: Physicochemical Characterization.

M. Vaccaro, A. Accardo, G. D'Errico, K. Schillén, A. Radulescu, D. Tesauro, G. Morelli and L. Paduano.
Biophysical Journal (2007) 93, 1736-1746.

4. Structural and Relaxometric Characterization of Peptide Aggregates Containing Gadolinium Complexes as Potential Tumour Specific Contrast Agents in MRI.

M.Vaccaro, G. Mangiapia, L. Paduano, E. Gianolio, A. Accardo, D. Tesauro, and G. Morelli.
ChemPhysChem (2007) 8, 2526-2538.

5. Investigation of the Adsorption of PEG1500-12-Acyloxystearate Surfactants onto Phospholipid Bilayers: An Ellipsometry and Cryo-TEM Study.

M. Vaccaro, C. von Corswant, and O. Söderman.

Biophysical Journal (2007) 93, 4300-4306.

6. Peptide Containing Vesicles as Selective Nanovectors for Therapeutics or Diagnostics.

A. Accardo, D. Tesauro, G. Morelli, L. Aloj, G. Mangiapia, M. Vaccaro, and L. Paduano.

ChemMedChem (2007) 3, 594-602.

7. Polymerized mixed aggregates containing gadolinium complex and CCK8 peptide.

M.Vaccaro, G. Mangiapia, A. Accardo, D. Tesauro, E. Gianolio, H. Frielinghaus, G. Morelli, and L. Paduano.

Colloid Polymer Science (2008) 286, 1643-1652.

8. Micelles Obtained by Aggregation of Gemini Surfactants Containing the CCK8 Peptide and a Gadolinium Complex.

A. Accardo, D. Tesauro, A. Morisco, G. Mangiapia, M.Vaccaro, E. Gianolio, R. K. Heenan, L. Paduano, and G. Morelli.

Submitted to Journal Biological Inorganic Chemistry.

9. Lipid Based Nanovectors Containing Ruthenium Complexes: A Potential Route in Cancer Therapy.

M. Vaccaro, R. Del Litto, G. Mangiapia, A. Carnerup, G. D'Errico, F. Ruffo and L. Paduano.

Submitted to ChemComm.

10. Colloidal Particles Composed of Amphiphilic Molecules Binding Gadolinium Complexes and Peptides as Tumor-Specific Contrast Agents in MRI:

Physico-Chemical Characterization.

M. Vaccaro, G. Mangiapia, A. Radulescu, K. Schillen, G. D'Errico, and L. Paduano. *Submitted to Soft Matter*.

Acknowledgements

It has been a pleasurable journey my experience as PhD student. Yes, if I should use one word to define my PhD, journey is the most appropriate due to my continuously getting around Europe. To thank all the persons that I met is a difficult task, but I need to express my gratitude to someone in particular.

Let's start form the beginning:

I wish to thank prof. Luigi Paduano (Gino) from University of Naples, Italy, for introducing me in the field of colloidal chemistry. Your first lesson has been love at the first sight with the subject. I could not have chosen a better course to strength my education! Gino, thanks also for the nice time spent together all around Europe. It will hard for me not have an audience to show my imitation of you, but above all I will miss your music!

I wish to thank prof. Piero Baglioni, University of Florence, Italy, and the CSGI (Italian Center for Colloid and Nano-Science) for the PhD scholarship.

I wish to thank dr. Gerardino D'Errico from University of Naples, Italy, for giving me the chance to go to Physical Chemistry 1, as Erasmus student.

I wish to thank all the persons at Physical Chemistry 1, University of Lund, Sweden, for feeling me at home in Sweden. *Jag är född att vara Svensk!!*

In particular, I want to acknowledge prof. Olle Söderman, who has been my supervisor, and then prof. Karin Schillén and prof Viveka Alfredsson for the scientific collaboration helping in light scattering and cryo-TEM measurements, respectively.

A thank to all my colleagues, PhD students and undergraduated students, for electing me the toastmaster of the Christmas Party 2004. I think I have been the first Italian toastmaster and still the only one in all Swedish history!

I wish to thank Pieter Saveyn, university of Gent, Belgium, for his patience in being *min bäst vän in Lund*!! I am still sorry for convincing you to follow me in Riga. I could not imagine ice creams in Latvia could be so dangerous ;-)

I wish to thank Christian von Corswant, Astrazeneca Mölndal Research Center, Sweden, for the fruitful collaboration and the nice day spent in Astrazeneca.

I want to show my gratitude to all the local contacts that in the different neutrons installations allowed running SANS experiments: dr. Aurel Radulescu and dr. Henrich Frielinghaus, Jülich Center for Neutron Science (Germany), dr. Richard K. Heenan, ISIS-Rutherford Appleton Laboratory (United Kingdom), dr. JoséTeixeira, Laboratoire Leon Brilluoin Saclay (France).

A special thanks to dr. Gaetano Mangiapia, University of Naples, Italy, for realizing all the program to fit SANS data, but thanks also for supporting me in my imitation of our supervisor (Gino).

Finally, I wish to thank my friends that I met during my stage in Procter&Gamble at Brussels Innovation Center (Belgium). In particular, I remember Thom Groot and Wim Garmyn for the nice atmosphere created in laboratory, Dora Gandicki and Penelope Coutroki for the Greek lessons, and Anna Gravina for all the dinners burnt in the oven.

Mauro

TABLE OF CONTENTS

1. Introduction

1.1 Aim of the Thesis

This thesis has been carried out at the Department of Chemistry of Naples University, Italy, and at the Department of Physical Chemistry 1 at Lund University, Sweden, during the period 2005-2008.

The aim of the thesis has been the design and the physico-chemical characterization of amphiphilic superstructures, such as micelles and liposomes, to be used as nano-devices in cancer diagnosis and therapy.

The past quarter century of outstanding progress in fundamental cancer biology has not translated into even comparable advances in the clinic. Inadequacy in the ability to administer therapeutic moieties, so that they will selectively reach the desired targets with marginal or no collateral damage, has largely accounted for this discrepancy.[1,2] Similar limitations apply to contrast agents for imaging applications.

There are two synergistic goals that should be striven for to increase the efficacy per dose of any therapeutic or imaging contrast formulation: to increase its targeting selectivity[3] and to endow the agent comprising the therapeutic or the diagnostic formulation with the means to overcome the biological barriers that prevent it from reaching its target.[4] An ideal therapeutic system would be selective directed against cell clusters that are in the early stages of the transformation towards the malignant phenotype.[5]

The realization of such a system faces different challenges, including the identification of suitable bio-active molecules or chemical processes able either to deliver the therapeutic/contrast agent toward the cancer cells or to avoid biological and biophysical barriers.

On these bases two different systems have been developed in the present research project: 1) The first system was formed by two amphiphilic unimers, one chelating a Gadolinium complex, that is the most common contrast agent used in *Magnetic Resonance Imaging* (MRI), the leading technique for the diagnosis of tumors, and the other one containing a peptide, the CCK8, showing high affinity for the cholecystokinin receptors which are overexpressed in different tumor pathologies. 2) The second system was formed by a unimer containing a pyridinium ring able to coordinate Ru(III) complexes, which offer new interesting perspectives in the selective attack of tumor metastases.

1.2 Surfactants in Aqueous Solution

1.2.1 Surfactants

The basic molecular architecture of surfactants is always based on the simultaneous presence in the same molecule of two or more groups of atoms that possess different affinities for the environmental (solvent). In most of the cases the solvent is water, and so we distinguish a hydrophilic part (the "polar headgroups") linked to a hydrophobic block made up by one or more hydrocarbon chains.[6]

Depending on the nature of the hydrophilic head, surfactants can be divided into ionic and non-ionic type. The ionic head can be negatively charged, such as in the case of carboxylates ($-COO^-$), sulfates ($-OSO_3^-$), sulfonates ($-SO_3^-$); or positively charged, with an quaternary ammonium head group ($-NH_3^+$,$-NR_3^+$); while the non-ionic head can be zwitterionic, two oppositely charged groups, or composed of an etoxylate chain $-(OCH_2\,CH_2)_mOH$.

1.2.2 Amphiphilic assembly processes

Depending on the chemical structure of the amphiphile, temperature, pH and ionic strength of the solution, nature and composition of the solvent, different kinds of aggregates with peculiar properties can be obtained. They originate by the assembly of surfactants in order to reduce the hydrocarbon-water repulsion and then

minimizes the total energy of the aggregate. It is possible to predict the type of phase that a surfactant forms using the **surfactant parameter** N_s:[7]

$$N_s = v/l \cdot a_0 \tag{1.0}$$

where v is the volume of the surfactant hydrophobic tail, l is the length of the hydrocarbon chain, and a_o is the effective area per head group.

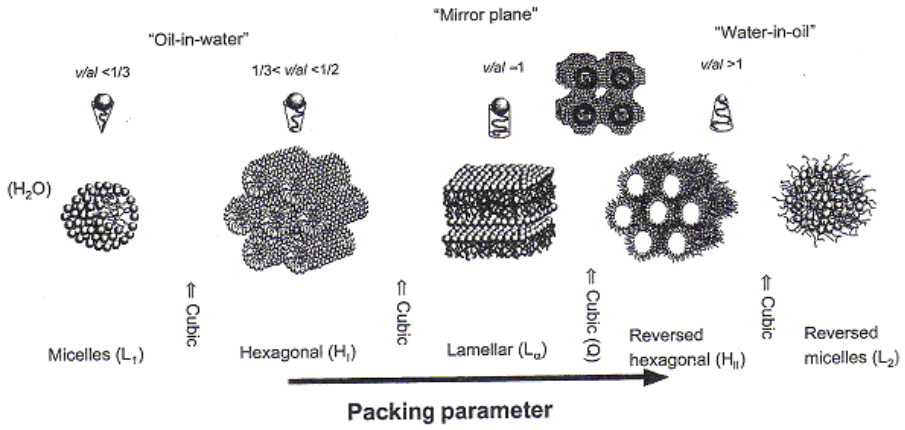

Figure 1.1: Schematic illustration of association structures formed in surfactant systems and their relative packing parameters.

For $N_s < 1/3$, spherical micelles will form, for $N_s = ½$ cylindrical micelles are expected instead.

Bilayers as well as bicontinous phases form for $N_s = 1$ while reverse structures are expected for $N_s > 1$.

The aggregates which have interested this thesis work are: micelles, vesicles and bilayers assemblies.

Micelles are the simplest and the most characterized self-organizing structures. The process of micellization is a start-stop process. This means that there is a well-defined point where process starts and one of stop too. The point of start is represented by the critical micellar concentration (CMC). The CMC is the lowest concentration where micelles are formed. Below CMC value the surfactants are in solution as free unimers, while above the CMC adding more surfactants produces more micelles with a well-defined aggregation number rather than larger micelles. The growth process is limited in fact from head-group head-group repulsion, so aggregates cease to grow when they reach a certain size.

The micellar aggregation process can be described by a stepwise association process, $S + S_{n-1} \leftrightarrow S_n$, but because it is almost impossible to specify all the K_n equilibrium steps, approximate models are used.[8] The most important models to describe the micellization process are the "isodesmic model" that assumes that K_n is independent of n and the "phase separation model" that approximates aggregation as a phase separation process. In particular, in the phase separation model the aggregation is described as a discontinuous process that shows an abrupt onset in a narrow concentration range, so this model is able to predict the CMC and is appropriate for surfactants with long hydrocarbon chains and low CMC, such as the surfactants used in this work.

The bilayer aggregation process is less studied than micellization process, because most experimental techniques are not sensitive enough to low concentrations. In fact,

the solubility of bilayer-forming monomers, such as phospholipids, which usually have two apolar chains, is much lower than micelle-forming surfactants solubility, which have generally one tail. For bilayers, the aggregation monomer's solubility defines the start of the process, but there is no molecular limit to bilayer growth in the lateral direction, so there is no a point of stop that limits the process of aggregation of bilayers whom thickness is a well-defined property determined by the length of the hydrocarbon chains. Lifetimes for micelles and bilayers are really different, for micelles it can vary from 10^{-3} to 10^{-1} s, while for bilayers the lifetime of the aggregate can vary from days to years. This difference reflects the fact that micelles are in dynamic equilibrium with free surfactants in the bulk aqueous solution, so surfactant in solution is continuously exchanged with surfactant in the micelle, causing the constant rupture and re-formation of micelles in solution. In contrast, vesicles are far less susceptible to break-down as a result of sluggish monomer exchange processes. Bilayers are the basic structural element in several phases, including lamellar liquid crystals and gel phases.The lamellar liquid crystal is the generic bulk phase of a bilayer-forming amphiphile, and it consists of a stack of bilayers, with the apolar chains behaving as in a liquid, separated by aqueous films. When a lamellar phase is cooled, it undergoes a phase change that can lead to the formation of a gel phase. Typical gel structures present crystallized alkyl chains while liquidlike solvent still exists between the bilayers.

The gel-to-liquid crystal transition can be studied by differential scanning calorimetry (DSC); two peaks can be observed, the first of which, the pre-transition, corresponds

to a disordering of the bilayer membrane in the absence of chain-melting, while the second one is very pronounced and corresponds to chain melting.[9]

Bilayers form the basic structural element in other ordered phases; in isotropic solutions they can form vesicles.

Vesicles are hollow spheres consisting of at least one surfactant bilayer, unilamellar vesicles, but they can also present more bilayers, multilamellar ones.

Vesicles are important biological structures, the surfactant bilayer mimics the lipid bilayer of cell membranes, in fact the cell is an example of a very complex biological vesicle.

Their ability to encapsulate an aqueous environment makes them suitable for many applications, above all, in pharmaceutical setting, where they are used as carriers of drugs[10] or as models for biological membranes.[11]

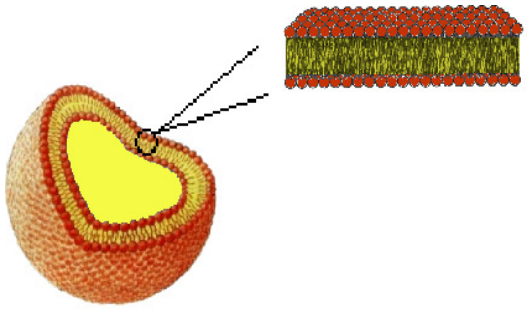

Figure 1.2: Schematic representation of a vesicular structure, observed on a little scale, its surface can be considered as a thickness of a lipidic bilayer.

Spontaneous vesicles of certain surfactants under favorable conditions have been reported, but vesicles are usually formed from lamellar dispersions with an input of energy. There are several ways to provide energy, the methods used in this work are: sonication and extrusion. The sonication method is a non selective way to produce vesicles, the sound waves tear the lamellae, which can reseal to form vesicles, the resulting consists in a distribution of unilamellar and small vesicles (SUV) with diameters in the range of 15-50 nm. In the extrusion method the lamellar suspension is forced through a polycarbonate filter with a defined pore size to yield particles having a diameter near the pore size of the filter used. Extrusion through filters with 100 nm pores typically produce large and unilamellar vesicles (LUV) with a mean diameter of 120-140 nm.

In any case vesicles produced with these two methods are metastable structures, this means that the vesicles will relax back to their equilibrium structure of lamellar phase, but this process is usually really sluggish, it can take days, months or years.

Khan et all have shown that the formation of stable vesicle is possible, without recourse to highly energetic methods, such as sonication and extrusion, using "catanionic surfactants".[12,13] Catanionic surfactants are equimolar mixtures of two oppositely charged surfactants, where the effective head group size becomes much smaller than the sum of the head group areas for the separate systems, since the amphiphiles attract one another by electrostatic interaction. According to the principle of reducing the head group area to obtain low radius curvature aggregate, it is possible to promote in solution the transition from micelles to vesicles in ionic systems modifying appropriately the pH. A rather large number of studies on the pH-

dependent behaviour of gemini surfactants, molecules made of two conventional surfactant units connected by a spacer, have been published in the recent years.[14, 15] In literature it is possible to find also different works about the inverse transition; non-ionic micelle-forming surfactants are especially adapt to yield vesicle to micelle transition of cationic unilamellar vesicles. All these studies reveal that the transition occurs by an intermediate stage, where rodlike and threadlike micelles are formed, confirming so the three-stage Lichtenberg model.[16, 17]

1.3 Surfactants in Pharmaceutics and Diagnostics

In the last years the use of nanovectors, namely supramolecular structures with dimensions of the order of nanometers, is becoming very appealing in the drug delivery field. They are able to carry an active substance through the aqueous biological system, and their typical size in the nanometer scale, which is of the same order of the human cells, allows them delivering the drug to the targeted site. However, drug delivery requires stringent conditions. The drug concentration must be in the therapeutic window, i.e. high enough to achieve a therapeutic effect at the site of action, but simultaneously low enough to avoid harmful side effects elsewhere. Then, the role of the supramolecular structures is not only to carry the drugs, but also to protect the active ingredients from destructive factor, and to control their spatial and temporal distribution through the biological system. Furthermore, the nanovector must be formed by molecules themselves non-toxic, that can be metabolized to harmless compounds.

Among the different nanovectors, those formed by amphiphilic molecules have recently drawn much attention owing to their good pharmacological properties. By operating on the different chemical structures of the amphiphilic molecules composing the super-aggregates, it is possible to build-up nanovectors different for shape, dimension and physico-chemical characteristics.

The most common structures are micelles and liposomes, whose physico-chemical characteristics have been discussed above. They possess some advantages as potential drug delivery systems, since they can encapsulate a variety of sparingly water-soluble

therapeutic and diagnostic agents. Such encapsulation substantially increases their bioavailability, protects them from destructive factors upon parenteral administration, and modifies their pharmacokinetics and biodistribution.

The most used amphiphilic aggregates for drug delivery purposes are liposomes. The first use of liposomes as nanovectors was in the anti-microbic and anti-fungal therapy. In fact, it is well-known that liposomes, given by endovenous injection, are assimilated by hepatic macrophages through the endocytosis mechanism that in turn is able to deliver them to lisosomes or to some other cytoplasmatic regions in which the drug can act.

Liposomes can be administrated not only via endovenous injection but also via: 1) aerosol, useful for pulmonary pathologies treatments, 2) subcutaneous or muscular injection able to transmit these nanovectors to the lymphatic ways, and 3) oral assumption.

Liposomes success in the field of drug delivery is due to several factors that can be summarized in the experimental evidence that these nanovectors are able to improve the therapy results respect to what is obtained administrating the same active principle in a more classic way.

The use of nanovectors such as liposomes allows reaching high concentration level of the drug in the ill tissues, but at the same time its inclusion into a supromolecular structure limits its toxicity preventing undesidered sides, concentration peak effects and prolonging the permanence time of the drug in the blood stream. Typical examples, confirming all this, are liposomes based doxorubicine that have been used

in the past for the treatment of Karposi sarcoma, while nowadays they are used in the breast and ovaries tumor therapy.

One limitation to the use of liposomes and micelles in pharmacology stayed in the fact that they often were recognized as extraneous bodies by the immunitary system with the consequence to be eliminated before they can reach and act on the ill tissues. Pegylated liposomes or micelles, namely aggregates covered by a polyethileneglycol film, are the right answer to this problem because polyethileneglycol is an inert chemical substance that does not alert the immunitary system. So tailored amphiphilic complexes freely circulate in the blood stream for 2-3 weeks and they have the time to get into the blood vessels generated the tumor itself. An example of this behavior is the pegylated doxorubicine (Caelyx®).

The inclusion of anti-neoplastic drugs into liposomes has been accepted by several pharmaceutical industries and several products have been put in the market. Hereafter, there is a list of liposomial formulations approved or in clinical experimentation.

Table. Liposomial formulation approved or in clinical experimentation.

Drug	**Commercial name**	**Therapeutical indication**
Daunorubicine	DaunoXome	Kaposi Sarcoma
Doxorubicine	Myocet	Breast cancer
Doxorubicine in pegylated liposomes	Doxil/Caelyx	Kaposi Sarcoma, Breast cancer, Ovaries cancer
Amphotericin B	AmBisome	Fungal inflammation
Cytarabine	DepoCyt	Meningitis
Vincristine	Onco TCS	Non-Hodgkin lymphoma
Lurtotecan	NX211	Ovaries cancer
Nystatin	Nyotran	Fungal inflammation
Retinoic Acid	Altragen	Leukaemia, Non-Hodgkin lymphoma, Renal cells carcinoma, Kaposi Sarcoma
Pt Complexes	Platar	Solid tumors

To further increase liposomal and micellar drug accumulation in the desired tissues and organs, thus maximizing the therapeutic efficacy of the drug and reducing its systemic side-effects, it is important to develop active targeting of particulates that carry physically entrapped drugs.

To attain active targeting of a drug carrier, nanovectors may be derivatized with ligands that bind to specific receptors expressed on target cells. The list of ligands that are used to derivatize nanovectors for selective drug delivery includes a wild range of synthetic and natural compounds of different chemical classes: antibodies or antibody fragments, low molecular weight organic molecules (e.g. folic acid) or natural peptides.

Immunoglobulins (Ig) of the IgG class and their fragments are the most widely used targeting moieties for amphiphilic aggregates, because the covalent binding to the aggregate surface or the hydrophobic insertion into the liposomal membrane or

micellar core don't affect either the integrity of the aggregate or the antibody properties. However, in spite of recent advances in antibody engineering, they remain expensive and time-consuming to produce, and problems with stability and storage exist. Moreover, the majority of antibody targeted aggregates accumulate in the liver as a consequence of insufficient time for the interaction between the target and the targeted liposomes.

Targeting tumours with folate-modified aggregates represents a popular approach, because folate receptors (FR) are frequently overexpressed in many tumour cells. Liposomal daunorubicin[18] as well as doxorubicin[19] have been delivered into various tumour cells through FR. Recently, the application of folate modified doxorubicin-loaded liposomes to the treatment of acute myelogenous leukaemia was combined with the induction of FR using all-trans retinoic acid.[20]

The use of peptides as targeting tools has been validated in a number of applications.[21] Small peptides are, in fact, excellent candidates for the development of target-specific pharmaceuticals, because they are easy to synthesize and modify, less likely to be immugenic, and can have fast blood clearance. One example are radiolabeled peptides which are used in nuclear medicine techniques to perform imaging or to deliver radiotherapeutic doses to cancer tissues overexpressing particular types of receptors, such as those for somatostatin.[22] In this case, a simple entity such as the radionuclide is driven by the peptide to target cells at higher concentrations compared to non-target organs.

1.4 Magnetic Resonance Imaging (MRI): A fundamental tool in tumor diagnosis

MRI is an imaging technique used in medical settings to produce high quality images of the inside of the human body. It measures the characteristics of hydrogen nuclei of the water contained in the human tissues, modified by chemical environment;[23, 24] providing the spatial distribution of the intensity of water proton signal in the volume of the body.

The spatial information is recovered through the additional application of three mutually perpendicular magnetic fields (gradient fields): one to select the slice and two to encode spatial information (Figure 1.3).

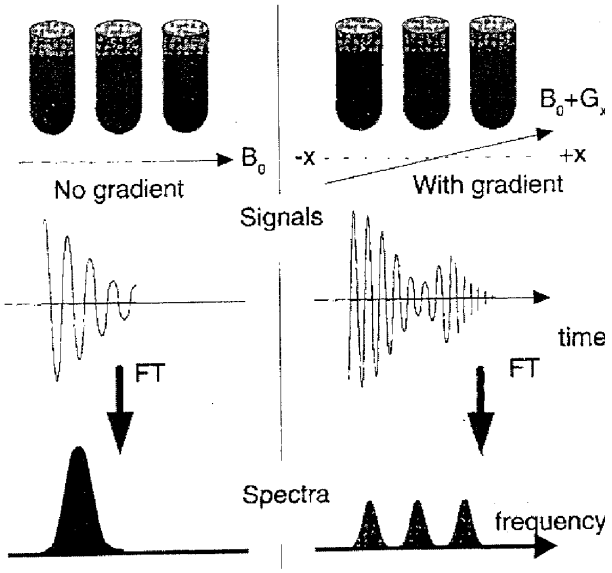

Figure 1.3: The signals and the spectra obtained from three water's samples in different positions on x axes. In presence of the gradient the signals are resolved and the separation depends from the spatial separation in the x versus and from the intensity of the gradient field.

The signal intensity in MRI depends on the amount of water in the given tissue and on the magnetic relaxation times T_1 and T_2, respectively the spin-lattice relaxation time and the spin-spin relaxation time.

The success of MRI is related to the coincidence that proton relaxation times are dependent on the physicochemical environment of a given tissue and so they are modified in presence of a pathological state. Thus, in conditions of optimal contrast, there is a clear distinction between healthy and diseased tissues.

The contrast in MR images is influenced by a range of factors such as the proton density and the relaxation times T_1 and T_2. The proton density in the tissue is obviously problematic to modify. The most modifiable factors are the magnetic relaxation times T_1 and T_2.[25] The spin-lattice relaxation time T_1 and the spin-spin relaxation time T_2 may be shortened considerably in presence of paramagnetic species leading to different effects. While shortening of T_1 leads to increase in signal intensity, shortening of T_2 produces broader lines with decreased intensity.[26] In current medical diagnostics, the most frequently used contrast agents (CA) are T_1 agents. The contrast agents contain magnetic centers that interact with water protons in exactly the same way as the neighboring protons, but with much stronger magnetic fields, and therefore, have a much greater impact on relaxation rates.

Among the paramagnetic species, due to its high number of unpaired electrons, the paramagnetic metal ion Gd^{3+} in its complexed form, otherwise it would be toxic, is the most diffused.

The first contrast agent approved for clinical use was the anionic complex Gd-DTPA (diethylenetriaminepentaacetate acid) under the trade name of Magnevist (Shering AG Germany). In Figure 1.4 are reported some examples of Gd^{3+} based contrast agents with the corresponding thermodynamic stability constants (usually between 10^{16} to 10^{23}) measured at 25° C and μ=0.1 M: Gd-DOTA (DOTA= 1,4,7,10-tetraazacyclo-dodecan-1,4,7,10- tetraacetic acid, Dotarem Guerbet SA, France), Gd-HPDO3A (PHDO3A=1,4,7,10-tetraazacyclo-dodecan-1-(2-hydoxypropyl)-4,7,10-triacetic acid; Prohance, Bracco Imaging, Italy) and Gd-DTPA-BMA (BMA= bismethylamide; Omniscan, Amersham-Hycomed, Norway) (Figure 1.2).

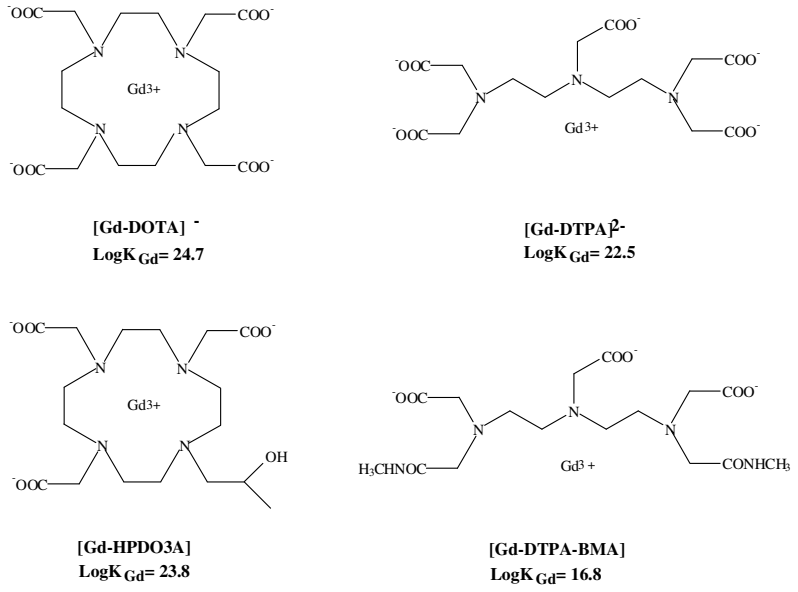

Figure 1.4: Schematic representation of four ligands whose, Gd^{3+} chelates are currently used as CA for MRI. Thermodynamic stabilities of the complexes at 25°C and μ=0.1 M are reported.

The efficiency of a CA, the capacity to shorten the longitudinal relaxation time of the water protons present in the coordination sphere of the metal complex, is expressed as proton relaxivity (r_1), which defines the increase in longitudinal water proton relaxation rate per millimolar concentration of Gd^{3+}.

The observed water proton longitudinal relaxation rate[27] (eq.1.1) in a solution containing a paramagnetic metal complex is given by the sum of three contributions:

$$R_1^{obs} = R_{1p}^{is} + R_{1p}^{os} + R_1^{w} \qquad (1.1)$$

where R_1^w is the water relaxation rate in the absence of the paramagnetic compound, R_{1p}^{is} the contribution due to the exchange of water molecules from the inner coordination sphere of the metal ion to the bulk water and R_{1p}^{os}, finally, the contribution of solvent molecules diffusing in the outer coordination sphere of the paramagnetic center. The overall paramagnetic relaxation enhancement ($R_{1p}^{is} + R_{1p}^{os}$) referred to by a 1 mM concentration of a given Gd^{3+} chelate is called relaxivity (Figure 1.5).

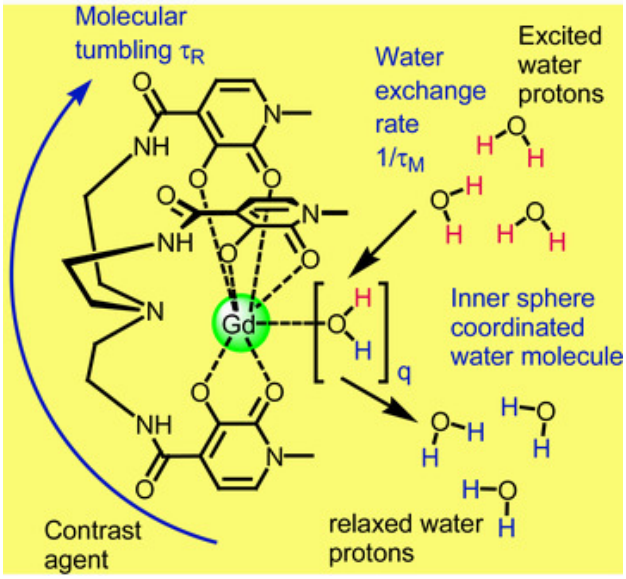

Figure 1.5: Schematic view of the relaxation mechanisms operating in an aqueous solution containing a paramagnetic Gd^{3+} chelate.

The inner sphere relaxation rate is described in terms of the following set of equations (eq. 1.2-1.4), which correspond to the model developed by Solomon-Bloembergen-Morgan:[28]

$$R_{1p}^{is} = \frac{c * q}{55.6} * \frac{1}{T_{1M}^{H} + \tau_M} \tag{1.2}$$

$$\frac{1}{T_{1M}^{H}} = Kf(\tau_C) \tag{1.3}$$

$$\frac{1}{\tau_C} = \left(\frac{1}{\tau_M} + \frac{1}{\tau_R} + \frac{1}{\tau_S} \right) \tag{1.4}$$

where: c is the molar concentration of the paramagnetic complex; q is the number of water molecules coordinated to the metal ion; τ_M is the mean residence lifetime; T_{1M} is their longitudinal relaxation time; K is the value of dipolar interaction between coordinated water's protons and the unpaired electrons; τ_R the reorientation correlation time; and τ_S is the electron spin relaxation time.

The ability of Gd^{3+} chelates to enhance the relaxivity is mainly determined by the value of their molecular reorientation time, τ_R, which depends upon the molecular dimension of the complexes. Therefore, the achievement of higher water proton relaxation rates may be pursued through the employment of macromolecular contrast agent, which allows also carrying a high concentration (10^{-2} M) of contrast agent. At this aim many supramolecular systems have been developed such as liposomes[29] and other microparticulates,[30] micelles,[31] dendrimers,[32] linear polymers,[33] proteins,[34] or peptides,[35] all of these derivatized with the metal-complex of interest. Among those carriers, micelle and vesicular aggregates have recently drawn much attention owing to their easy controlled properties and good pharmacological characteristics.

1.5 Metal Complexes in tumor therapy

Since 1965, when the neoplastic activity of cis-Platinum was discovered,[36] this transition metal has been becoming one of the most used chemicals in the treatment of some tumoral diseases; such as testicle, mammalian, uterine and ovarian cancers.[37] Many Pt-based complexes have been synthesized, the most successful are: cis-Platinum, Carbo-Platinum[38] and Oxali-Platinum[39].

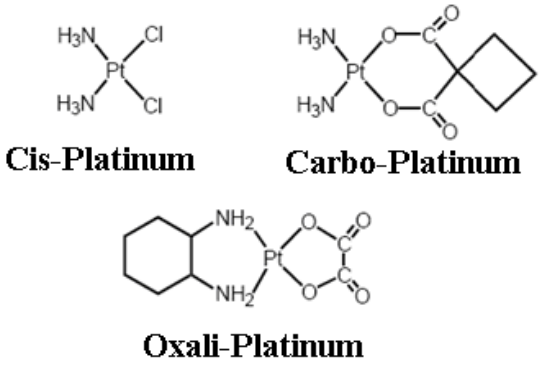

Figure 1.6: Schematic structures of some Platinum complexes.

In 1979 the Food and Drugs Administration adopted cis-Pt as human drug. Nevertheless other transition metals have been taken into account in the cancer treatment with the aim to substitute Pt, because of its gastric and renal toxicity. The use of cis-Pt is also limited by problems connected with the resistance induced in patients and for its chemo-activity only on few tumoral forms.[40]

It has been proposed that Pt-complexes renal and gastric toxicity is the consequence of the inactivation of sulfured enzymes due to the bonds that Pt directly forms with the sulfur sites.

The setting-up of sulfured chemo-protectors, mainly thiols and thiocarbamates, is a good strategy to overcome this problem. In fact, these chemicals are able to bind Pt ions not allowing their direct interaction with sulfured enzymes; but although this winning strategy, the toxicity of Pt-based drugs remains considerable. This is the reason why researchers are paying attention on other metals,[41] such as Titanium[42], Rhodium[43], Iridium[44] and Ruthenium[45]. In relation to this last metal, it is Ru^{+2} (from now on Ru(II)), that shows good anti-tumoral and anti-metastatic activity [46], together with a lower toxicity in comparison with that of Pt complexes. In particular Ru(II)-amine complexes are at present preferred for the reproducibility of their synthesis and for the stability of the complexes, but above all because of their specificity for proteins, oligonucleotides and nucleic acids of specific tissues.[47]

Although only Ru(II), among all the Ru oxidation states shows anti neoplastic activity, Ru(III) can also be employed in drug preparation. In fact Ru(III) can be activated through the so named “Activation by Reduction Mechanism”. This mechanism consists in the *in vivo* reduction of Ru(III) to Ru(II) with the aid of glutathione (GSH) or of other reducing proteins.[48]

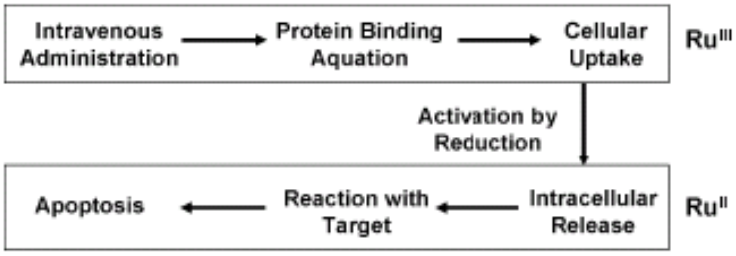

Figure 1.7: Suggested mode of action of Ru-based anticancer agents.

It is well-known that the growth of tumoral tissues needs a large quantity of oxygen for the formation of new blood-vessels (angiogenesis). However these vessels are not able to satisfy the continuous request of oxygen of the tumor cells. This gives rise to a mechanism of cellular hypoxia[49] that has two important consequences. First, the tumor cells are compelled to migrate towards more oxygenated regions so starting the metastasis production. Second, the tumor cells dependent on glycolysis mechanism much more, in order to satisfy the request of energy and this has the secondary effect to produce an excess of lactic acid that lowers pH inside tumor cells.[50]

Furthermore, there are evidences that hypoxia favors the binding of Ru-complexes to DNA,[51] while it does not favor the binding of Pt-based drugs. The reason of this different mechanism probably stays in the octahedral geometry of Ru complexes in comparison with the planar geometry of Pt complexes.[52]

The first Ruthenium based compound has been the so named NAMI, Na[transRuCl4(DMSO)(Na)], that showed encouraging antitumoral properties. This

molecule has a pseudo-octahedral form with the four chlorines in equatorial position and the DMSO in axial.

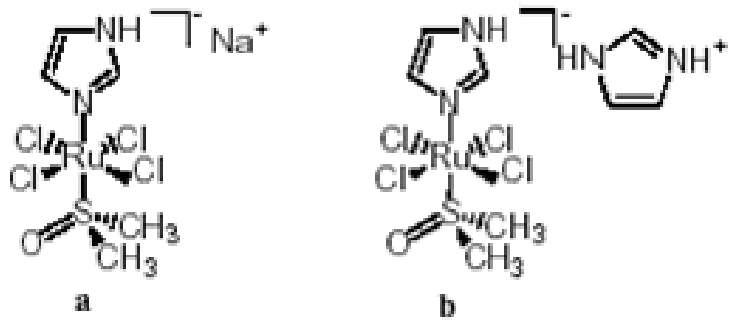

Figure 1.8: Chemical structures of NAMI (a) and NAMI-A (b).

NAMI, then, was modified in NAMI-A, designed and synthesized by the research group of prof. Gianni Sava, university of Trieste, substituting the counterion Na^+ with the imidazole group. This substitution gave rise to a more stable complex, such that in 1999 the clinical trial of this compound started.[36] It is supposed that NAMI-A is able to modify the gene expression of metastases cell, blocking the genes that sustain the malignant phenotype and activating, instead, the genes that regulate the normal growth and death of cells.

Although a rather large number of studies on Ruthenium complexes have been published in the recent years,[53] up to date in literature no examples of nanovectors carrying Ruhenium complexes are reported.

2. The Systems Studied

2.1 Peptides and Gd Complexes Containing Colloidal Assemblies as Tumor Specific Contrast Agents in MRI.

The first system, that has been designed and characterized during this PhD thesis, has been a new amphiphilic supramolecular contrast agent able to give good and resolved images of human tissues and organs in Magnetic Resonance Imaging.

The system should present two important aspects:

1) to display a very high relaxivity value
2) to be selective for cancer cells

The two aims have been simultaneously achieved by working out mixed systems formed by two different amphiphilic unimers, one containing the chelating moiety DTPAGlu, capable of forming stable complexes with Gd^{3+} ions, and the other one the bioactive peptide CCK8.

The first unimer had a double alkylic chain bound through a lysine residue to the DTPAGlu chelating agent (N,N-bis[2-[bis[2-(1,1-dimethylethoxy)-2-oxoethyl]amino]ethyl]-L-glutamic acid). The second unimer contained the same lipophilic moiety bound through an oxyethylene glycol spacer to the C-terminal cholecystokinin octapeptide amide (CCK 26-33 or CCK8). CCK8 is the C-terminal sequence of the cholecystokinin hormone and provides the binding sequence for the cholecystokinin receptor subtypes A and B (CCKA-R and CCKB-R).[54] Overexpression

of both of these receptor subtypes has been demonstrated in certain human tumours: CCKA-R is overexpressed in pancreatic cancer, and CCKB-R is found in small cell lung cancer, colon and gastric cancers, medullary thyroid carcinomas, astrocitomas and stromal ovarian tumors.

We have carried out several attempts to optimize the design of the CCK8 unimer, varying the length of the spacer situated between the double tail and the CCK8. In fact, the spacer should be long enough to assure an efficient exposure of the peptide on the external surface of the aggregate and at the same time short enough to favor the formation of vesicles.[55]

The system so formulated, containing both unimers, has been investigated in different conditions of pH and ionic strength, due to the variety of environmental conditions the contrast agent may experience in the blood stream.

2.2 Lipid Based Nanovectors Containing Ruthenium: A New Approach in Cancer Therapy

Recently Ruthenium complexes have shown great potentialities in clinical use, but in spite of that in the open literature up to date no example of nanosystem carrying Ruthenium is reported. The use of nanovectors as carriers for Ruthenium complexes can improve the therapeutic efficacy of these complexes and reduce their systemic side-effects.

The basic idea behind the project developed in this PhD thesis is the synthesis of a new amphiphilic molecule constituted by two oleoyl chains bound to an uridine residue containing a pyridinium ring able to coordinate a Ruthenium (III) complex.

The molecules so designed can aggregate in nanovectors with different shape and size, such as spherical or rod-like micelles, vesicles/liposomes or other nanostructures.

The amphiphilic unimer coordinating the Ruthenium, baptized DOPURu, has been lodged in lipid bilayer formed by DOPC (1,2-Dioleoyl-*sn*-Glycero-3-Phosphocholine) and DOPE (1,2-Dioleoyl-*sn*-Glycero-3-Phosphoethanolamine), to reduce the commercial cost of the final formulation. PC and PE polar heads are the most abundant in plasma membranes and are known to be compatible with cells.

The system so formulated should guarantee an:

1) Increased solubility of Ruthenium complexes in the bloodstream.

2) Prolongation of the drug circulation time by protecting Ruthenium complexes from enzymatic and/or environmental degradation.

3) Reduced Ruthenium complexes toxicity.

These goals will be obtained because:

1) The lodgement of Ruthenium complexes in amphiphilic nanovectors consents to carry a higher amount of drug in the bloodstream compared to the case when it is administrated as free complex.

2) The amphiphilic nanovectors are able to protect the Ruthenium complexes from enzymatic and/or environmental degradation that they could experience circulating in bloodstream.

2) and 3) The presence of a poly(ethylene glycol)chain, PEG, in the backbone of our molecules, allows protecting Ruthenium complexes from enzymatic or environmental degradation, increasing so their circulation time in the bloodstream. A long time permanence of Ruthenium complexes in the bloodstream is advantageous from a therapeutic point of view, since the rapid uptake of colloidal drug carriers by RES (reticulo-endothelial system) would result in a fast reaching of the dose-limiting toxicity.

3. Experimental Section

3.1 Unimers Synthesis

3.1.1 Synthesis of the Unimers Binding Gd and Peptides

The unimers employed in the first project were synthesized by prof. Carlo Pedone's research group (CIRPeB, Naples, Italy).

The synthesis was carried out in solid phase (SPPS) by conjugation of DTPAGlu chelate or CCK8 peptide molecule (Figure 3.1) on a double hydrophobic tail of 18 carbon atoms.

We used two C18 chains to mimic the phospholipid bilayer of the cell membrane and to avoid so a possible cytholitic effect on the cells.

DTPAGlu is the chelating agent used to coordinate Gd^{3+} ion. It's a DTPA analog endowed of one carboxylic group more than DTPA molecule. This function permits to bind it on the double C18 chain and continue to preserve eight positions for the complexation of the paramagnetic ion.[56]

The CCK8 peptide monomer was synthesized binding the alkylic chains on the terminal amino group of CCK8 to assure that the peptide is still able to recognize selectively the cholocystokinin receptors (CCK_A-R and CCK_B-R), that are over-expressed in tumoral processes. In fact, structural modifications on the N-terminal of

the CCK8 should not affect receptor binding for both subtypes, because this part is distant from the receptor fragment and points towards the extra-cellular space.

Some non-ionic ethoxylic spacers (AdOO) were placed between the peptide and the alkylic moiety in order to improve the hydrophilicity of the CCK8 peptide, and its exposition on the external aggregate surface.

To improve the exposition of the peptide fragment, it was also synthesized another monomeric compound, where ethoxylic spacers were replaced by a poly(ethylene glycol) molecule.

Notwithstanding the very promising properties of the already reported target-specific contrast agents, we thought that an increase of the efficacy in the development of selective contrast agents in MRI could be obtained by including, in the same molecule, all three fundamental tasks that are required: 1) a bioactive peptide, 2) a gadolinium complex, and 3) a hydrophobic moiety. We have, therefore, synthesized a new monomer with an “upsilon” shape (MonY; Figure 3.1), where a lysine residue is derivatized on its three reactive functions with: 1) the CCK8 peptide bound to the lysine carboxylic function and spaced by two oxyethylene linkers 2) the DTPAGlu chelating agent covalently bound to the side-chain ε-amino group and 3) a double C18 alkyl chain, where each chain was bound to the lysine α-amino group.

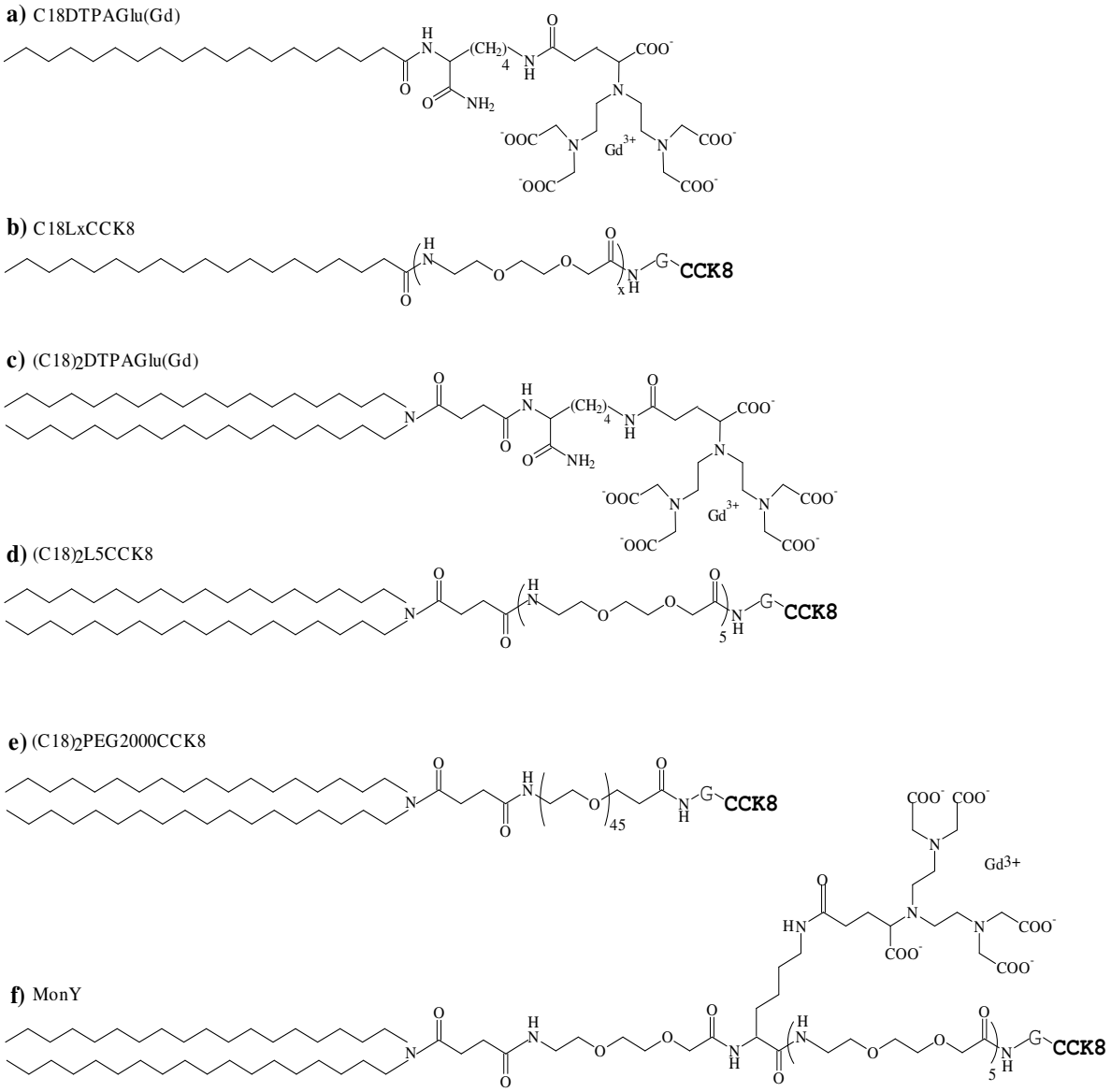

Figure 3.1: Schematic representation of the synthesized unimers. The amino acid sequence of CCK8 peptide is reported by using the one-letter amino acid code.

3.1.2 Synthesis of the Unimer Binding Ru(III)

The synthesis of the unimer binding Ru(III) has been carried out by Dr. Raffaella Del Litto and Prof. Francesco Ruffo.

The new amphiphilic ligand, baptized DOPU, has been obtained from an uridine derivative by introduction of a pyridine function on the uracile base. The hydrophobe of the molecule is constituted by a double C18 alkyl chain attached to the C2 and C3 of the sugar ring, whereas in position C5 an hydrophilic PEG-350 residue is present (see figure 3.2).

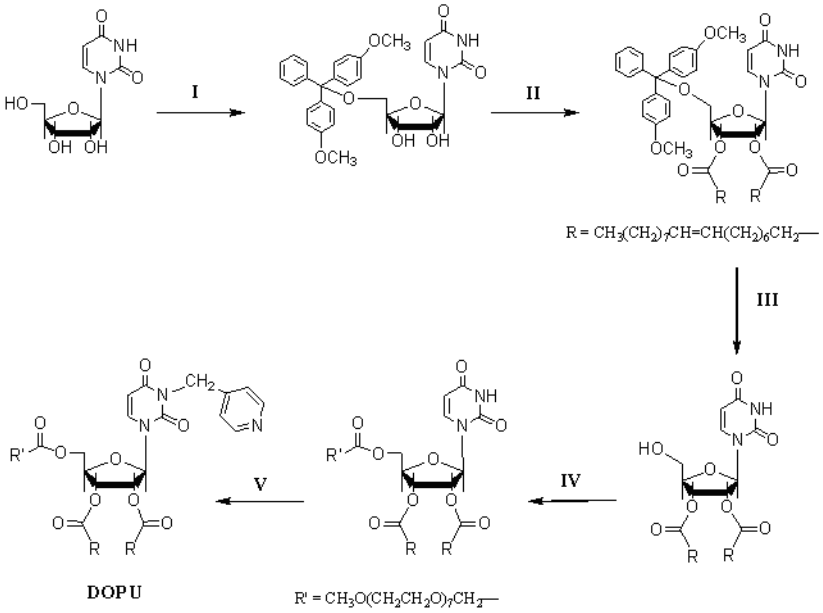

Figure 3.2: Scheme of synthesis of DOPU unimer: I) nucleoside protection by dimethoxynitrile, II) alkyl chain introduction, III) nucleoside deprotection, IV) PEG350 residue introduction, V) pyridine function introduction.

The ligand unimer DOPU has been coordinated to Ru(III) by displacing a DMSO molecule from the suitable precursor $[(DMSO)_2H][RuCl_4(DMSO)_2]$, as shown in figure 3.3.

According to the stoichiometry of the reaction, the anionic molecule binding ruthenium $[RuCl_4(DMSO)(DOPU)]^-$ is accompanied by the protonated unimer $[(DOPU)H]^+$ as counterion.

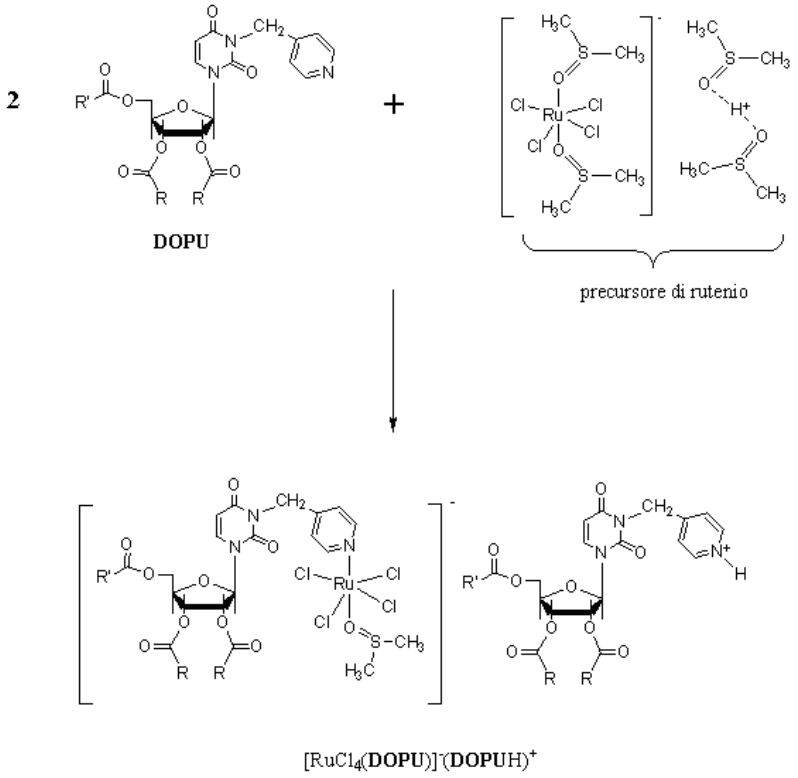

Figure 3.3: Scheme of the synthesis of DOPURu

3.2 Sample Preparation

The method of preparation of samples was evolved more times during the thesis, in order to find the right procedure to favor the formation of vesicles.

The ordinary methods of sonication and extrusion were both used to give energy as much as possible to the system and to support so the formation of vesicles.

All solutions were prepared by weighing; the solvent used was bi-distilled water or a buffer solution.

Two different types of buffer solutions were used depending on the environmental conditions. For physiological condition, pH 7.4, a 0.10 M phosphate buffer solution was used, while for lower pH values a 0.10 M citric acid/phosphate buffer, that mixed at different ratios allowed moving from pH 7 to pH 3. pH measurements were made by using pH-meter MeterLab PHM 220. The pH-meter was calibrated with standards at pH 7, pH 10, and pH 3.

The amphiphile unimers dissolved in the aqueous solvent were successively undergone to sonication for half a hour at 25°C in a bath-sonicator. Finally the resulting was extruded, pushing it 11 times through a polycarbonate membrane with 100 nanometer pore size, to homogenize the size of vesicles.

4. Results and Discussion

4.1 Binary system: $(C18)_2$DTPAGlu-water

DLS measurements have shown that in $(C18)_2$DTPAGlu solution, extruded at physiological pH, there is the contemporary presence of two different aggregates.

Figure 4.1a shows the relaxation time distributions for 1 mM $(C18)_2$DTPAGlu at different pH values. At pH 7.4 the distribution is clearly bimodal with well-separated modes, and in particular the fast mode has a higher amplitude than the slow mode. The relaxation rates ($\Gamma = \tau^{-1}$) for the fast and the slow modes were measured at different q values. The linear relation of the relaxation rates confirms that both modes are due to translational diffusion processes, attributed to two different complexes, with apparent translational diffusion coefficients D_{fast} = (30.3 ± 0.4) × 10^{-12} m^2s^{-1} and D_{slow} = (3.2 ± 0.5) × 10^{-12} m^2s^{-1} respectively, see table 1. The Stokes-Einstein equation may be used to evaluate the hydrodynamic radius, R_H at infinite dilution:

$$R_H = \frac{k_B T}{6\pi\eta_0 D_0} \tag{4.1}$$

where D_0 is the translational diffusion coefficient at infinite dilution, k_B is the Boltzmann constant, T is the absolute temperature and η_0 is the solvent viscosity. Due to the high dilution (10^{-4} mol kg^{-1}) and high ionic strength of the systems, we have approximately $D \approx D_0$ so eq. 1 can be reasonable used to estimate the hydrodynamic radius of the aggregates.

The R_H values obtained for the slow and fast modes were (620±90) and (66±1) Å respectively, see table 1, and they are compatible with bilayer structures, such as vesicles, and micelles with an elongated shape.[57]

The relaxation time distribution of the $(C18)_2$DTPAGlu solution at physiological pH collected in Figure 4.1a reveals the contemporary presence of micelles and bilayer structures or vesicles and that the dominant aggregates present in the system are micelles. The magnitude of the peak of this latter is sensibly higher than that corresponding to the vesicles.

The intensity scattering profile collected by SANS confirmed these results, showing at intermediate q range ($0.02 < q/Å^{-1} < 0.06$) a rising peak coming from the presence of micelles, whereas at low q values a q^{-2} decay typical of double layer scattering (see figure 4.2). Structural parameters of the aggregates have been obtained by fitting experimental data through an appropriate model (see appendix 2), and they are reported in table 2. Micelles have been modelled as rodlike micelles with a length of ~ 200 Å and a radius of ~ 40 Å, while the bilayer thickness of vesicles was estimated to be around 70 Å.

Variation of pH has a drastic effect on the size distribution of the aggregates. An overall view of the aggregation behavior may be obtained by plotting the intensity correlation functions or the relaxation time distributions obtained from RILT analysis of the former as a function of pH at a fixed scattering angle ($\theta = 90°$) (Figure 4.1 a-b). Figure 4.1 b shows that the time correlation function of scattered intensity $g^{(2)}(t)-1$ translates to longer decay time as pH decreases, indicating a growth in the size of the aggregates. In particular in the pH range between 7.4 and 5.0 the

relaxation time distributions (Figure 4.1 a) are substantially unvaried; the distributions are bimodal and the high amplitude peak at faster relaxation times corresponds to the diffusion of micelles.

As pH decreases from 5.0 to 4.0, the picture changes: the distribution becomes almost monomodal and shifts toward slower relaxation times as expected for larger aggregates. Thus, subsequent acidification results in a further shift to slower times of the relaxation time. SANS measurements have highlighted that at pH 4.5 micelles increase their length from ~ 200 Å to ~ 700 Å.

Further acidification at pH 3 favors the formation of vesicles, whose radius is 740 ± 30 Å and thickness is 47 ± 5 Å.

The results from the DLS and SANS measurements clearly show that the aggregation behavior is pH sensitive, this because of the presence of five carboxylic groups in the surfactant head-group.

At physiological pH the tendency to form bilayer structures is sensible reduced, owing to the high negative actual charge of the surfactant head-group, which cause a strong head groups repulsion. At lower pH (pH 5.0 – 4.0) the size distributions change as expected in light of the carboxylic acids pKa ~ 4.5.[58] In fact around this pH the DTPA group should be partially uncharged, supporting the formation of large and low curvature aggregates, such as bilayer aggregates or vesicles.

Thus for $(C18)_2$DTPAGlu-water binary system, we have observed a micelle-to-vesicle transition, which confirms the three-stage Lichtenberg model.[16, 17]

We have found the following sequence of aggregation states as the solution pH was decreased from pH 7.4 to 3.0 (see figure 4.3):

rodlike micelles ⟶ threadlike micelles ⟶ vesicles

The cryo-TEM images collected in figure 4.3 give a clear indication of the structural evolution of the aggregates formed by $(C18)_2$DTPAGlu as a function of the pH. The cryo-TEM results confirm a gradual transition upon decreasing pH from small rod-like micelles (pH=7.4) to thread-like micelles (pH = 4.5), and finally to vesicles (pH = 3.0). At physiological pH, micelles are visualized in the image as dark dots, because objects with a size of about 5-6 nanometers are in the limit of the resolution of electron microscopy technique used (see figure 4.3 a). At pH 4.5 micelles change their shape and appear in the vitrified sample as threads with slightly swollen end caps (figure 4.3 b).We note the aggregates seen in the image are characterized by a low contrast, which is typical of micelles. At pH 3 the images are dominated by the presence of vesicles, as foreseen from the DLS and SANS measurements. Most of the vesicles are unilamellar, see Figure 4.3 c, with a mean radius in the range of 700÷1000 Å. This value is in agreement with the apparent hydrodynamic radius estimated by the DLS experiments.

FIGURES

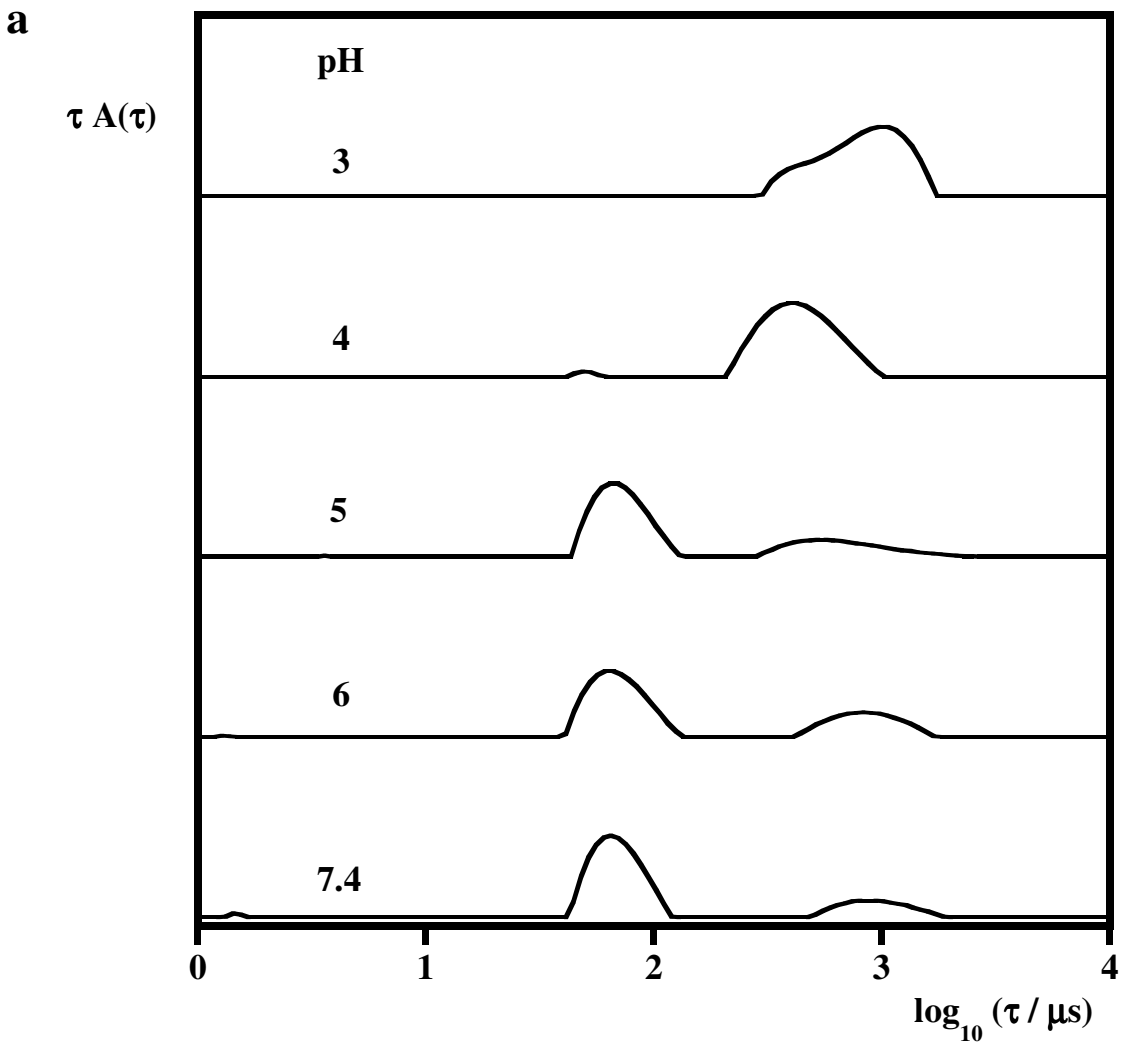

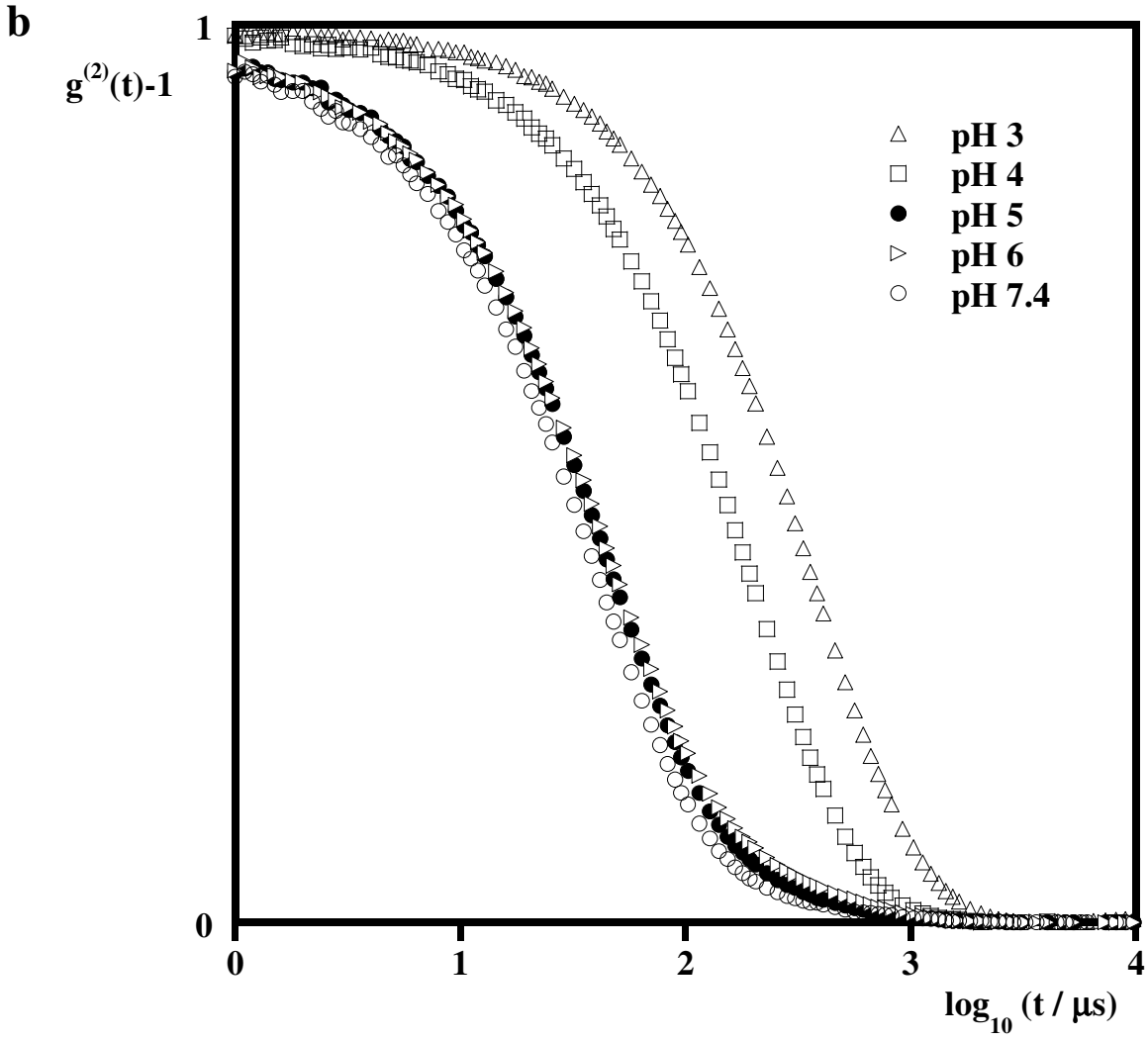

Figure 4.1: (a) Relaxation time distributions at θ = 90° for 1mM $(C18)_2$DTPAGlu aqueous solution as function of pH; (b) Intensity correlation functions at θ = 90° for 1mM $(C18)_2$DTPAGlu aqueous solution as function of pH.

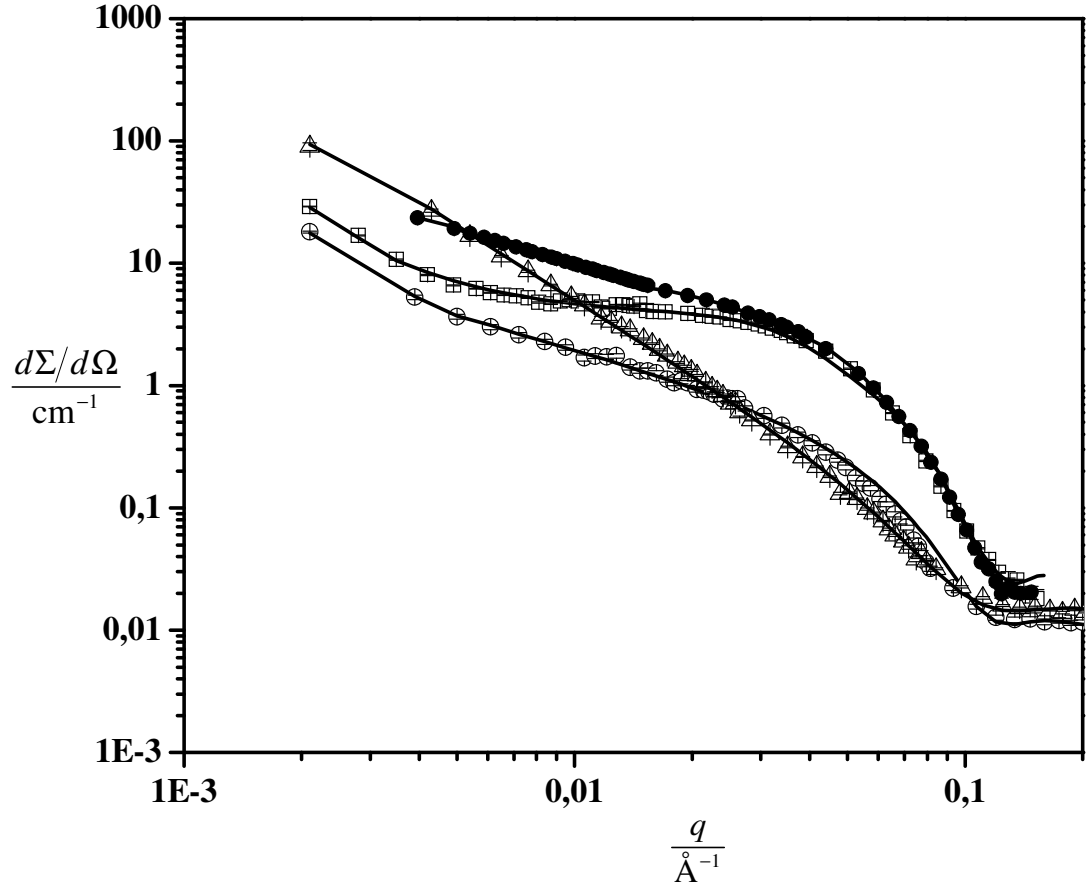

Figure 4.2: Scattering intensity profile for $(C18)_2$DTPAGlu-D_2O at pH 7.4 (□), $(C18)_2$DTPAGlu-D_2O at pH 4.5 (○), $(C18)_2$DTPAGlu -D_2O at pH 3 (△), and $(C18)_2$DTPAGlu-D_2O at pH 7.4 not extruded (●).(—) Fitting curve to the experimental data through the model reported in the appendix.

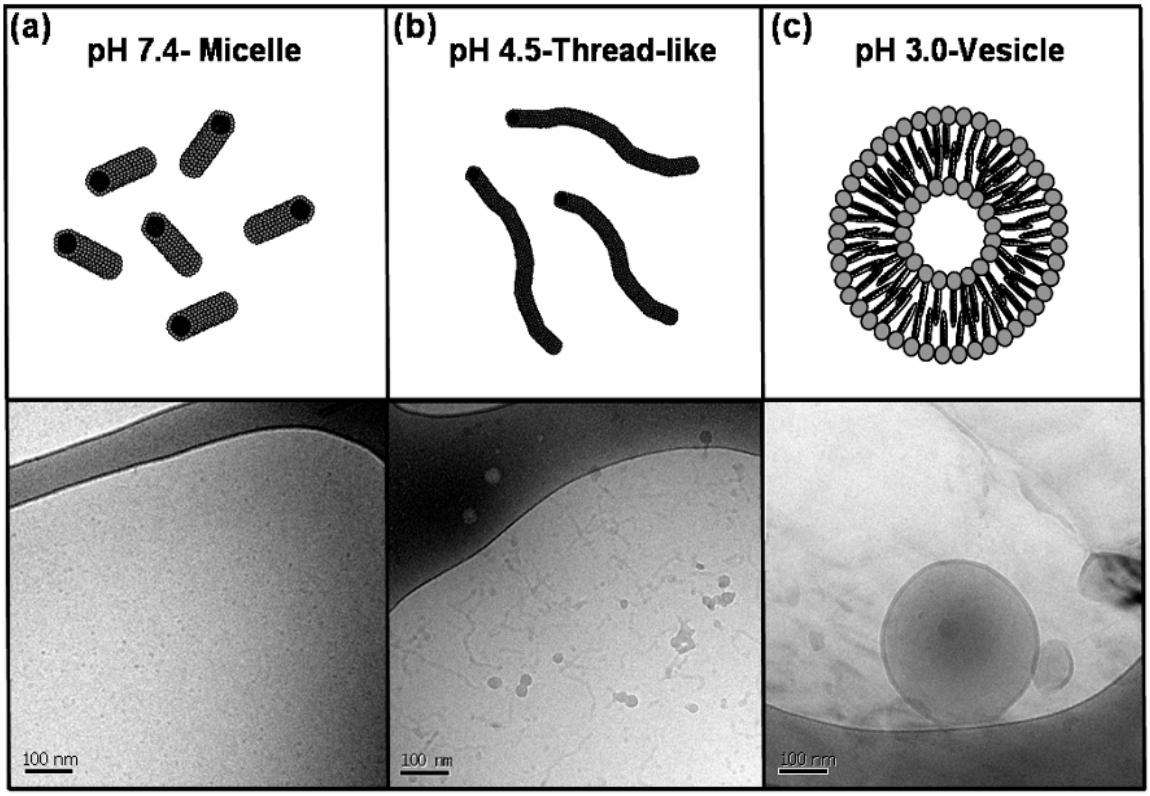

Figure 4.3: Cryo-TEM image for 1mM $(C18)_2$DTPAGlu-water at different pH values: (a) at pH 7.4 micelles appear as black dots which are difficult to distinguish from the background; (b) at pH 4.5 thread-like micelles are observed (circular stains are artifacts); (c) at pH 3 vesicles appear unilamellar with a radius in the range of $700 \div 1000$ Å.

TABLES

Table 1. Diffusion coefficients and hydrodynamic radii obtained from DLS measurements for the systems studied at different pH values. The terms fast and slow refer to micelles and bilayer structures respectively.

Systems	pH	$D_{fast}\times10^{11}$ (m^2s^{-1})	R_H (Å)	$D_{slow}\times10^{12}$ (m^2s^{-1})	R_H (Å)
$(C18)_2$DTPAGlu (0.0001 mol kg^{-1}) – water	7.4	3.03±0.04	66±1	3.2±0.5	620±90
$(C18)_2$DTPAGlu (0.0001 mol kg^{-1}) – water	6	3.01±0.01	66±1	2.81±0.11	710±40
$(C18)_2$DTPAGlu (0.0001 mol kg^{-1}) – water	5	2.91±0.03	68±1	3.1±0.3	650±60
$(C18)_2$DTPAGlu (0.0001 mol kg^{-1}) – water	4			5.0±1	400±80
$(C18)_2$DTPAGlu (0.0001 mol kg^{-1}) – water	3			2.7±1	740±30

Table 2. Structural parameters of the aggregates at different pH values determined by Small-Angle Neutron Scattering (SANS). The terms N_{agg}, R and l refer to the aggregation number, the radius and the height of the micelles respectively, whereas d refers to the thickness of the bilayer structures.

Systems	pH	N_{agg}	R (Å)	l (Å)	d (Å)
$(C18)_2$DTPAGlu (0.00079 mol kg $^{-1}$)-water	7.4	125±15	39±3	198±21	72±9
$(C18)_2$DTPAGlu (0.00079 mol kg $^{-1}$)-water (not extruded)	7.4	102±10	38±4	108±39	
$(C18)_2$DTPAGlu (0.00063 mol kg $^{-1}$)-water	4.5	771±80	36±2	710±60	61±8
$(C18)_2$DTPAGlu (0.00063 mol kg $^{-1}$)-water	3				47±5

4.2 Binary system: $(C18)_2$DTPAGlu(Gd)-water

Systems where gadolinium ion was complexed by the chelating agent unimer exhibited quite similar relaxation time distributions and cross scattering profiles (see figures 4.4 and 4.5) to the systems in uncomplexed form when compared at the same condition of pH; although, as highlighted by SANS, double layer structures over the entire pH range were generally observed. In particular, DLS measurements have shown that below pH 6.0 the distribution becomes already monomodal. The relative amplitude for the slow mode increases on the expense of the fast mode yielding to a single peak positioned at a slower relaxation time at pH 4.0, see figure 4.4.

The presence of Gd^{3+} ions produces a mild effect for the pH reduction, because it reduces the actual charge of the surfactant from -5 to -2. Thus, for these systems, formation of low and large curvature aggregates, such as open bilayers, is supported, and this tendency is further enhanced upon lowering the pH.

At physiological pH, the cryo-TEM micrographs showed open bilayer structures and elongated and thick structures similar to fibers, corresponding to cylindrical micelles, see figure 4.6a. Upon decreasing pH, the images are dominated by the presence of bilayers structures as predicted by DLS and SANS results that are summarized in tables 3 and 4. The images collected for the system at pH 3.0 showed clearly the presence in solution of vesicles (figure 4.6 b) and open bilayers, similar to those visualized at pH 7.4. The radius of vesicles is ranged between 500 and 600 Å (table 3). The latter structures, whereas, appear as hollow tubes having a thickness of around 60 Å with well marked edges. The edges appear quite dark probably because

of the presence of the gadolinium, which is oriented toward the aqueous phase. These aggregates, as confirmed by DSC experiments, represent “gel phases” containing bilayers with crystallized hydrocarbon chains separated by liquid-like solvent whose gel to liquid-crystalline phase transition temperature T_m is around 70°C.[8]

FIGURES

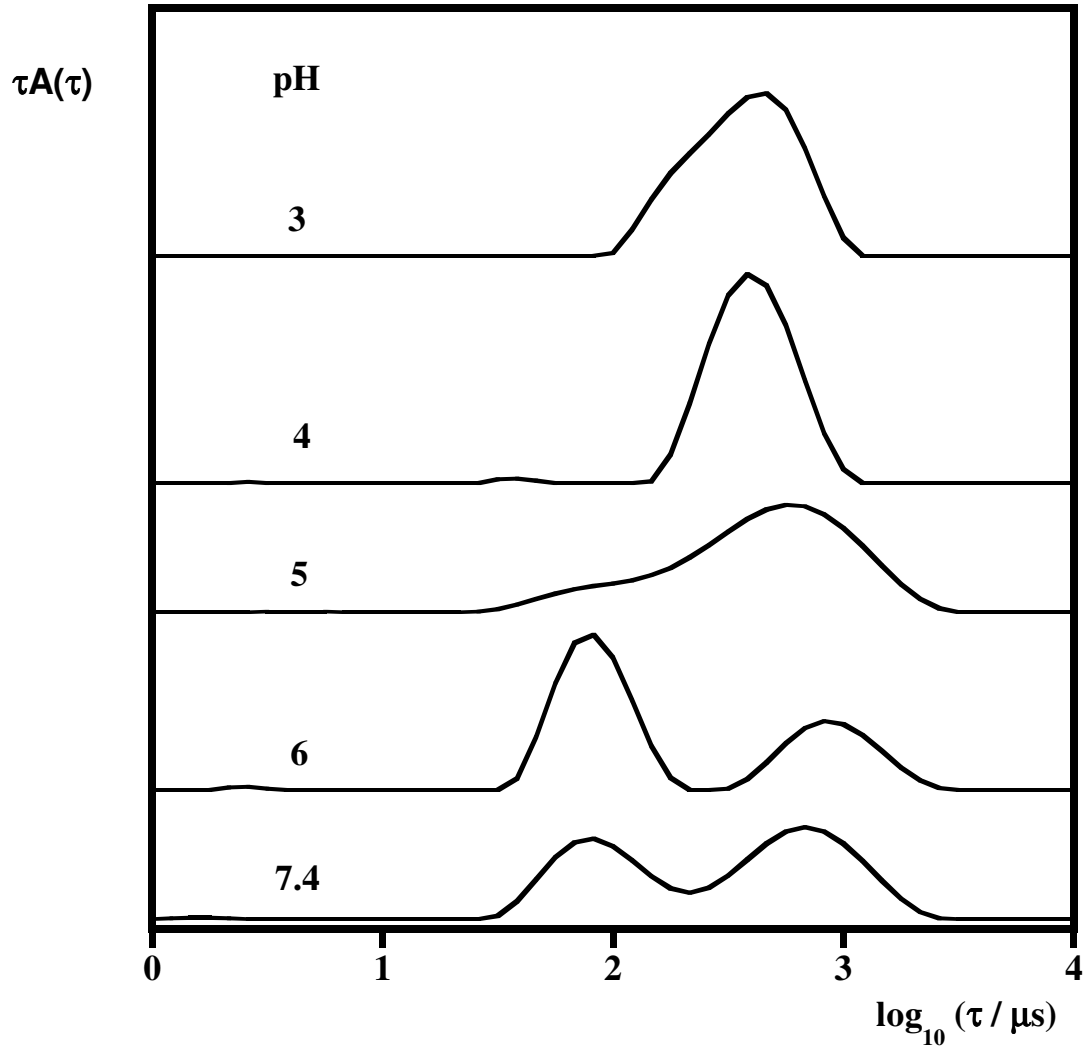

Figure 4.4: Relaxation time distributions at θ = 90° for 1mM $(C18)_2$DTPAGlu(Gd) aqueous solution as function of pH.

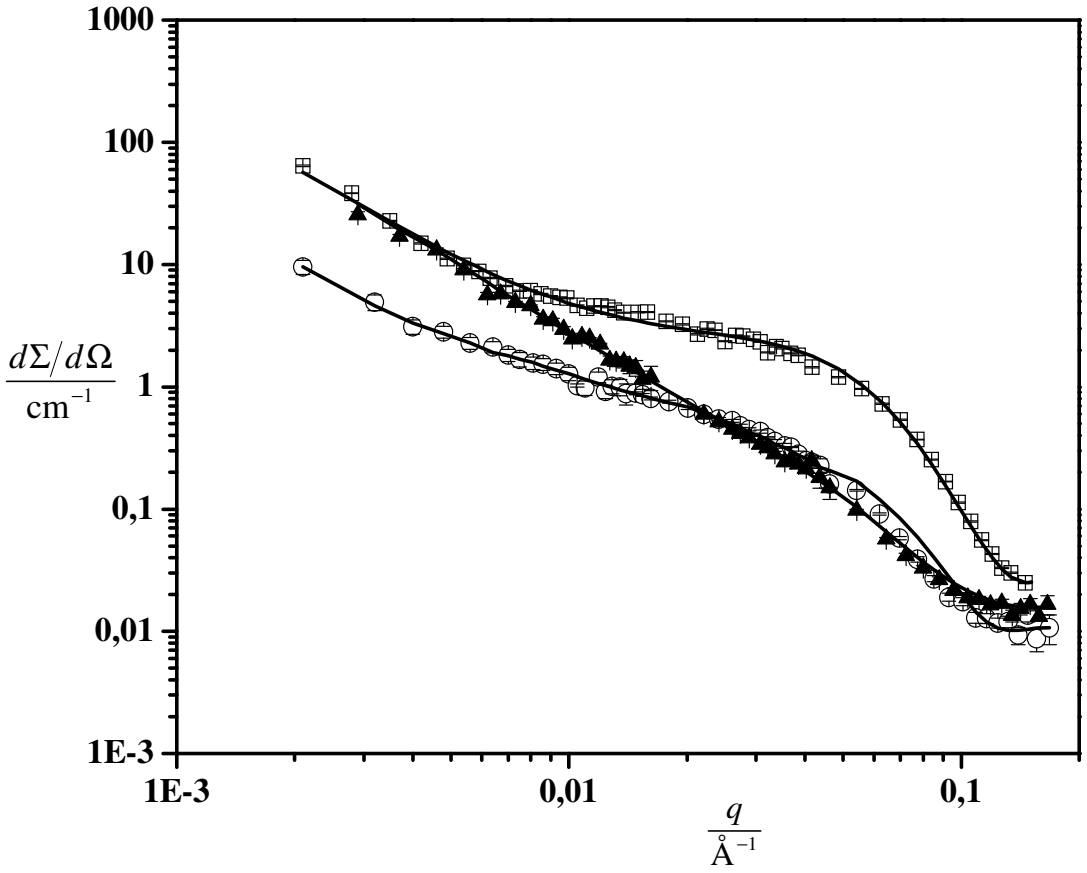

Figure 4.5: Scattering intensity profile for $(C18)_2$DTPAGlu(Gd)-D_2O at pH 7.4 (□), $(C18)_2$DTPAGlu(Gd)-D_2O at pH 4.5 (○) and $(C18)_2$DTPAGlu(Gd) -D_2O (▲).(—) Fitting curve to the experimental data through the model reported in the appendix.

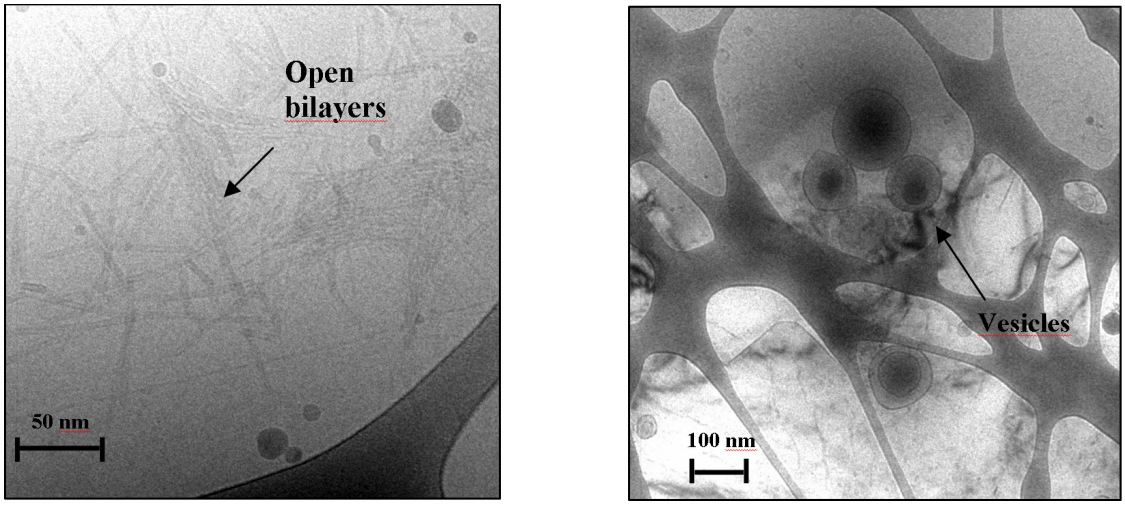

Figure 4.6: Selected cryo-TEM images for 1mM $(C18)_2$DTPAGlu(Gd)-water at different pH values: (a) at pH 7.4 open bilayers and cylindrical micelles similar to fibers appear (circular stains are artifacts); (b) at pH 3 vesicles with a radius in the range of 500 ÷ 600 Å.

TABLES

Table 3. Diffusion coefficients and hydrodynamic radii obtained from DLS measurements for the systems studied at different pH values. The terms fast and slow refer to micelles and bilayer structures respectively.

Systems	pH	$D_{fast}\times10^{11}$ (m^2s^{-1})	R_H (Å)	$D_{slow}\times10^{12}$ (m^2s^{-1})	R_H (Å)
$(C18)_2$DTPAGlu(Gd) (0.0001 mol kg^{-1}) -water	7.4	2.64±0.05	76±1	4.1±0.3	490±50
$(C18)_2$DTPAGlu(Gd) (0.0001 mol kg^{-1}) – water	6	2.64±0.03	76±1	3.2±0.4	620±80
$(C18)_2$DTPAGlu(Gd)(0.0001 mol kg^{-1}) – water	5	2.50±0.05	80±2	4.3±0.2	460±20
$(C18)_2$DTPAGlu(Gd) (0.0001 mol kg^{-1}) – water	4			5.6±0.3	360±20
$(C18)_2$DTPAGlu(Gd) (0.0001 mol kg^{-1}) – water	3			6.3±0.2	320±20

Table 4. Structural parameters of the aggregates at different pH values determined by Small-Angle Neutron Scattering (SANS). The terms N_{agg}, R and l refer to the aggregation number, the radius and the height of the micelles respectively, whereas d refers to the thickness of the bilayer structures.

Systems	pH	N_{agg}	R (Å)	l (Å)	d (Å)
$(C18)_2$DTPAGlu(Gd) (0.00063 mol kg $^{-1}$) -water	7.4	110±10	35±3	233±30	52±5
$(C18)_2$DTPAGlu(Gd) (0.00063 mol kg $^{-1}$) -water	4.5	723±65	34±2	741±82	53±8
$(C18)_2$DTPAGlu(Gd) (0.00063 mol kg $^{-1}$) -water	3				51±6

4.3 Ternary systems: $(C18)_2$DTPAGlu-$(C18)_2$PEG2000CCK8-water and $(C18)_2$DTPAGlu-$(C18)_2$L5CCK8- water

Once optimized the design of the chelating agent unimer; we then have carried out several attempts to optimize the design of the CCK8 unimer, varying the length of the spacer situated between the double tail and the CCK8. In fact, the spacer should be long enough to assure an efficient exposure of the peptide on the surface of the aggregates, as above mentioned, and in the meanwhile short enough to favor vesicles formation. Our study has been dealt with two unimers (see figure 3.1), one where the spacer consisted of 5 units of 8–amino-3,6-dioxaoctanoic acid ($(C18)_2$L5CCK8), and the other one where the spacer was a poly(ethylene glycol) chain with an average molecular weight 2000 ($(C18)_2$PEG2000CCK8).

In figure 4.7 a we have reported the time correlation function of scattered intensity $g^{(2)}(t)$-1 for both systems. The correlation function translates to longer decay time as the length of the spacer diminishes, indicating a growth in the size of the aggregates. In particular DLS measurements (figure 4.7 b) have shown for the $(C18)_2$DTPAGlu-$(C18)_2$PEG2000CCK8 system a monomodal distribution corresponding to diffusion process of a complex with $D = (1.7 \pm 0.1) \times 10^{-12}$ m^2s^{-1}; whereas for the $(C18)_2$DTPAGlu-$(C18)_2$L5CCK8 system the distribution was bimodal, indicating the presence of two aggregates with $D_{fast} = (30.9 \pm 0.9) \times 10^{-12}$ m^2s^{-1} and $D_{slow} = (2.9 \pm 0.2) \times 10^{-12}$ m^2s^{-1}, respectively (see table 5). The dimension of the PEG coil is decisive in establishing the kind of aggregate, but also in assuring an efficient exposure of the peptide beyond the surface of the aggregate (see figure 4.9). Structural data obtained by SANS

measurements are reported in table 6 and they have been used to estimate the percentage of covered surface by the PEG coil, that for $(C18)_2$DTPAGlu-$(C18)_2$L5CCK8 is ~ 20%, while for $(C18)_2$DTPAGlu-$(C18)_2$PEG2000CCK8 is ~ 50%. A value of covered surface too high could reveal unfavorable for medical purposes, since it could prevent the contact between the peptide and the membrane receptors. Thus, our attention has been focused on $(C18)_2$DTPAGlu-$(C18)_2$L5CCK8 system. The relaxation time distribution for this system shows a similar profile to the corresponding binary system, but with respect to this latter in mixed aggregates the presence of the peptide unimer favors the formation of bilayer structures. As indicated by the magnitude of the relaxation time distribution, that in the same condition (total concentration, pH) appear sensibly larger than that found for the pure $(C18)_2$DTPAGlu binary system. The presence of uncharghed peptide unimer that interposes between the charged headgroups of the chelating agent unimer decreasing the strong headgroup-headgroup electrostatic repulsions supports the formation of larger aggregates with a lower radius of curvature. SANS results have shown the extension of the q^{-2} increases as the amount of $(C18)_2$L5CCK8 in the aggregates raises.

FIGURES

a

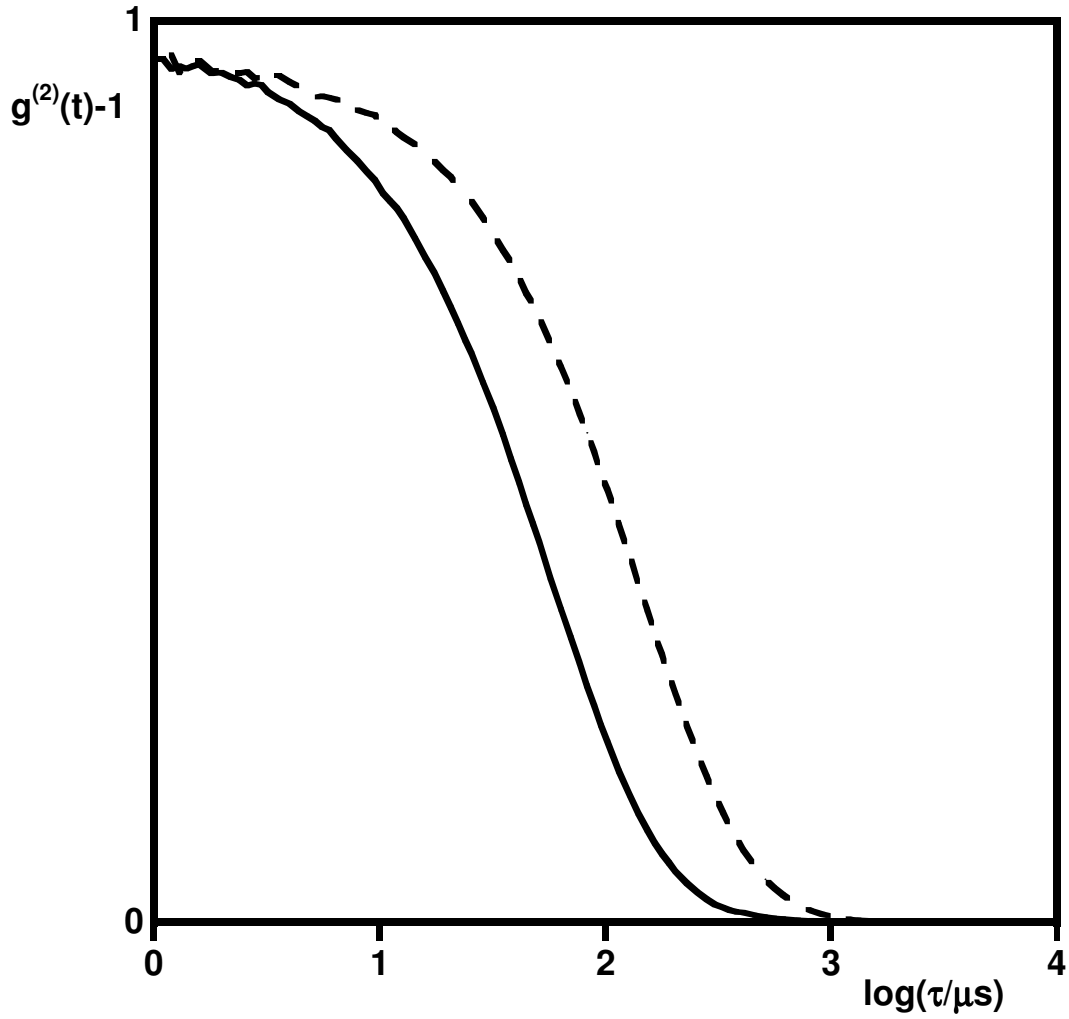

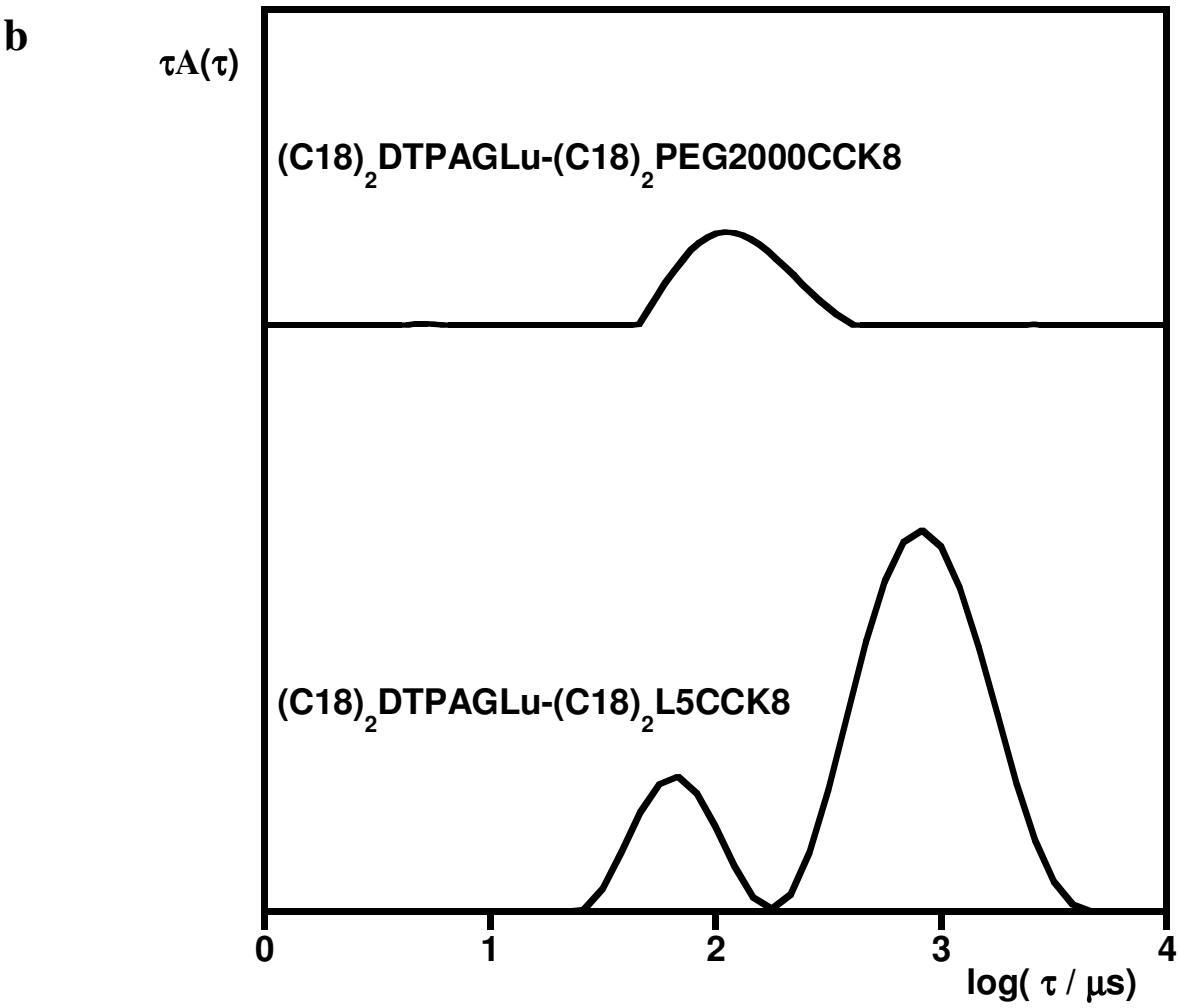

Figure 4.7: Intensity correlation functions at θ = 90° for 1mM $(C18)_2$DTPAGlu-$(C18)_2$PEG2000CCK8 (solid line) and $(C18)_2$DTPAGlu-$(C18)_2$L5CCK8 (dashed line) aqueous solutions; (b) Relaxation time distribution θ = 90° obtained from regularized inverse Laplace transformation of the intensity correlation function for $(C18)_2$DTPAGlu-$(C18)_2$L5CCK8 and $(C18)_2$DTPAGlu-$(C18)_2$PEG2000CCK8 aqueous solutions.

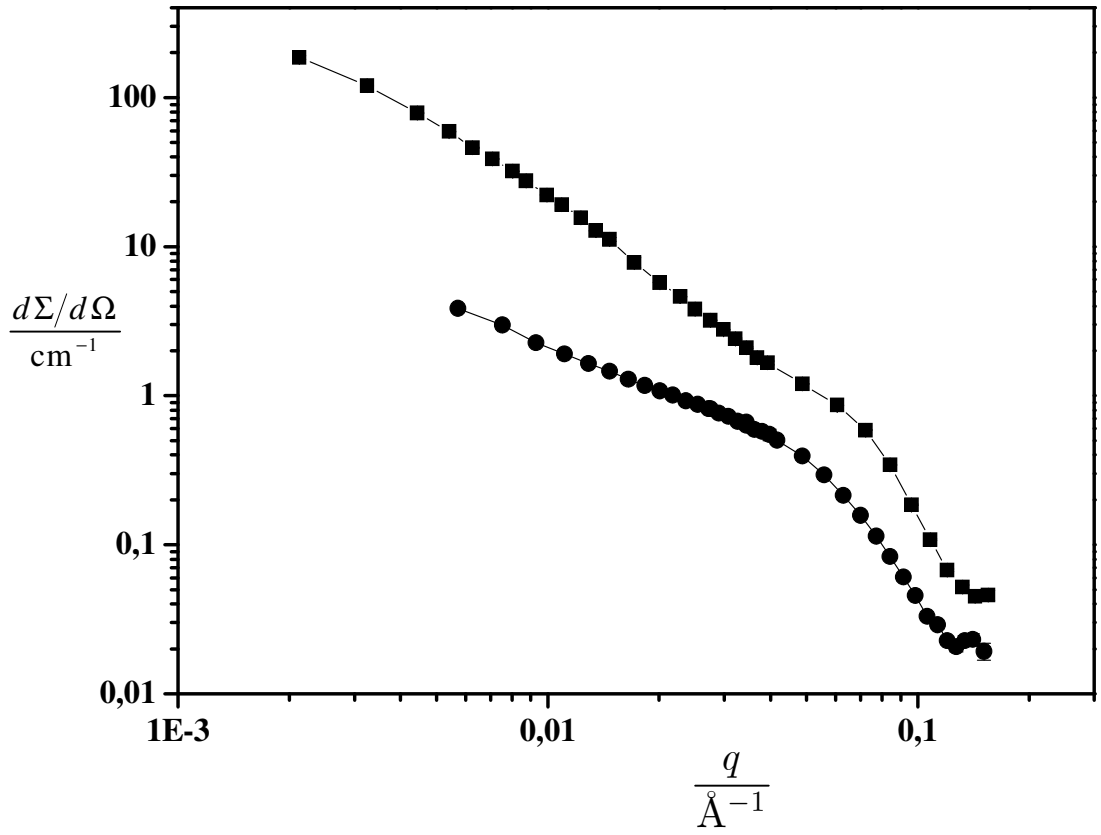

Figure 4.8: Scattering intensity profile for the following systems: $(C18)_2$DTPAGlu-$(C18)_2$PEG2000CCK8-D_2O (●),$(C18)_2$DTPAGlu-$(C18)_2$L5CCK8-D_2O (■). (–) Fitting curve to the experimental data through the model reported in the appendix.

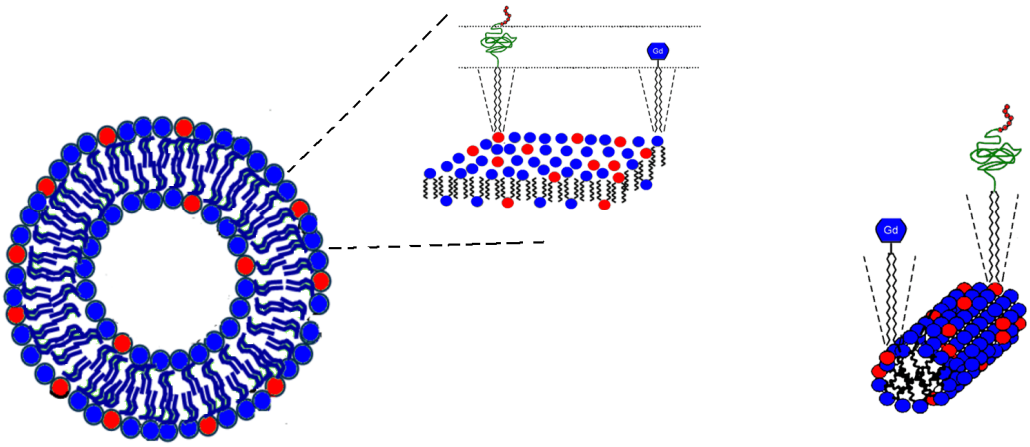

Figure 4.9: Schematic picture of the aggregates formed by our molecules according to SANS measurements.

TABLES

Table 5. Diffusion coefficients and hydrodynamic radii obtained from DLS measurements for the systems studied at different pH values. The terms fast and slow refer to micelles and bilayer structures respectively.

Systems	pH	$D_{fast} \times 10^{12}$ ($m^2 s^{-1}$)	R_H (Å)	$D_{slow} \times 10^{12}$ ($m^2 s^{-1}$)	R_H (Å)
$(C18)_2$DTPAGlu (0.00030 mol kg^{-1}) - $(C18)_2$L5CCK8 (0.00012 mol kg^{-1})-water	7.4	30.9±0.9	64±2	2.9±0.2	690±40
$(C18)_2$DTPAGlu (0.00032 mol kg^{-1}) - $(C18)_2$PEG2000CCK8 (0.00015 mol kg^{-1})-	7.4			1.7±0.1	125±25

Table 6. Structural parameters of the aggregates at different pH values determined by Small-Angle Neutron Scattering (SANS). The terms N_{agg}, R and l refer to the aggregation number, the radius and the height of the micelles respectively, whereas d refers to the thickness of the bilayer structures.

Systems	pH	N_{agg}	R (Å)	l (Å)	d (Å)
$(C18)_2$DTPAGlu (0.00030 mol kg^{-1})– $(C18)_2$L5CCK8 (0.00012 mol kg^{-1})-water	7.4	310±60	36±7	262±32	68±9
$(C18)_2$DTPAGlu (0.00032 mol kg^{-1}) - $(C18)_2$PEG2000CCK8 (0.00015 mol kg^{-1})-water	7.4	120±10	32±4	200±20	

4.4 Ternary system: $(C18)_2$DTPAGlu(Gd)-$(C18)_2$L5CCK8- water

The complexation of DTPAGlu with the paramagnetic Gd^{3+} ion decreases strongly the actual charge of the headgroup of the surfactant, and consequently also the high electrostatic repulsions between the different headgroups; favoring in turn the formation of vesicular aggregates. This is observed from the DLS results, where the relaxation time distribution was bimodal, as in the gadolinium free case, but was clearly dominated by the slow mode (see figure 4.10). The apparent translational diffusion coefficients obtained for the fast and slow modes were D_{fast} = (33.2 ± 0.2) × 10^{-12} m^2s^{-1} and D_{slow} = (2.5 ± 0.3) × 10^{-12} m^2s^{-1}, with corresponding R_H values of 61 ± 4 and 810 ± 110 Å (see table 7). These results are in agreement with the SANS results, where a scattering profile with a power law of q^{-2} spans over a larger q range, as shown in figure 4.11. The thickness of the lamellar aggregate containing gadolinium ion decreases from (68±9) to (53±8) Å, as shown in table 8. This suggests a better packing of the molecules in the double layer due the decrease of the electrostatic repulsions.

The aggregation behavior for $(C18)_2$DTPAGlu(Gd)-$(C18)_2$L5CCK8 ternary system has also been studied as pH function, as shown in figures 4.9 and 4.10. The pH values selected for this study were pH 7.4, that corresponds to physiological pH condition; pH 4.5, because of the pK_a of carboxylic acids; and finally pH 3, since extracellular fluid of tumor cells is acidic. The decrease of pH leads to the formation of larger aggregates, such as the vesicular structures, that are further favored by the presence of the uncharged unimer $(C18)_2$L5CCK8 (figure 4.10). In fact previous investigations

have shown that in the absence of $(C18)_2L5CCK8$, the $(C18)_2$DTPAGlu system (as free base or as Gd^{3+} complex) at pH 4.5 forms either vesicles or micelles; in contrast when the $(C18)_2L5CCK8$ is incorporated in the aggregates the micelles disappear in the system.

Cryo-TEM images have shown at physiological pH the presence of elongated micelles, which appear as fibers, and planar symmetric bilayers. The latter appears as stiff tubular molecular arrangements long about 150 nanometers (figure 4.12 a). The images reveal that these bilayer structures tend to crowd all together forming a sort of texture having an asymmetric geometry. Upon lowering pH, as shown by scattering techniques, the tendency to form bilayer structures increases. At pH 3 the images were characterized by the presence of planar bilayers coexisting with vesicles with a diameter of around 120 nanometers (see figure 4.12 b).

FIGURES

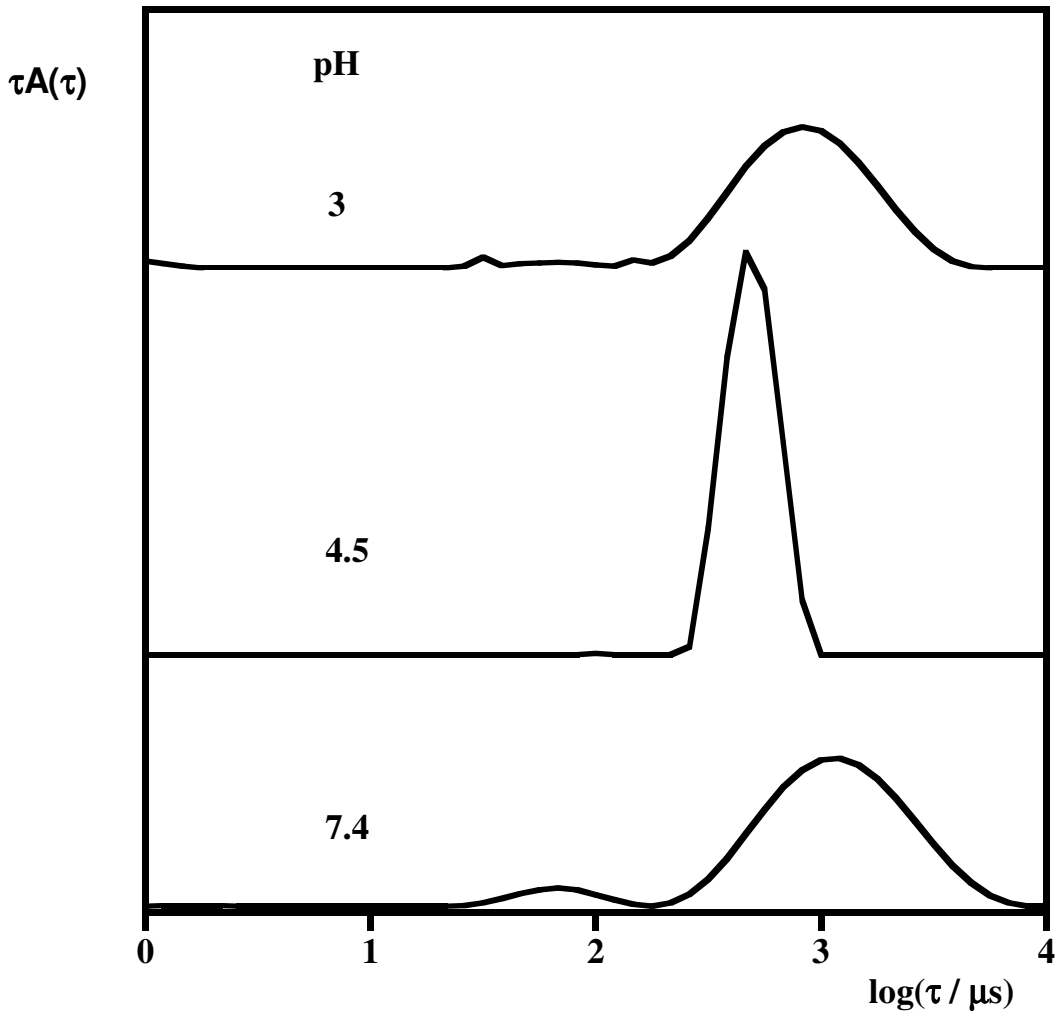

Figure 4.10: Relaxation time distribution θ = 90° obtained from regularized inverse Laplace transformation of the intensity correlation function for $(C18)_2$DTPAGlu(Gd)-$(C18)_2$L5CCK8 as a function of pH.

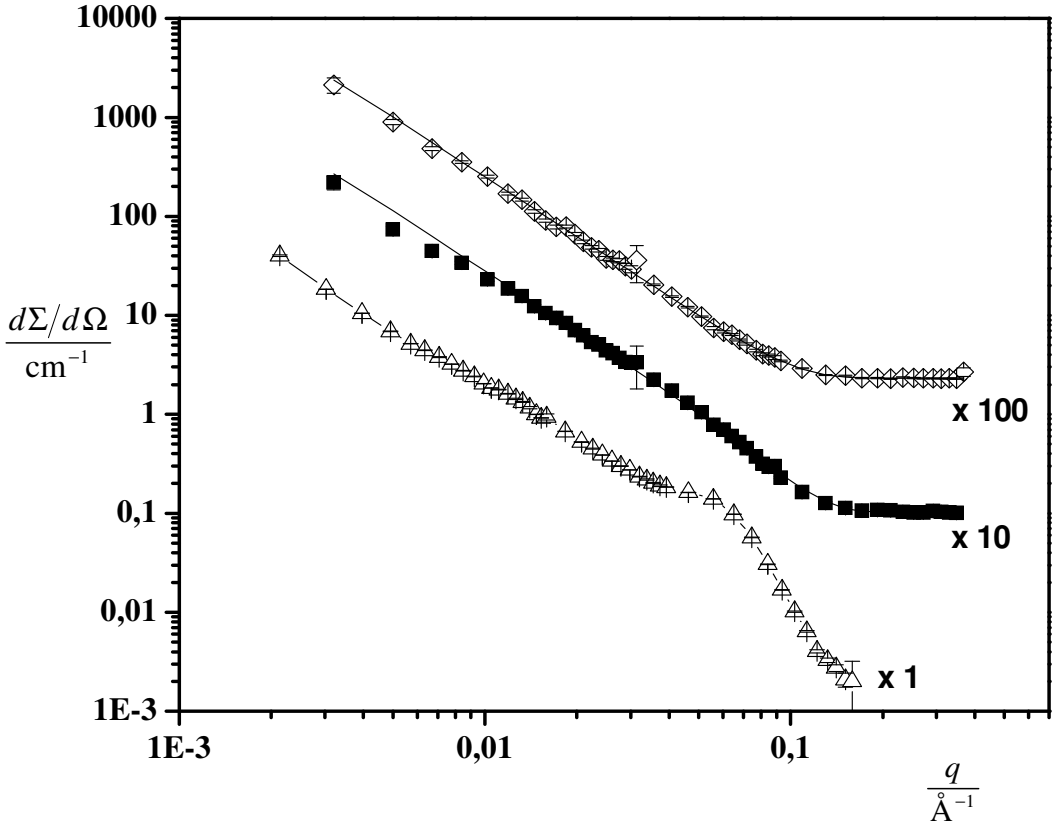

Figure 4.11: Scattering intensity profile for the following systems: $(C18)_2$DTPAGlu(Gd)-$(C18)_2$L5CCK8-D_2O at pH=7.4 (△),$(C18)_2$DTPAGlu(Gd)-$(C18)_2$L5CCK8-D_2O at pH=4.5 (■), $(C18)_2$DTPAGlu(Gd)-$(C18)_2$L5CCK8-D_2O at pH=3 (◇). (–) Fitting curve to the experimental data through the model reported in the appendix. For a better comparison, cross sections have been multiplied for a scale factor.

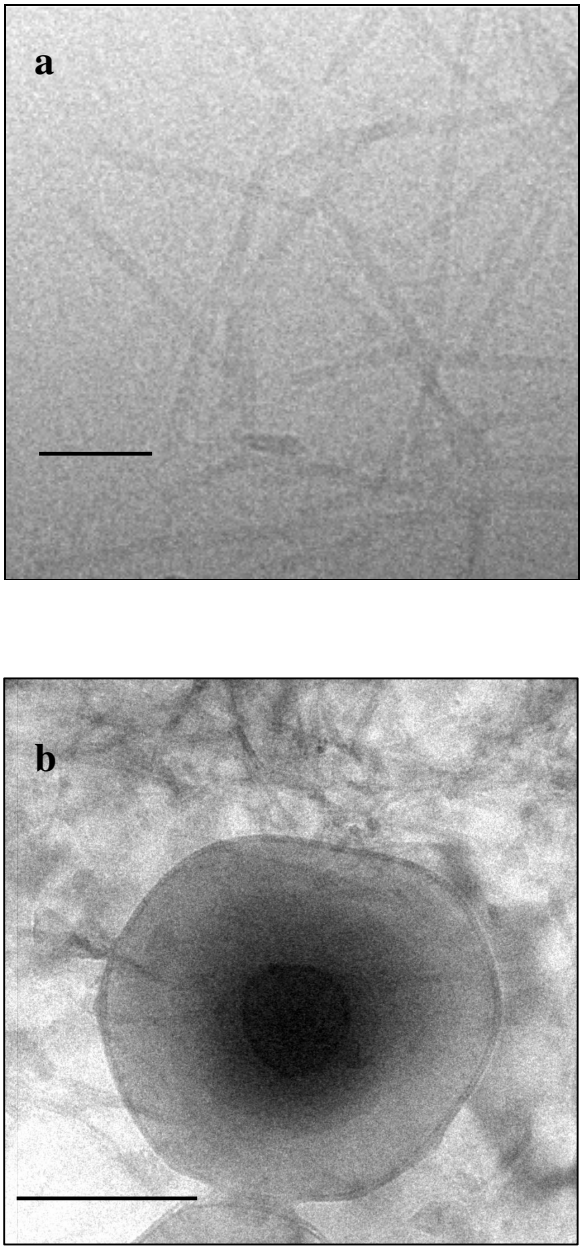

Figure 4.12: Selected cryo-TEM images for $(C18)_2$DTPAGlu(Gd)-$(C18)_2$L5CCK8 at different pH conditions: (a) pH 7.4, sandwiched bilayer structures; (b) pH 3, enlargement of the image of a vesicle. Scale bar = 50 nm.

TABLES

Table 7. Diffusion coefficients and hydrodynamic radii obtained from DLS measurements for the systems studied at different pH values. The terms fast and slow refer to micelles and bilayer structures respectively.

Systems	pH	$D_{fast}\times10^{12}$ (m^2s^{-1})	R_H (Å)	$D_{slow}\times10^{12}$ (m^2s^{-1})	R_H (Å)
$(C18)_2$DTPAGlu(Gd) (0.00030 mol kg^{-1}) - $(C18)_2$L5CCK8 (0.00013 mol kg^{-1})-water	7.4	33.2 ±0.2	61±4	2.5±0.3	810±110
$(C18)_2$DTPAGlu(Gd) (0.00032 mol kg^{-1}) - $(C18)_2$L5CCK8 (0.00015 mol kg^{-1})-water	4.5			4.6±0.3	429±26
$(C18)_2$DTPAGlu(Gd) (0.00032 mol kg^{-1}) - $(C18)_2$L5CCK8 (0.00016 mol kg^{-1})-water	3			2.9±0.2	669±40

Table 8. Structural parameters of the aggregates at different pH values determined by Small-Angle Neutron Scattering (SANS). The terms N_{agg}, R and l refer to the aggregation number, the radius and the height of the micelles respectively, whereas d refers to the thickness of the bilayer structures.

Systems	pH	N*agg*	*R* (Å)	*l* (Å)	*d* (Å)
$(C18)_2$DTPAGlu(Gd) (0.00030 mol kg^{-1}) - $(C18)_2$L5CCK8 (0.00013 mol kg^{-1})-water	7.4	270±40	33±5	269±42	53±8
$(C18)_2$DTPAGlu(Gd) (0.00032 mol kg^{-1}) - $(C18)_2$L5CCK8 (0.00015 mol kg^{-1})-water	4.5				44±6
$(C18)_2$DTPAGlu(Gd) (0.00032 mol kg^{-1}) - $(C18)_2$L5CCK8 (0.00016 mol kg^{-1})-water	3				44±9

4.5 Binary system: MONY-water and Ternary system: DOPC-MONY-water

A further upgrade of the supramolecular system, studied up to now, is represented by the design and synthesis of a molecule containing contemporarily both active principles, and named as MonY.

The relaxation time distribution for the binary system MonY–H_2O (Figure 4.13), obtained by regularized inverse Laplace transformation (RILT) of the correlation function, was bimodal at all angles studied and consisted of a fast and a slow peak. Both peaks corresponded to the translational diffusion process of aggregates, because the relaxation rates had a linear dependence on the square of the magnitude of the scattering vector q. Inspection of Table 9 shows that R_H is (48±1) and (645±20) Å for the fast and slow peaks, respectively.

Thus, the relaxation time distribution of the MonY–H_2O system reveals the presence in solution of small micelles and larger aggregates, probably liposomal structures. The dominant aggregates in solution are micelles, even if the fast and slow peaks have a similar amplitude. In fact, we are considering an intensity-weighted distribution and not a number distribution. This leads to a dominance of the larger objects in the distribution, even if they are fewer in quantity.

SANS measurements confirmed DLS results; in figure 4.14 the scattering cross sections $d\Sigma/d\Omega$ obtained for the binary system MonY–D_2O is represented. Inspection of the data reveals the presence of two different regions: a first region (q>0.01 $Å^{-1}$) where the trend of a typical form factor of spherical or ellipsoidal micelles with weak

or negligible interactions is present; and a second region (q< 0.01 Å^{-1}) where an increasing of the magnitude of $d\Sigma/d\Omega$ holds. In this case, the data scale with a power law $d\Sigma/d\Omega \propto q^{-2}$ that can be ascribed to the scattering of the vesicular surfaces present in the system, induced by the extrusion process. Table 10 reports the parameters obtained from the fitting procedure. From the inspection of the table, it is possible to observe that MonY form oblate ellipsoidal aggregates composed by around 30 unimers per aggregate, and where the ratio between the micellar axes is ~1.7. Structural data of vesicles have not been obtained in this case, since the number of data does not allow performing an accurate analysis.

DLS and SANS measurements were also carried out on the mixed systems DOPC–MonY–H_2O, in order to determine the maximum MonY amount in the lipid bilayer such vesicular structures are not destabilized.

Figure 4.13 displays the structural evolution of the aggregates obtained by assembling DOPC and MonY at different molar ratios. For a mixed sample containing 30% molar ratio of MonY, the distribution was bimodal and dominated by the slow peak; the fast peak (see arrow) had a very small amplitude. The relaxation rates ($\Gamma=\tau^{-1}$) for the fast and slow modes were measured at different q values. The linear relation of the relaxation rates confirms that both modes were due to translational diffusion processes, attributed to two different complexes with apparent translational diffusion coefficients D_{fast} =(3.64±0.06)×10^{-11} m^{2}s^{-1} and D_{slow} =(2.9±0.1)×10^{-12} m^{2}s^{-1}, respectively (see Table 9). The corresponding hydrodynamic radii were (55±9) and (690±20) Å for the fast and slow modes, respectively. Scattering cross sections for

this system confirmed DLS data. They showed a power-law $d\Sigma/d\Omega \propto q^{-1}$, typical of rod–like structures, but for q< 0.009 Å^{-1} the scattering of vesicular bilayers was observed ($d\Sigma/d\Omega \propto q^{-2}$), even if, like for the binary systems, number of data does not allow performing an accurate analysis. Concerning the analysis of rod-like micelles, the missing of the Guinier regime for such systems prevent to have an estimation of the length of these structures, but the q^{-1} regime is enough extended to have a reasonable value of the transversal radius r of rods. We have estimated that the radius value should be (35±1) Å (table 10).

The increasing of the amount of DOPC in the mixed system results in a drastic change of the characteristics of scattering data. In fact, upon decreasing the MonY content (R= 80:20) the relaxation time distribution becomes monomodal, with a well-defined slow peak corresponding to liposomes (see figure 4.13). Concerning SANS data, the scattering cross sections for the systems, where the molar ratio was 80/20 or higher, scaled with a power law q^{-2} characteristic of scattering of planar sheets. DOPC molecules, as already known, form vesicular aggregates that retain their shape and characteristics until the MonY amount is smaller than 20% of the total concentration. In any case, a difference in absolute units of $d\Sigma/d\Omega$ occurs among the DOPC/D_2O systems and the ternary samples where the power law $d\Sigma/d\Omega \propto q^{-2}$ holds. This leads us to conclude that vesicles should be mixed aggregates formed by DOPC and MonY.

Cryo-TEM images confirmed scattering data. Figure 4.15 displays that the sample DOPC–MonY 80/20 was full of liposomes with a diameter ranging between 50 and 150 nm.

FIGURES

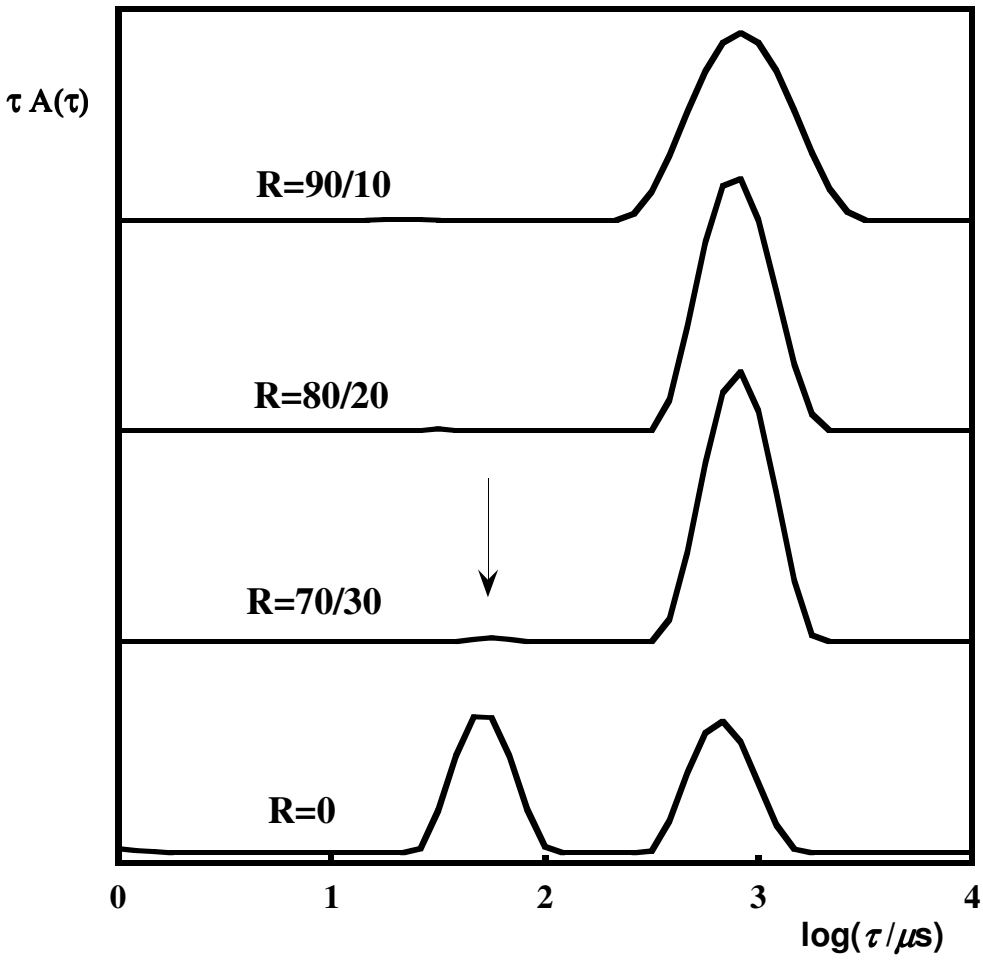

Figure 4.13: Relaxation time distributions at θ=90° for DOPC–MonY–H_2O ternary systems at different molar ratios (R=0, 70:30, 80:20, 90:10).

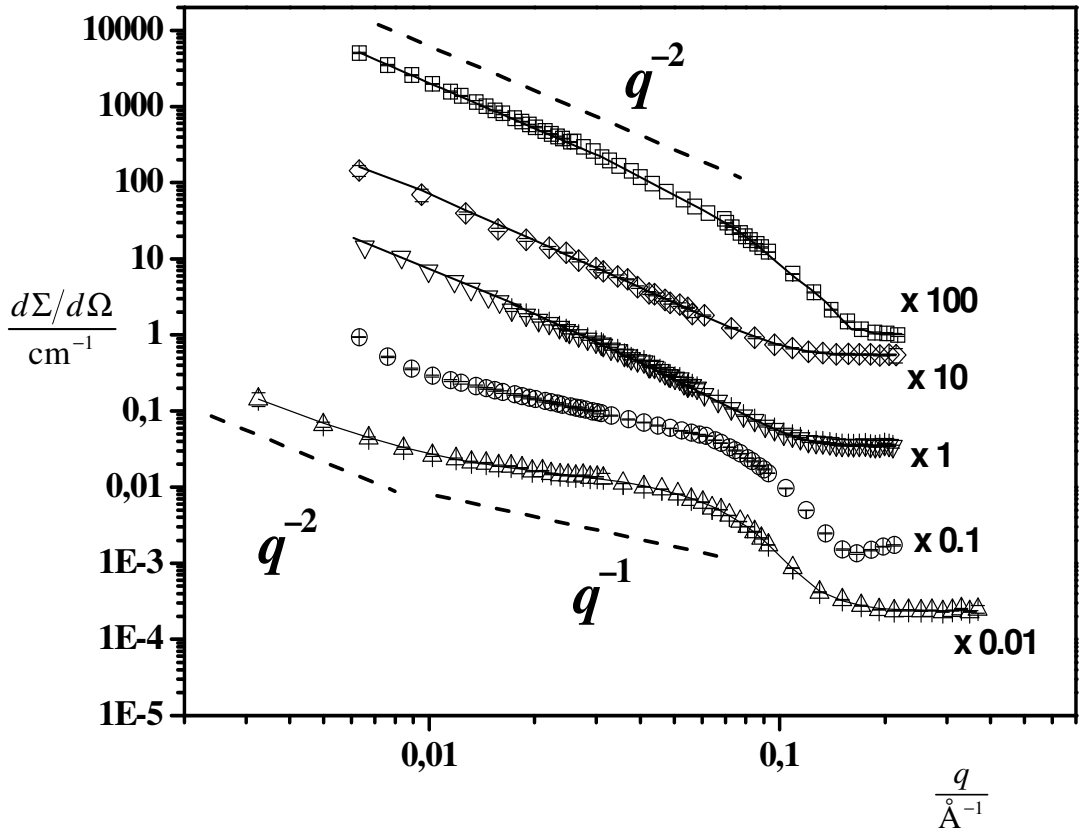

Figure 4.14: Scattering cross sections obtained at 25 °C for the following systems: (△) MONY- D_2O (c=2.1×10^{-3} mol kg^{-1}), (○) DOPC–MonY–D_2O (c=2.1×10^{-3} mol kg^{-1}, R=70:30); (▽) DOPC–MonY–D_2O (c=1.9×10^{-3} mol kg^{-1}, R=80:20); (◇) DOPC–MonY–D_2O (c=1.7×10^{-3} mol kg^{-1}, R=90:10); (□) DOPC-D_2O (c=2.5×10^{-3} mol kg^{-1}). Curves fitted to the experimental data through an appropriate model are also reported. For a better comparison, cross sections have been multiplied for a scale factor.

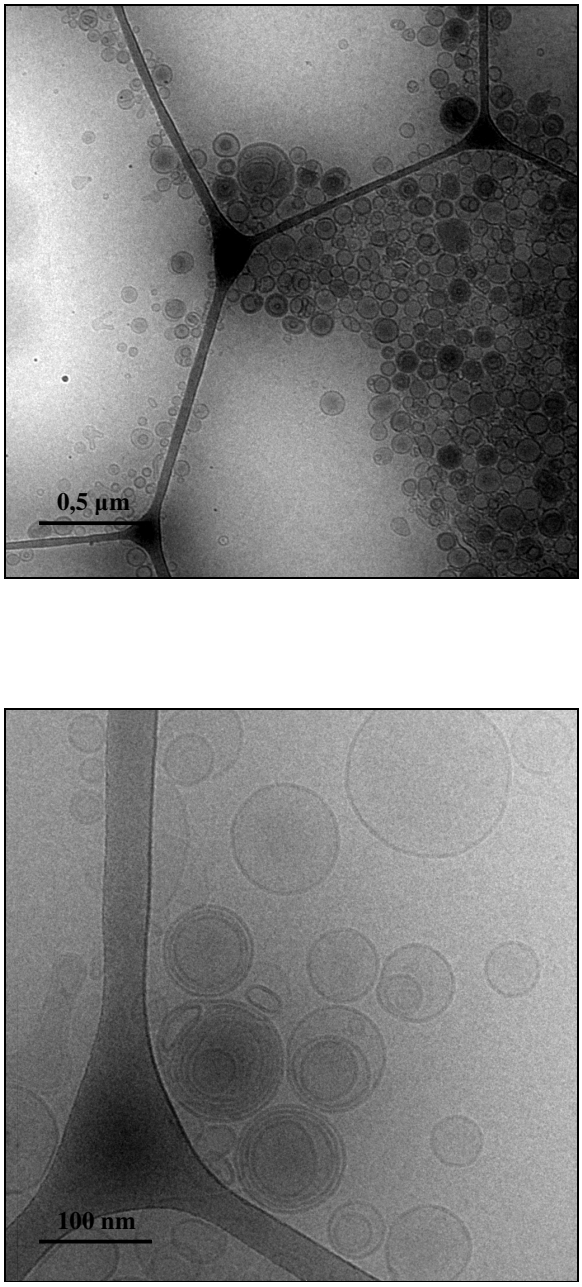

Figure 4.15: Selected cryo-TEM image for mixed system DOPC–MonY-water (R=80:20)

TABLES

Table 9. Diffusion coefficients and hydrodynamic radii obtained from DLS measurements for the systems studied at different molar ratios phospholipid/unimer. The terms fast and slow refer to micelles and bilayer structures, respectively.

Systems	*R*	$D_{fast} \times 10^{12}$ ($m^2 s^{-1}$)	R_H (Å)	$D_{slow} \times 10^{12}$ ($m^2 s^{-1}$)	R_H (Å)
MONY(0.00476mol kg^{-1}) - water	0	41.4 ±0.1	48±1	3.1±01	645±20
DOPC (0.00150 mol kg^{-1}) – MONY(0.00064 mol kg^{-1})-water	70/30	36.4±0.6	55±9	2.9±0.1	690±20
DOPC(0.00154 mol kg^{-1}) – MONY (0.00039 mol kg^{-1})-water	80/20			2.8±0.1	700±20
DOPC (0.00032 mol kg^{-1}) – MONY(0.00024 mol kg^{-1})-water	90/10			2.9±0.1	690±20

Table 10. Fitting parameters obtained from SANS data at 25°C for the systems MonY–D_2O DOPC–MonY–D_2O and DOPC- D_2O through the equations reported in the text. The table displays the concentrations of the two solutes, the ratio $R = {c_{DOPC}}/{c_{MONY}}$, the radius of cylinders r the three main semiaxis of the micellar hydrophobic core (a, b and c), the thickness of the micellar hydrophilic shell δ and the micellar aggregation number N_{agg}. Finally, for the vesicular aggregates, the double layer thickness τ is reported.

$\frac{c_{DOPC}}{\text{mmol kg}^{-1}}$	$\frac{c_{MonY}}{\text{mmol kg}^{-1}}$	R	$\frac{r}{\text{Å}}$	$\frac{a}{\text{Å}}$	$\frac{b}{\text{Å}} = \frac{c}{\text{Å}}$	$\frac{\delta}{\text{Å}}$	N_{agg}	$\frac{R_g}{\text{Å}}$	$\frac{R_g^{GUIN}}{\text{Å}}$	$\frac{\tau}{\text{Å}}$
0	4.76	0		9 ± 1	27 ± 1	15 ± 1	32 ± 1	29 ± 2	28 ± 1	–
0	1.20	0		10± 1	27 ± 1	16 ± 1	34 ± 1	30 ± 2	29 ± 2	–
1.50	0.64	70/30	35 ± 1							
1.50	0.39	80/20		–	–	–	–	–	–	38 ± 1
1.54	0.24	90/10		–	–	–	–	–	–	37 ± 2
2.54	0	∞		–	–	–	–	–	–	36 ± 1

4.6 Binary system: MONY(Gd)-water and Ternary system: DOPC-MONY(Gd)- water

MonY(Gd) containing systems were also studied. For the binary system MonY(Gd)–H_2O the relaxation time distribution was bimodal and dominated clearly by the large-amplitude fast peak (see figure 4.16). Both peaks were found to have a linear dependence with respect to q^2. The diffusion coefficients were D_{fast}=(4.15±0.03)×10^{-11} and D_{slow}=(3.4±0.3)× 10^{-12} m^2s^{-1}, and the hydrodynamic radii were (48±1) and (580±50) Å for the fast and the slow modes, respectively (Table 11). These values are similar to those corresponding to the Gd-free case; this indicates that the gadolinium complex does not modify significantly the kind and size of aggregates in solution. This observation is in agreement with SANS data, the structural data collected are similar to those of MONY-D_2O binary system, as reported in table 12. The inspection of the scattering cross section reveals, also in this case, the presence of two different regions: one at high q values where a power law $d\Sigma/d\Omega \propto q^{-1}$ typical of rod like structures holds, and an other region at low q where the power law $d\Sigma/d\Omega \propto q^{-2}$ holds due to the presence of bilayer structures.

Measurements were also carried out in mixed systems DOPC–MonY(Gd) to optimize the MonY(Gd) content in the lipid bilayer, and to find hence, as in the previous case, the right molar ratio between the two molecules where liposomes are the favored structures. At R=70:30 the relaxation time distribution was bimodal, as shown in figure 4.16. The diffusion coefficients obtained from the moments of the distribution

were D_{fast} =(2.90±0.09)×10^{-11} and D_{slow} = (2.7±0.1)×10^{-12} m^{2}s^{-1}, and these values can be attributed to micellar and bilayer structures diffusing in solution. As for gadolinium uncomplexed systems, at R=80:20 the distribution appeared monomodal. This finding suggests that at this ratio the presence of MonY(Gd) did not destabilize the lipid bilayer, in fact when the ratio $R = c_{DOPC}/c_{MONY(Gd)}$ is high enough (80:20) mixed vesicular structures formed by DOPC and MonY(Gd) molecules are present in solution. The values of the double-layer thickness τ, extracted by SANS measurements and reported in table 12, showed values 35÷40 Å, that are comparable with those found for the ternary systems containing MonY in its uncomplexed form (≈ 37 Å). The radii of the vesicles measured by cryo-TEM (figure 4.18), analogously, ranged between 50-150 nm, as in the previous case.

Indeed, liposome destabilization occurs when the volume fraction of MonY in the liposome bilayer reaches a value of ≈50%. This value has been calculated using the thickness of the bilayer, as obtained by SANS data, and the radius measured by cryo-TEM.

FIGURES

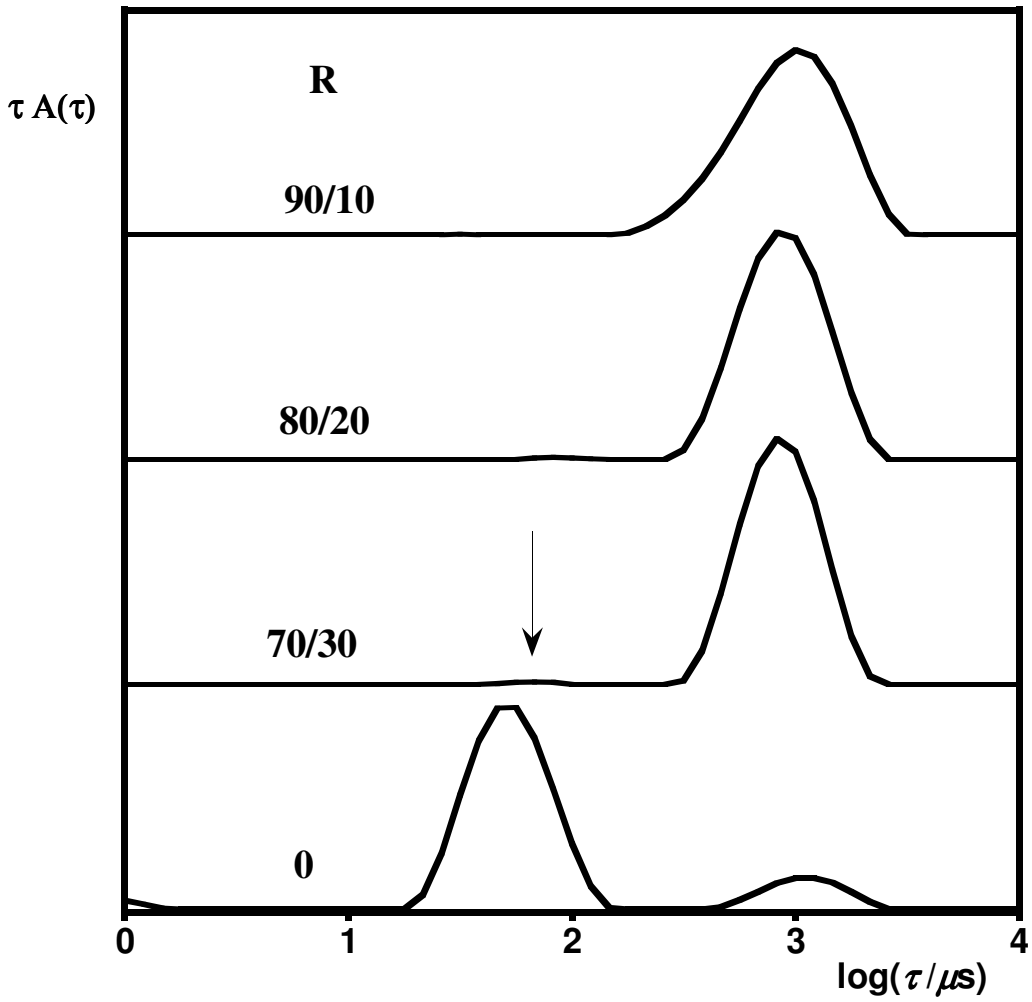

Figure 4.16: Relaxation time distributions at θ=90° for DOPC–MonY(Gd)–H_2O ternary systems at different molar ratios (R=0, 70:30, 80:20, 90:10). The arrow indicates the fast peak.

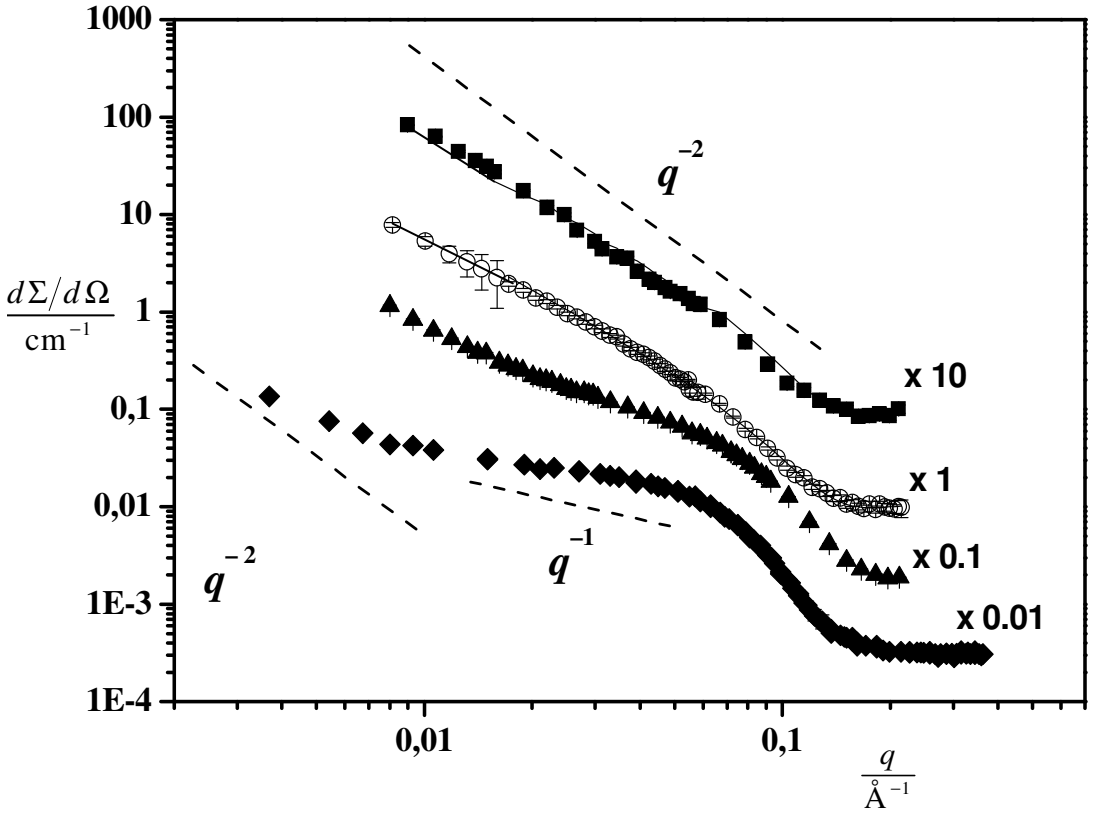

Figure 4.17: Scattering cross sections obtained at 25 °C for the following systems: (◆) MONY(Gd)-D_2O (c=3.0×10^{-3} mol kg^{-1}), (▲) DOPC–MonY(Gd)–D_2O (c=1.8×10^{-3} mol kg^{-1}, R=70:30); (○) DOPC–MonY(Gd)–D_2O (c=1.7 ×10^{-3} mol kg^{-1}, R=80:20); (■) DOPC–MonY(Gd)–D_2O (c=1.7×10^{-3} mol kg^{-1}, R=90:10). Curves fitted to the experimental data through an appropriate model are also reported. For a better comparison, cross sections have been multiplied for a scale factor.

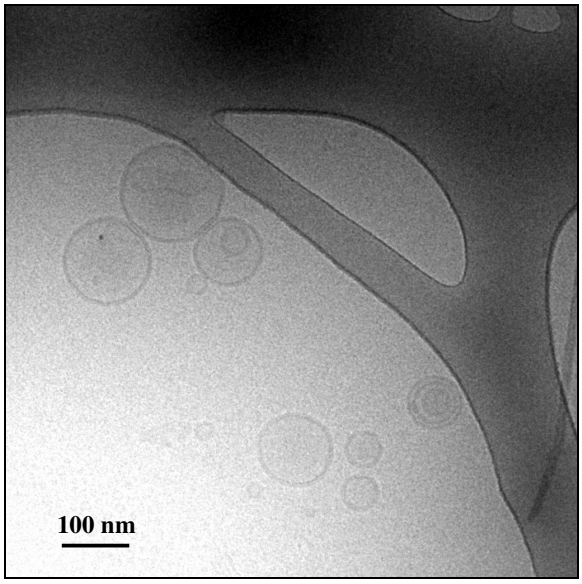

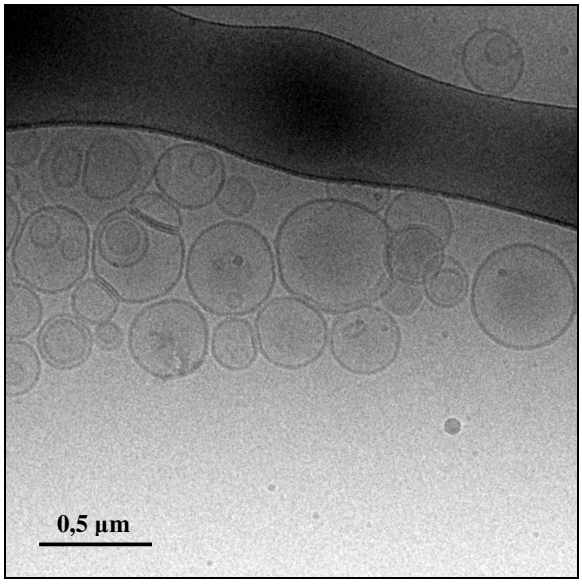

Figure 4.18: Selected cryo-TEM image for mixed system DOPC–MonY(Gd)-water (R= 80:20)

TABLES

Table 11. Diffusion coefficients and hydrodynamic radii obtained from DLS measurements for the systems studied at different molar ratios phospholipid/unimer. The terms fast and slow refer to micelles and bilayer structures, respectively.

Systems	*R*	$D_{fas}\times10^{12}$ (m^2s^{-1})	R_H (Å)	$D_{slow}\times10^{12}$ (m^2s^{-1})	R_H (Å)
MONY(Gd)(0.0016 mol kg^{-1}) - water	0	41.5 ±0.1	48±1	3.4±03	580±50
DOPC (0.00137 mol kg^{-1}) – MONY(Gd)(0.00048 mol kg^{-1})-water	70/30	29.0±0.1	70±2	2.7±0.1	730±30
DOPC(0.00139 mol kg^{-1}) – MONY(Gd) (0.00027 mol kg^{-1})-water	80/20			2.6±0.1	750±30
DOPC (0.00134 mol kg^{-1}) – MONY(Gd)(0.00014 mol kg^{-1})-water	90/10			2.7±0.1	735±30

Table 12. Fitting parameters obtained from SANS data at 25°C for the systems MonY(Gd)–D_2O and DOPC–MonY(Gd)–D_2O through the equations reported in the text. The table displays the concentrations of the two solutes, the ratio $R = {c_{DOPC}}/{c_{MONY(Gd)}}$, the radius of cylinders r the three main semiaxis of the micellar hydrophobic core (a, b and c), the thickness of the micellar hydrophilic shell δ and the micellar aggregation number N_{agg}. Finally, for the vesicular aggregates, the double layer thickness τ is reported.

$\frac{c_{DOPC}}{\text{mmol kg}^{-1}}$	$\frac{c_{MonY(Gd)}}{\text{mmol kg}^{-1}}$	R	$\frac{r}{\text{Å}}$	$\frac{a}{\text{Å}}$	$\frac{b}{\text{Å}} = \frac{c}{\text{Å}}$	$\frac{\delta}{\text{Å}}$	N_{agg}	$\frac{R_g}{\text{Å}}$	$\frac{R_g^{GUIN}}{\text{Å}}$	$\frac{\tau}{\text{Å}}$
0	1.60	0		10 ± 1	27 ± 1	16 ± 1	36 ± 1	30 ± 2	29 ± 1	–
0	3.00	0		10 ± 1	27± 1	16 ± 1	35 ± 1	30 ± 2	29± 1	–
1.37	0.48	70/30	34 ± 1							
1.39	0.27	80/20		–	–	–	–	–	–	35± 1
1.34	0.14	90/10		–	–	–	–	–	–	39 ± 2

4.7 Pseudo-Binary system: DOPURu-water

DOPURu vesicles were characterized by means of different techniques: dynamic light scattering (DLS), electron paramagnetic resonance (EPR), small-angle neutron scattering (SANS), and cryo-transmission electron microscopy (cryo-TEM).

For DOPURu-water pseudo-binary system, the relaxation time distribution, obtained by regularized inverse Laplace transformation of the correlation function, was monomodal and consisted of a well-defined peak (see figure 4.19). The diffusion coefficient D was estimated from the slope of the relaxation rate Γ, which is obtained from the first moment of the translational mode, as function of q^2. The value obtained was $D = (3.1\pm0.2)\times10^{-12}$ m^2s^{-1}, whereas the value of the apparent hydrodynamic radius, R_H, evaluated using the Stokes-Einstein equation, was (700±50) Å (see table 13). This suggests that the molecule of new synthesis assemblies in aqueous solution forming aggregates larger than micelles, whose size is comparable to that of vesicles.

EPR spectrum for DOPURu-water pseudo-binary system was indicative of the presence of bilayer structures (see Figure 4.20). DOPURu-water dispersions were EPR silent, indicating the formation of aggregates in which the closeness between metal ions promotes strong spin exchange phenomena. In these conditions, the DOPURu structuring in the system can be investigated by using a proper spin-probe. EPR spectrum for phosphatidyl-choline spin-labeled on the 5-C atom of the sn-2 chain (5-PCSL), inserted in DOPURu membranes (1:100 5-PCSL/DOPURu molar ratio), was indicative of the presence of bilayer structures. The outer hyperfine

splitting, $2A_{max}$, measured as the difference between the low-field maximum and the high-field minimum (59.81±0.15) G was significantly higher than that observed for typical phospolipids (52.47±0.03) G, such as for DOPC (1,2-Dioleoyl-sn-Glycero-3-Phosphocholine) and DOPE (1,2-Dioleoyl-sn-Glycero-3-Phosphoethanolamine). This suggests that the spin-labeled chains in DOPURu were lodged in a more rigid bilayer membrane with respect those lodged in DOPC and DOPE bilayer.

SANS investigation confirmed the presence of vesicles in solution. The scattering cross section $d\Sigma/d\Omega$ showed, at low q range, a power law $q^{-\alpha}$ ranging as $2<\alpha<4$ (see figure 4.21). This is typical of multilamellar vesicles, as also proved by cryo-TEM images, see figure 4.22, where unilamellar vesicles coexist with multilamellar ones.

Thus, the SANS data were fitted through a model that accounted for the coexistence in the system of unilamellar and multilamellar vesicles. The structural parameters extracted from the SANS fitting procedure revealed that bilayer of the vesicles had a thickness, τ, of (35±3) Å. In particular the multilamellar ones showed an average number of lamellae, M, ≈ 3, while the average spacing, *d*, between the centers of two lamellae was about (50±1) Å.

Cryo-TEM micrographs, shown in figure 4.22, were in agreement with EPR and scattering techniques results. The images showed the presence of vesicles of various types, unilamellar and multilamellar, with a radius of about 600-700 Å.

Figure 4.23 represents a cartoon of how the system formulated should work.

FIGURES

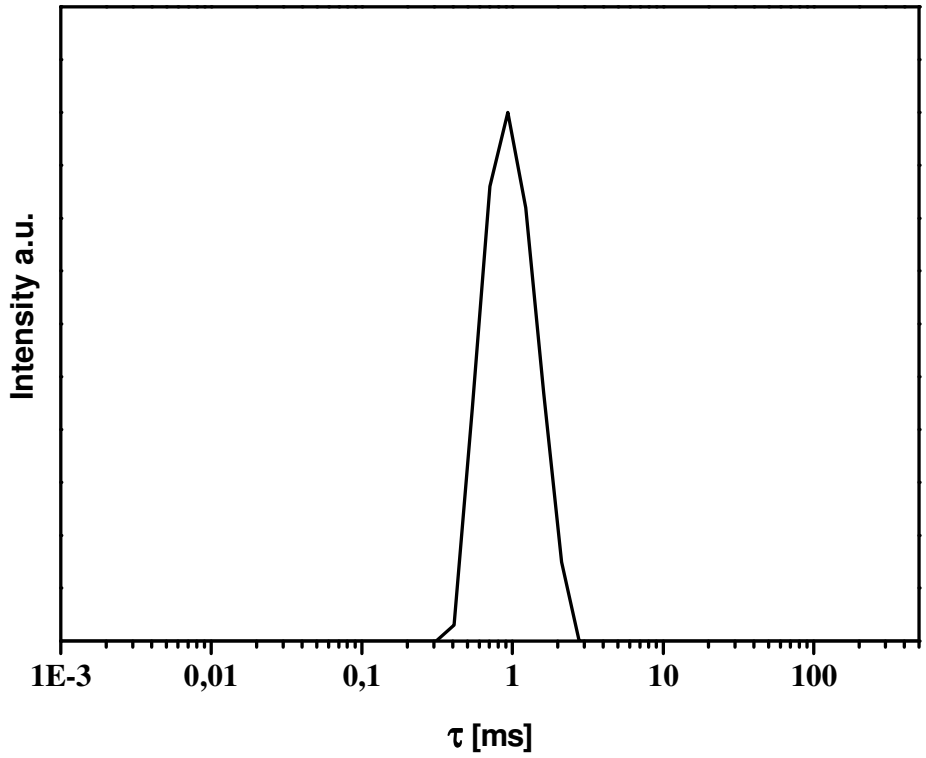

Figure 4.19: Relaxation time distributions at θ=90° for DOPURu-water pseudo-binary system.

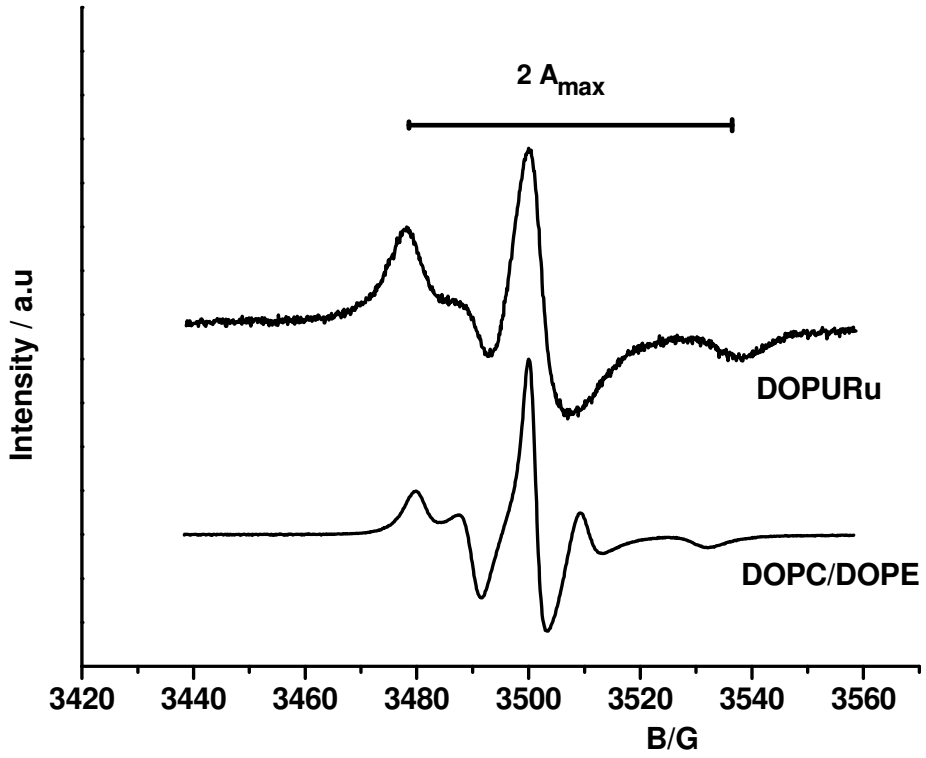

Figure 4.20: EPR spectra obtained at 25°C for 5-PCSL inserted in DOPURu and DOPC-DOPE membranes, respectively.

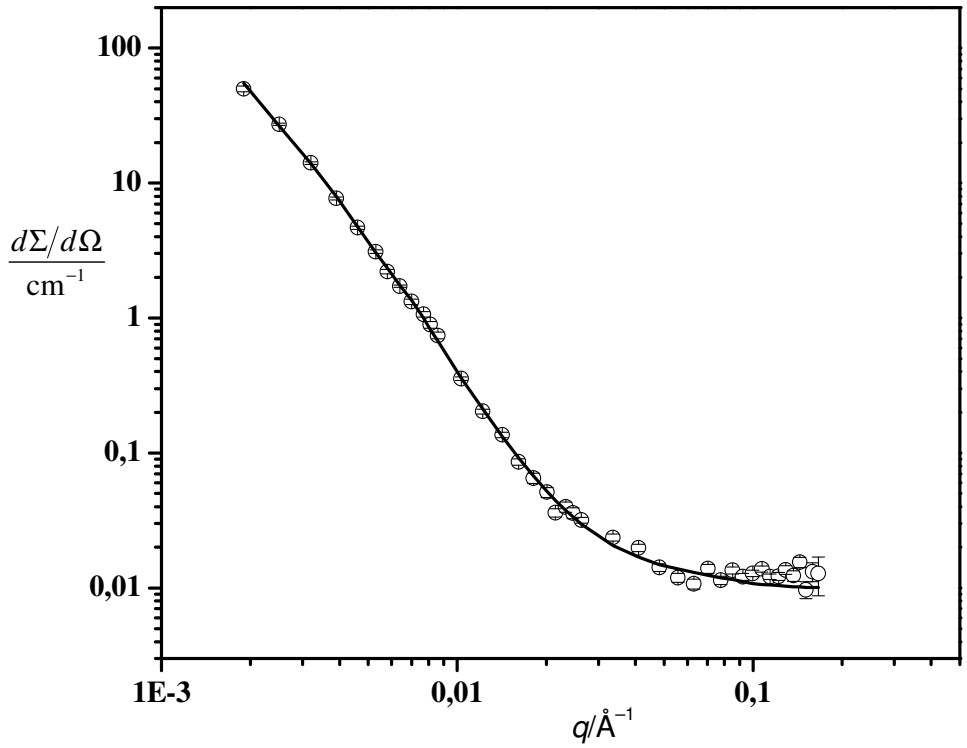

Figure 4.21: Scattering cross sections obtained at 25 ºC for DOPURu-water pseudo-binary system together with the curve obtained from the fitting model.

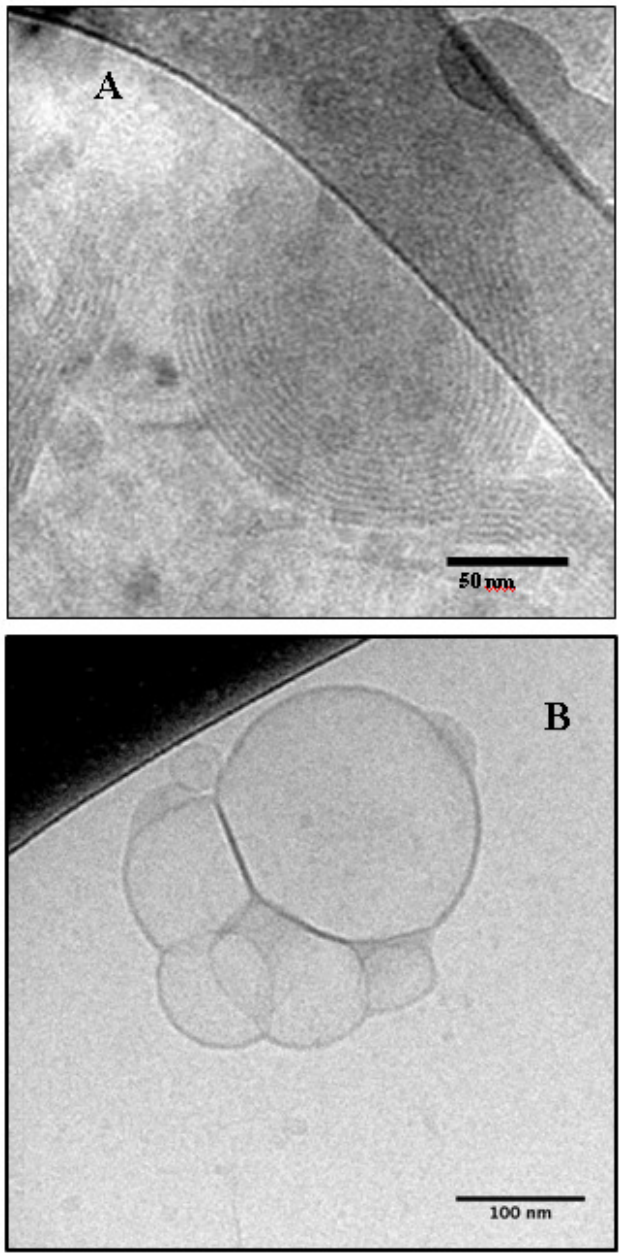

Figure 4.22: Cryo-TEM images showing (A) oligolamellar and (B) unilamellar vesicles. (Globular stains in figure 4A are artifacts).

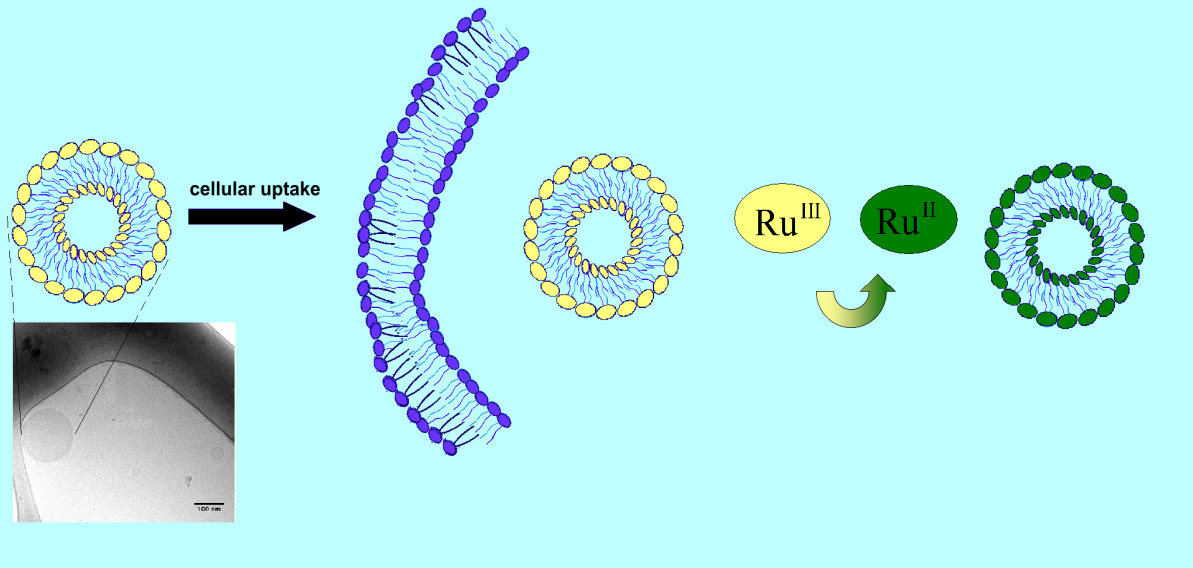

Figure 4.23: Schematic representation of the system should work.

4.8 Pseudo-Quaternary system: (DOPC-DOPE)-DOPURu-water

The amphiphilic molecule coordinating the Ruthenium, DOPURu, has been lodged in mixed liposomes of DOPC (1,2-Dioleoyl-*sn*-Glycero-3-Phosphocholine) and DOPE (1,2-Dioleoyl-*sn*-Glycero-3-Phosphoethanolamine), to reduce the commercial cost of the final formulation. PC and PE polar heads are the most abundant in plasma membranes and are known to be compatible with cells.

The aggregation behavior of the (DOPC-DOPE)-DOPURu-water quaternary system has been studied as a function of DOPURu amount by means of different techniques. Figure 4.24 shows the relaxation time distributions collected by DLS. All the analyzed systems were characterized by the presence of one single broaden peak. The R_H of the aggregates ranged from (880±70) to (750±80) Å, and was consistent with the presence of bilayer aggregates, such as vesicles.

SANS measurements confirmed the presence in solution of bilayer aggregates for the quaternary systems at all molar ratios studied (70:30, 60:40 and 50:50). The scattering cross sections $d\Sigma/d\Omega$ showed, at low q range, a power law $q^{-\alpha}$ ranging as $2<\alpha<4$ (see Figure 4.25). In particular, at lower surfactant/phospholipid ratios (60:40 and 50:50) the scattering cross sections appeared different compared to that of DOPC-DOPE pure system. A diffraction peak was visible at intermediate q range, rising probably from intra-lamellar interference, whereas at low q range the slope was ranging between q^{-3} and q^{-4}.

EPR study for the pseudo-quaternary systems, analogously to the binary system, was performed introducing in the bilayer membrane an opportune probe: 5-PCSL. EPR

spectra (see figure 4.26) evidenced that for the quaternary system 70:30 phospholipid/surfactant molar ratio the $2A_{max}$ assumes a value (52.40±0.10) G, and is similar to that registered for the DOPC-DOPE pure system. This suggests that in correspondence of this molar ratio, the DOPC-DOPE bilayer is not significantly perturbed by the presence of DOPURu.

On these bases, cryo-TEM investigation was carried out on the aqueous system (DOPC-DOPE)-DOPURu 70:30. In figure 4.27 are reported selected cryo-TEM images. The images show a rich variety of aggregates: unilamellar vesicles, cubosomes and vesicles with a highly ordered cubic inner structure.

FIGURES

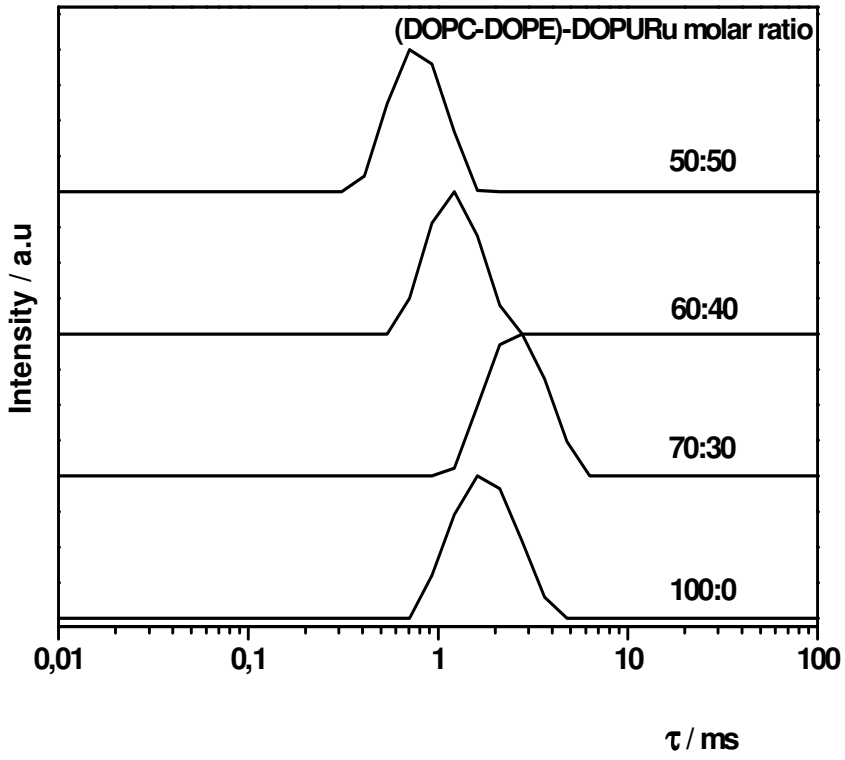

Figure 4.24: Relaxation time distributions for the (DOPC-DOPE)/DOPURu-water quaternary systems at different phospholipid/surfactant molar ratios: 70:30, 60:40, 50:50.

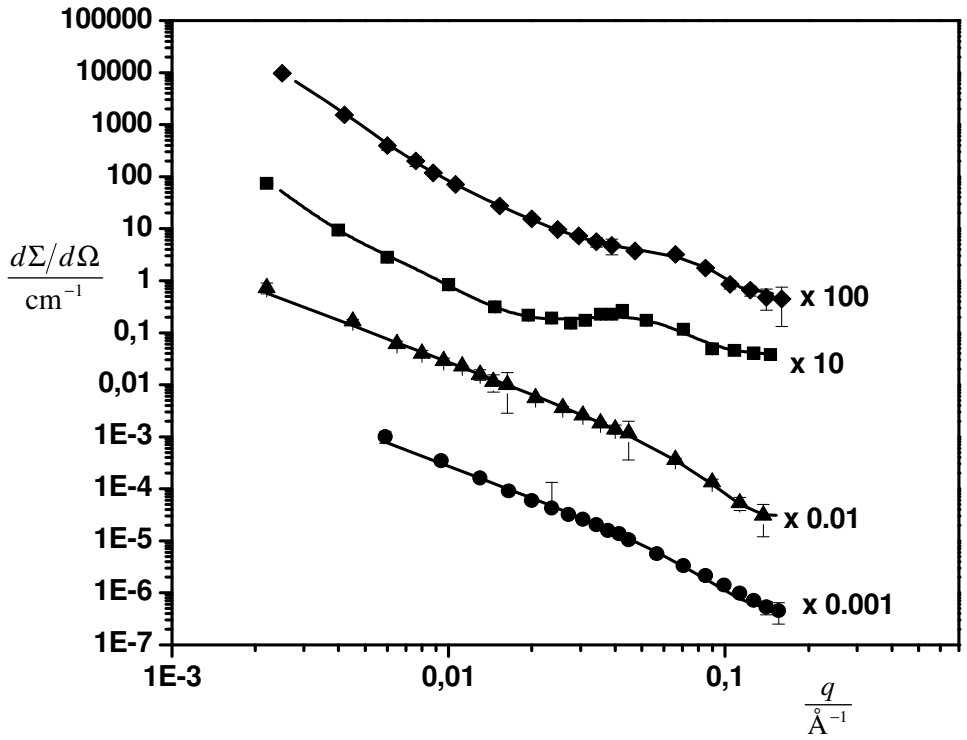

Figure 4.25: Scattering cross sections obtained at 25 ºC for the following systems: (●) DOPC–DOPE–D_2O, (▲) (DOPC–DOPE)–DOPURu–D_2O (R=70:30), (■) (DOPC–DOPE)–DOPURu–D_2O (R=60:40), (◆) (DOPC–DOPE)–DOPURu–D_2O (R=50:50). For a better comparison, cross sections have been multiplied for a scale factor. Lines are a guide for the eye.

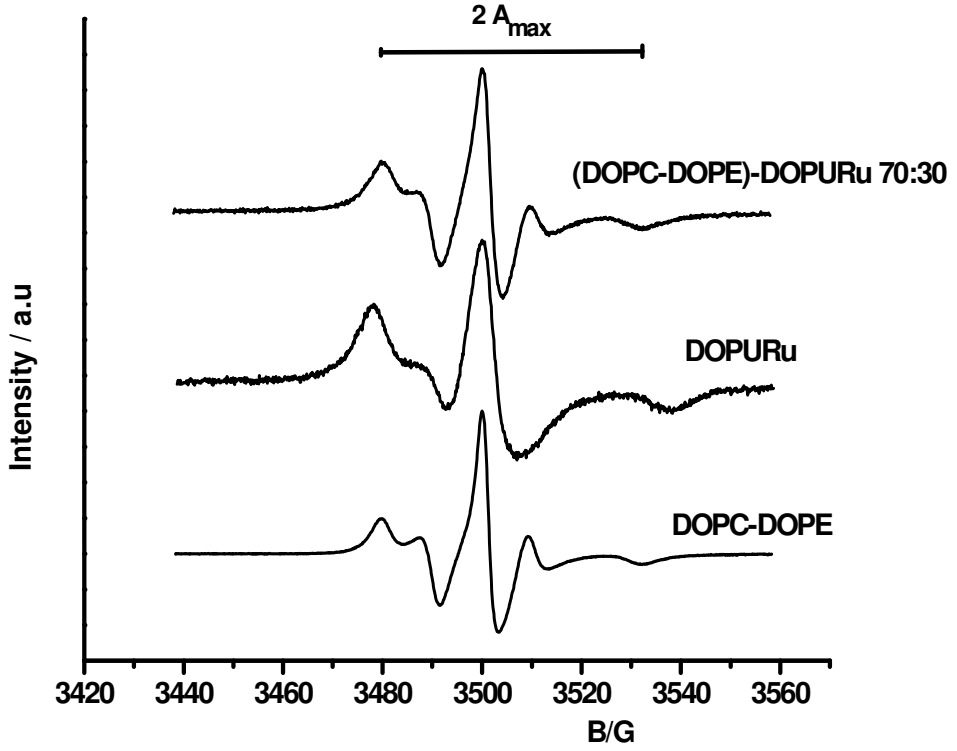

Figure 4.26: EPR spectra obtained at 25°C for 5-PCSL inserted in (DOPC-DOPE)-DOPURu, DOPURu and DOPC-DOPE membranes, respectively.

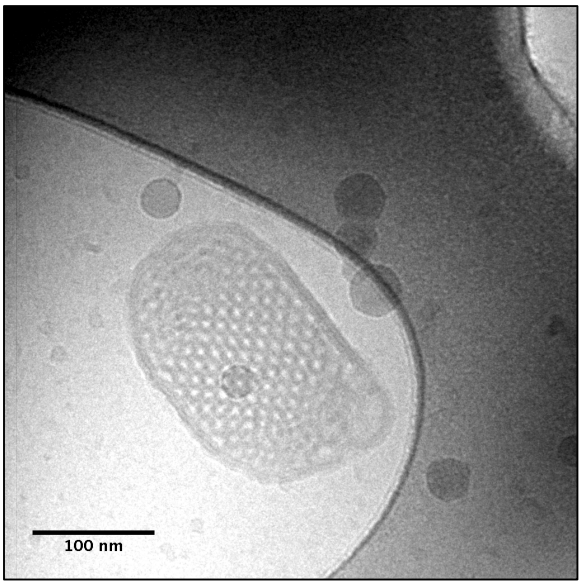
100 nm

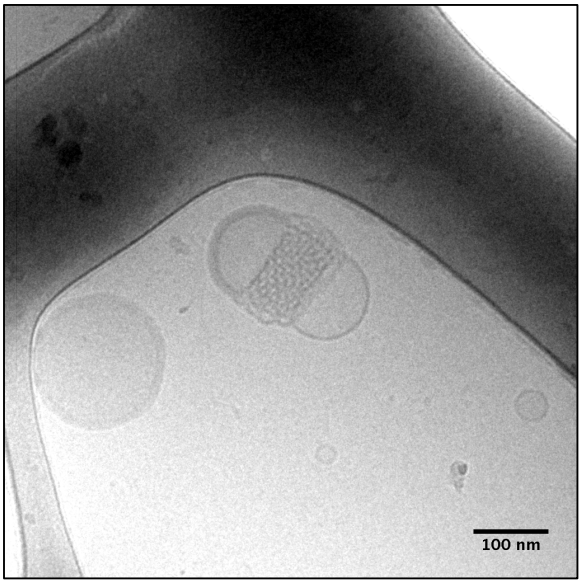
100 nm

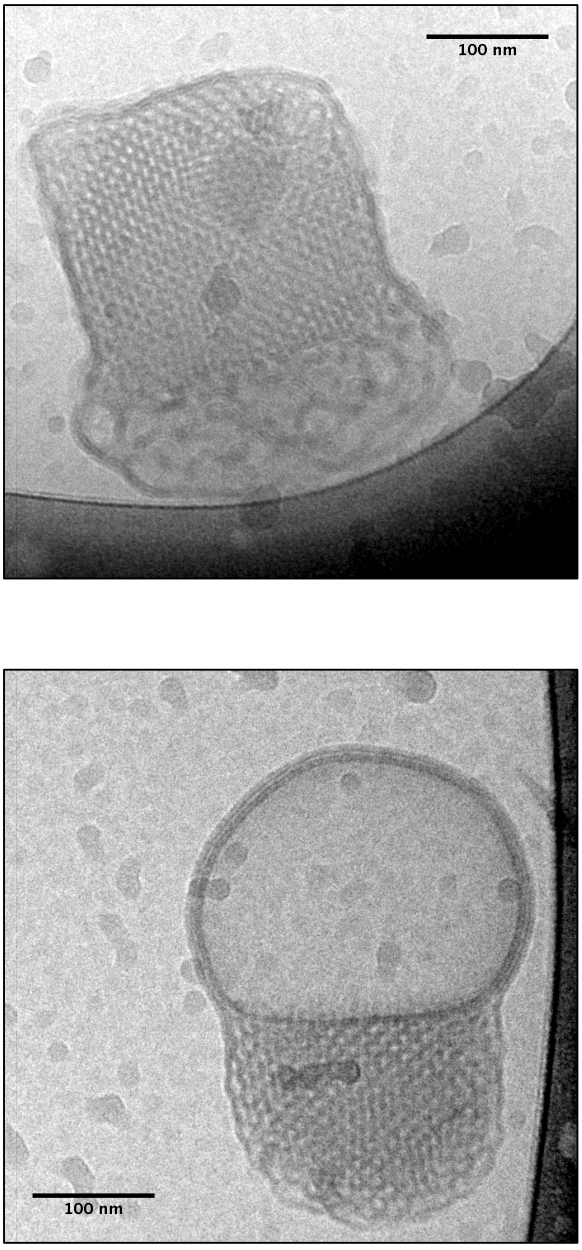

Figure 4.27: Cryo-TEM images for (DOPC-DOPE)-DOPURu 70:30 system. The images show the coexistence of unilamellar vesicles with cubosomes.

TABLE

Table 13. Diffusion coefficients and hydrodynamic radii obtained from DLS measurements for the systems studied at different molar ratios phospholipid/unimer. The terms fast and slow refer to micelles and bilayer structures, respectively.

Systems	*R*	$D \times 10^{12}$ ($m^2 s^{-1}$)	R_H (Å)
DOPC–DOPE–water	∞	3.2±0.3	650±60
(DOPC–DOPE) –DOPURu–water	70/30	2.5±0.2	880±70
(DOPC–DOPE) –DOPURu–water	60/40	2.6±0.3	850±100
(DOPC–DOPE) –DOPURu–water	50/50	2.9±0.3	750±80
DOPURu–water	0	3.1±0.2	700±50

5. Conclusions

The present PhD thesis work has dealt with the development and the upgrade of innovative amphiphilic supramolecular systems to be used in cancer diagnosis and therapy.

Two are the main systems that have been formulated during these 3 years of PhD: one based on Gadolinium complexes to be employed as contrast agent in Magnetic Resonace Imaging, and the other one consisting in a nano-vector able to deliver Ru (III), the most promising metal for cancer therapy.

The most remarkable aspect of these systems is their bio-selective behavior toward the ill tissues. Two different strategies have been followed to achieve this goal: the first system was able to carry a high amount of Gd (III) ions towards tumor cells by means of the presence of a peptide, CCK8, on the external surface of the aggregates; the second system, whereas, was able to deliver cytotoxic Ru (II) by a mechanism of activation *in situ*; thanks to the internal reductive environment typical of cancer cells Ru (III) reduces to Ru (II).

The physico-chemical characterization of the systems, here presented, has significantly supported the understanding with regard to their aggregation behavior and structural properties. In particular, it has been shown that structural properties can be modified and tuned according to the exigencies for a future clinical use of the systems.

Collection of structural data allowed, for instance, determining the critical molar ratio DOPC-MONY or (DOPC-DOPE)/DOPURu where bilayer aggregates are stable.

Bilayer aggregates, such as vesicles or cubosomes, are characterized by sluggish monomer exchange processes. This feature makes this kind of aggregates less dangerous for cellular membranes compared to micelles, and therefore their use is more favored.

An other important example is the determination of the right length of the spacer in the peptide unimer $(C18)_2$LxCCK8, such that the bio-active sequence of CCK8 was well-exposed and well-separated on the external surface of the aggregates, and able, thus, to interact with its target membrane receptors.

Particular emphasis has been provided to the study of the aggregation behavior as pH function. Recent studies have revealed, in fact, that the extracellular fluid of tumor cells has a pH lower than that of healthy tissues, so that there has been an increasing demand in current clinic for pH-responsive systems.

Gadolinium containing systems demonstrated particularly suitable as pH-sensitive aggregates, this because of the high actual charge of the head group of the chelating agent unimer $(C18)_2$DTPAGlu.

Upon decreasing the pH value in solution, a micelle-to-vesicle transition in three stages has been observed:

rodlike micelles ⟶ threadlike micelles ⟶ vesicles

as result of the screening of the intra-aggregate electrostatic repulsions among the different head-groups. This property of the system can be applied to realize pH-

responsive MRI contrast agents able to supply the *in vivo* pH mapping of tissues in tumor diagnosis.

The findings presented in this study opens up novel and interesting opportunities to investigate surfactant aggregation properties, that may be exploited in several applications, such as in drug and gene delivery or in medical diagnostic.

The active principles used can be easily substituted from new ones, in order to make more appealing the formulated systems from an applicative point of view. At this aim, we are considering different bio-active molecules, such as the hyaluronic acid (HA) for its applications in lung cancer therapy and the octreotide, a peptide analogous of the somatostatine, for breast cancer. In the first case, we are carrying out in laboratory experiments, in order to bind covalently fragments of HA on the external surface of DOPE liposomes by means of the formation directly in the bulk of a peptide bond between the ethanolamine of DOPE and the carboxylic groups of HA. In the second case, a molecule with similar characteristics to $(C18)_2L5CCK8$ has been synthesized (see figure 6.1).

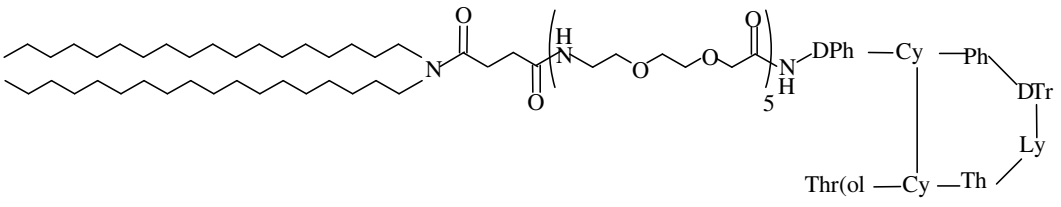

Figure 5.1: Schematic representation of the unimer $(C18)_2L5$Octreotide.

Appendix 1

6. DOES THE SYSTEM WORK?

The applicative properties of the Gadolinium containing systems have been studied in specialized centers in Italy.

The two main aspects have been investigated:

1) relaxivity evaluation by water proton relaxation measurements (NMRD);

2) selectivity assay for cancer cells by test *in vivo* on mice.

6.1 Water proton relaxation measurements

Water proton relaxation measurements were carried out by prof. Silvio Aime's group (Departement of Chemistry IFM, University of Turin).

The complexation of DTPAGlu chelating agent with gadolinium ions has been carried out on micellar solution.

Upon addition of increasing amounts of a concentrated $GdCl_3$ solution to the $(C18)_2$DTPAGlu water solution, the chelating ligand DTPAGlu became progressively saturated. The Gd^{3+} titration was followed by measuring ^1H-relaxation rates.

The proton relaxivity value measured, at 20 MHz and 298 K, for binary system $(C18)_2$DTPAGlu(Gd)-D_2O was 17.5±1.7 $mM^{-1}s^{-1}$. This value is markedly larger than that measured for the simple complex DTPAGlu(Gd), 6.2±06 $mM^{-1}s^{-1}$. The slow

rotation of the $(C18)_2$DTPAGlu(Gd) micelle decreases the longitudinal relaxation time of the water protons bound to the Gd^{3+} and produces a substantial raise of the relaxivity.

Relaxivity measurements on $(C18)_2$DTPAGlu(Gd)-$(C18)_2L_5$CCK8-D_2O and $(C18)_2$DTPAGlu(Gd)-$(C18)_2$PEG2000CCK8-D_2O ternary systems were performed using mixed micelles prepared with $(C18)_2$DTPAGlu(Gd). The measured relaxivity values for these species were 16.3±1.6 mM^{-1} s^{-1} and 13.4±1.3 mM^{-1} s^{-1} respectively at 20 MHz and 298 K (Figure 6.1).

Finally, for MONY(Gd)-D_2O and DOPC-MONY(Gd)-D_2O systems the values obtained were 15.0± 1.5 mM^{-1} s^{-1} and 12.7±1.3 mM^{-1} s^{-1}, respectively.

FIGURES

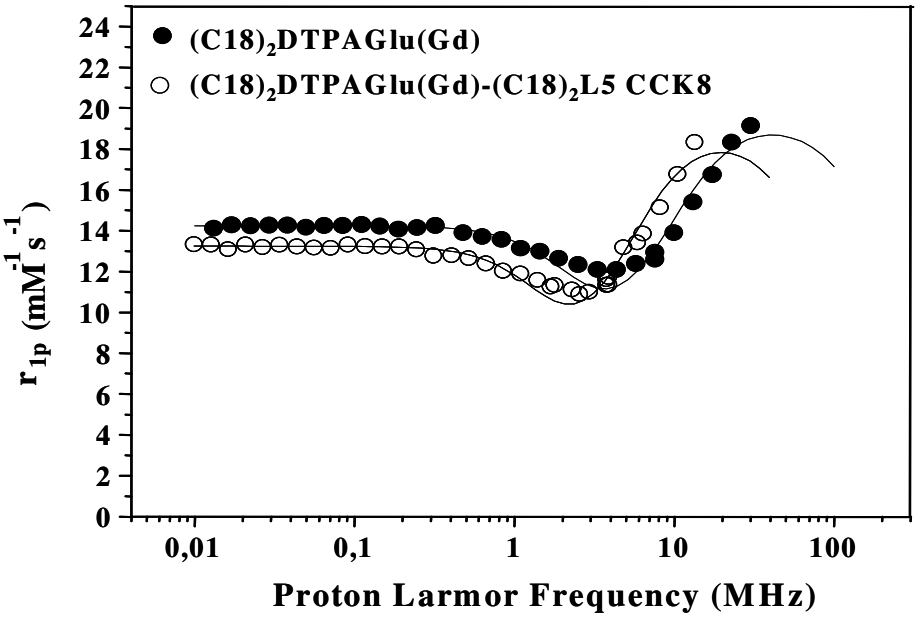

Figure 6.1: Nuclear Magnetic Resonance Dispersion profiles of $(C18)_2$DTPAGlu(Gd)-$(C18)_2$L5CCK8-D_2O (○) , $(C18)_2$DTPAGlu(Gd)-D_2O (●) solutions at pH 7.4 and 25°C, normalised to 1 mM concentration of Gd^{3+} ion.

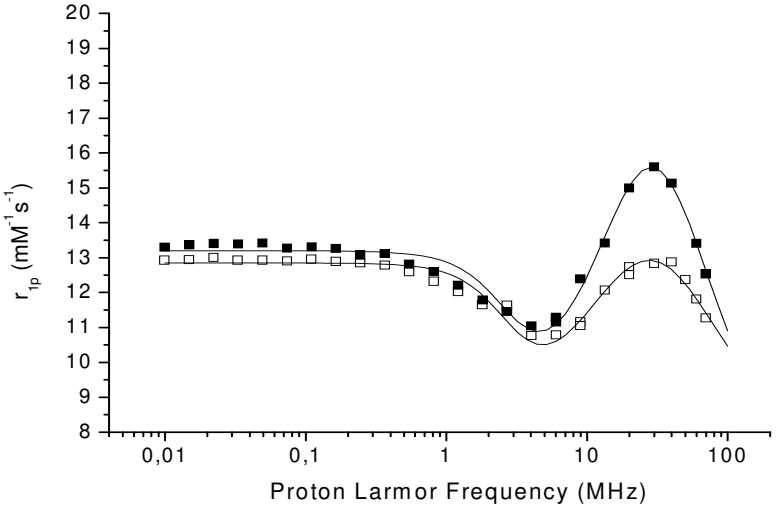

Figure 6.2: Nuclear Magnetic Resonance Dispersion profiles of MONY(Gd) (■), DOPC-MONY(Gd)-D_2O (□) solutions at pH 7.4 and 25°C, normalised to 1 mM concentration of Gd^{3+} ion.

TABLE

Table 6.1: Relaxivity values measured at 20 MHz and 298 K.

Systems	$r_{1p}(mM^{-1}s^{-1})$
DTPAGlu(Gd) – D_2O	6.2±0.6
$(C18)_2$DTPAGlu(Gd) – D_2O	17.5±1.7
(C18)DTPAGlu(Gd) – $(C18)_2L_5$CCK8 – D_2O	16.3±1.6
$(C18)_2$DTPAGlu(Gd) – $(C18)_2$PEG2000CCK8– D_2O	13.4±1.3
MONY(Gd) – D_2O	15.0±1.5
DOPC-MONY(Gd) – D_2O	12.7±1.3

6.2: *In Vivo* Evaluation of the system

In vivo evaluation of the mixed aggregates was performed to verify the bio-specificity of the supramolecular aggregates formulated in this thesis.

The experiments consisted in nuclear medicine tests, that were carried out by dr. Luigi Aloj at the Italian National Institute for Tumours, G. Pascale, Naples, Italy.

The experiments were realized on mice, where two different type of tumours were allowed to grow for two weeks. One tumour was selective for the CCK8 peptide, and it was placed in the left thigh of the mice, while the other one not showing affinity for CCK8, it was used as control tumour and was placed in the right thigh.

The aggregates injected in the mice were mixed aggregates, containing the peptide monomer, $(C18)_2$PEG2000CCK8, and the chelating agent monomer binding In^{3+}, $(C18)_2$DTPAGlu(In). $(C18)_2$DTPAGlu(In)-$(C18)_2$Peg2000CCK8 aggregates were prepared by dissolving monomers at a 5 to 1 ratio (chelator containing vs peptide containing) with final concentration in the 10^{-2} M range. Trace amounts of ^{111}InCitrate were added and the suspension was allowed incubating at room temperature for 30 min. Proof of aggregate formation and labelling with ^{111}In was obtained by gel filtration chromatography in comparison to In-Citrate which was run as control.

The aggregates prepared as described above were injected into nude mice bearing subcutaneous xenografts in opposite thighs (receptor positive in left thigh, receptor negative in right thigh). One hundred μL of ^{111}In labelled aggregate suspension was injected in the tail vein of the animals. After 16 h the animals were killed, imaged with

a medium energy collimator equipped clinical gamma camera, and subsequently dissected to evaluate organ distribution of radioactivity.

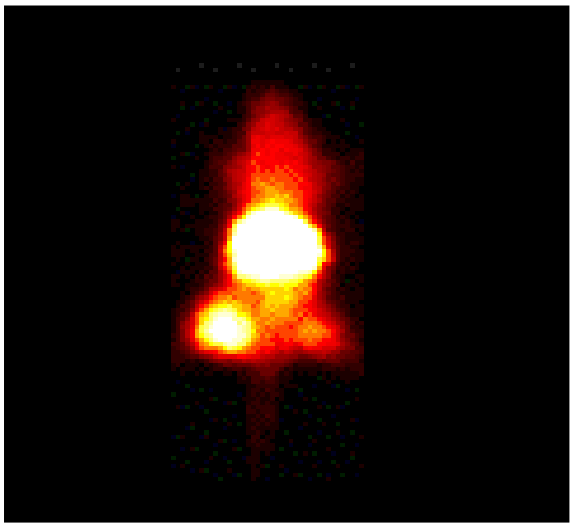

Figure 6.2: γ-camera image obtained at16 hours the injection after injection of the aggregates.

The figure 6.2 shows a gamma camera image. The receptor overexpressing tumour compatible for CCK8 peptide clearly shows higher uptake compared to the control tumour. Radioactivity levels were elevated in blood and in all high blood pool organs (liver, spleen). There appeared to be no overall loss of radioactivity from the animals over the 16 h observation period, indicating the aggregates were extremely stable. The receptor expressing tumours were the highest concentrating tissue after liver and spleen. On average CCKBR overexpressing xenografts contained 6.9 $\pm$ 1.7 % of injected dose per gram (%ID/g) against 5.1 $\pm$ 1.1 %ID/g for control tumours (mean $\pm$ SD).

This confirmed that the aggregates were able to recognize selectively the cholocystokinin receptors (CCK_A-R and CCK_B-R) over-expressed in the left thigh

tumour. But, it is noteworthy that a great amount of radioactivity was accumulated in correspondence of the liver and the spleen (the yellow spot in the middle of the mouse body), indicating a problem of expulsion from the body of the aggregates by urinary vie.

Appendix 2

7.1: Dynamic Light Scattering (DLS)

The dynamic light scattering (DLS) is a technique widely used to study the dynamical properties of colloidal dispersions.

In a DLS experiment the fluctuations of the scattered light intensity are measured as a function of time at a constant scattering angle. These intensity fluctuations occur because the particles in solution are in constant motion, the Brownian motion. The analysis of the intensity fluctuations allows the determination of the distribution of diffusion coefficients of the particles, which are converted then into a size distribution using established theories.[59,60] In DLS the temporal variation of the intensity is measured and is represented usually through the so-called intensity autocorrelation function. Since, in general, it is not convenient to deal with a large intensity values as function of time, one reduces the intensity fluctuations to the autocorrelation function $G^{(2)}(t)$. The intensity correlation function measures the correlation between the intensity value $I(t)$ at a generic time (t) and the intensity value $I(t+t_d)$ being t_d the time delay.

$$G^{(2)}(t) = I\langle I(q,0)I(q,t)\rangle = \lim_{T\to\infty}\int_{-T}^{T} I(q,t')I(q,t'+t)dt' \qquad (7.1)$$

where $I(q,0)$ and $I(q,t)$ are the intensities of the scattered light at delay time $t=0$ and $t=t$, respectively.

Its normalized value, $g^{(2)}(t)$, is defined by :

$$g^{(2)}(t) = \frac{G^{(2)}(t)}{G^{(2)}(0)} \tag{7.2}$$

where $G^{(2)}(0)$ is the time-averaged value of the square intensity, i.e. $\langle I(t)^2 \rangle$.

The models used in the fitting procedures are expressed with respect to the normalized time correlation function of the electric field, $g^{(1)}(t)$, because the time correlation function of scattered light is not simply related to the motion of the molecules.

$$g^{(1)}(t) = \frac{\langle E^*(q,0)E(q,t) \rangle}{\langle E^*(q,0)E(q,0) \rangle} \tag{7.3}$$

The two normalized time correlation functions are related by Siegert's relationship:[61]

$$g^{(2)}(t) - 1 = \beta \left| g^{(1)}(t) \right|^2 \tag{7.4}$$

where $\beta (\leq 1)$ is the coherence factor, which accounts for deviation from ideal correlation and depends on the experimental geometry.

For a monodisperse system, $g^{(1)}(t)$ will decay as a single exponential function with a characteristic relaxation time τ :[62]

$$g^{(1)}(t) = \exp(-t/\tau) \tag{7.5}$$

whereas for a polydisperse system $g^{(1)}(t)$ will be multiexponential and may be expressed as a Laplace transformation of a distribution of relaxation times, $A(\tau)$:

$$g^{(1)}(t) = \int_{-\infty}^{+\infty} \tau A(\tau) \exp(-t/\tau) d \ln \tau \tag{7.6}$$

where $\tau = \Gamma^{-1}$ and Γ is the relaxation or frequency rate.

The relaxation time distribution $\tau A(\tau)$ is obtained by regularized inverse Laplace transformation (RILT) of the measured intensity correlation function using calculation algorithms. In the analyses in this work, algorithms of two commercial programs have been used: REPES,[63,64] incorporated in the GENDIST analysis package,[64,65] and RILT incorporated ALV-5000/E software.

The relaxation rate Γ is obtained from the first moment of the relaxation time distribution, and from its value is possible to estimate the apparent translational diffusion coefficient D , through this relation:

$$D = \lim_{q \to 0} \frac{\Gamma}{q^2} \tag{7.7}$$

where q is the absolute value of the scattering vector ($q = 4\,\pi n_o \sin(\theta/2) / \lambda$, where n_o is the refractive index of the solvent, in this work is water, λ is the incident wavelength and θ is the scattering angle).

D is, thus, obtained from the slope of Γ as a function of q^2, where Γ is measured at different scattering angles.

The diffusion coefficient D obtained in a DLS experiment is believed to be the mutual diffusion coefficient. The Brownian motion generates concentration fluctuations that in turn produce a chemical potential gradient and the associated flow is proportional to this gradient through a coefficient called the mutual diffusion coefficient, which can be described by Fick's second law:[59,66]

$$D = \frac{1}{6\pi\eta R}\left(\frac{\delta\pi}{\delta c}\right) \tag{7.8}$$

where π is the osmotic pressure of the dispersion and c is the concentration of the solute.

In particular for infinite dilute dispersions:

$$\pi = cK_BT \Rightarrow \left(\frac{\delta\pi}{\delta c}\right) = K_BT \tag{7.9}$$

D reduces to the self-diffusion coefficient D_0 and we obtain the Stokes-Einstein equation:

$$D = \frac{K_B T}{6\pi\eta R} \tag{7.10}$$

7.2 Small angle neutron scattering (SANS)

SANS is a small angle scattering technique that exploits the wave-particle duality of the neutron and its unique nuclear properties to provide information about the size (length scale varies from 1 to 1000 nm) and shape of molecules and their assemblies. In SANS, the scattering vector q is used to describe the relationship between the incident and the scatter wavevectors. Its module, q, is the independent variable in a SANS experiment and has magnitude $q = 2\pi \sin(\theta/2)/\lambda$ and dimensions of (length)$^{-1}$. By combining q with the Bragg law of diffraction, one obtains the simple and useful relationship: $d = 2\pi/q$, from which the molecular-level length scale (d) at any accessible q can be obtained. The dependent variable in a SANS experiment is the differential scattering cross-section, (dΣ/dΩ), improperly also called intensity of scattering $I(q)$. Scattering cross section $d\Sigma/d\Omega$ contains information on interactions, size and shapes of aggregates present in the system, and can be expressed for a collection of monodisperse bodies as [67]

$$\frac{d\Sigma}{d\Omega}(q) = n_p P(q) S(q) + \left(\frac{d\sigma}{d\Omega}\right)_{\text{inch}} \tag{7.11}$$

where n_p represents the number density of the scattering object present in the system, $P(q)$ and $S(q)$ are respectively the form and the structure factor of the scattering particles, whereas $(d\Sigma/d\Omega)_{\text{inch}}$ takes into account for the incoherent contribution to the cross section measured, mainly due to the presence of hydrogenated molecules. The

form factor contains information on the shape of the scattering objects, whereas the structure factor accounts for inter-particle correlations and is normally important for concentrated or charged systems. Provided that solutions are quite dilutes ($c<10^{-3}$ mol kg^{-1}) the structure function $S(q)$ can be approximated to the unity, and the scattering cross section is reduced to

$$\frac{d\Sigma}{d\Omega}(q) = n_p P(q) + \left(\frac{d\sigma}{d\Omega}\right)_{\text{inch}} \tag{7.12}$$

Microstructural parameters of the aggregates have been obtained by applying the appropriate model to the experimental SANS data. Experimental data have shown in the analyzed systems the existence of cylindrical micelles and/or the presence of vesicular aggregates.

Scattering from cylindrical structures is characterized by a region where the $d\Sigma/d\Omega \sim q^{-1}$ power law dependence holds. The single particle form factor for such micelles can be written as [68]

$$P(q) = (\rho_c - \rho_0)^2 \pi R^2 l \int_0^{\pi/2} \frac{\sin^2\left(q\frac{l}{2}\cos\phi\right)}{\left(q\frac{l}{2}\cos\phi\right)^2} \frac{9\left[j_1(qR\sin\phi)\right]^2}{(qR\sin\phi)^2} \sin\phi \, d\phi \tag{7.13}$$

where l is the length of the cylinders, R the radius of the base, whereas j_1 is the first order Bessel function and $\rho_c - \rho_0$ the scattering length density difference between the cylinders and the solvent.

Vesicular aggregates cannot be observed in their completeness since the Guinier region of such objects falls almost completely in the USANS domain. As consequence

the SANS region is characterized by a power law $d\Sigma/d\Omega \sim q^{-2}$ due to the scattering of vesicular double layer. Indeed the q range spanned by the SANS measurements is such to allow regarding the vesicles as randomly oriented planar sheets for which the form factor can be expressed by [69]

$$P(q) = 2\pi(\rho_c - \rho_0)^2 Sd^2 \frac{1}{q^2} \frac{\sin^2\left(\frac{qd}{2}\right)}{\left(\frac{qd}{2}\right)^2} \tag{7.14}$$

where d is the plane thickness, and S is the plain surface per unit volume.

Scattering from solutions containing cylindrical structures has been analyzed by using eqs 7.12 and 7.13, whereas in the systems containing vesicles aggregates, eqs 7.12 and 7.14 have been used. Systems containing both the objects have been treated assuming each kind of aggregate scattered independently from the other and expressing the cross section as the sum of the form factors weighted for two scale factors (K_{cyl}, K_{sheets}) the relative number density of the objects

$$\frac{d\Sigma}{d\Omega}(q) = n_p K_{cyl} P_{cyl}(q) + K_{sheets} P_{sheets}(q) + \left(\frac{d\sigma}{d\Omega}\right)_{\text{inch}} \tag{7.15}$$

and treating the scale factors as adjustable parameters.

7.3 Cryo-Transmission electron microscopy (Cryo-TEM)

Structures formed by amphiphilic molecules can be visualized by several microscopy techniques, but the more promising is the transmission electron microscopy, which was originally developed by Knoll and Ruska in Germany in the 1930's.

In a transmission electron microscope, a beam of electrons is sent trough a thin sample. An electron source situated at the top of the instrument emits electrons, which are accelerated by a high voltage. The wavelength of the electrons is dependent on the accelerating voltage of the microscope. The electron source, the so-called filament, usually consists of a LaB_6 cathode. The electron beam is focused onto the specimen by condenser lenses. The objective lens, situated below and around the specimen, forms the image and controls the contrast. Finally a set of projector lenses enlarges the image and projects it onto fluorescent screen. The image can also be transferred to a photographic film or an electron sensitive camera. To perform TEM experiments is necessary to respect some requests: the samples must be thin enough (< 0.25 μm) to permit electrons to pass through them, moreover, to prevent image blurring, all motion on the supramolecular scale must be arrested. To achieve these conditions, different ways of preparation of TEM sample have been developed, one of them is the so called Cryogenic TEM, which is based on the rapid freezing of sample. In fact, with the term cryo-TEM, we mean transmission electron microscopy of thin vitrified aqueous films, kept at liquid nitrogen temperature,[70,71] in order to reduce the vapour pressure and to stop all the supramolecular motions.

Figure 7.1: Picture of the cryo-electron microscope used, a Philips CM120 BioTWIN operating at 120 kV.

This technique has during the last 10 years contributed significantly to the understanding of the numerous, and often complex, structures formed by amphiphilic molecules in dilute aqueous solutions.[72,73]

In the cryo-TEM method the solution is applied to a microscopy grid in such a way that a very thin aqueous film is formed, which then is plunged into a cooling medium, such as ethane just above its freezing point, where the film rapidly vitrifies, without crystallisation. The grid with the vitrified film is then transferred to the microscope, and examined at liquid nitrogen temperature in transmission mode. The structures, which in this way are captured in the vitrified film, are so quickly vitrified that normally no important reorganisation takes place.

The fact that the film is thin in the middle and thicker at the edges can introduce a size separation, small objects will tend to be accumulated in the middle of the film and larger objects at the edges.

A limiting factor is represented by the contrast, it derives from the difference in electron density between the atoms of the amphiphile and the surrounding water, and it is necessary to underfocus the image to improve the contrast.

Other limiting factors are due to the dimensions of the aggregates: the smallest size that can be resolved is about 4-5 nm, so micelles are seen only as dots, the upper size, instead, is about 500 nm.

The technique is generally perfect to visualize structures as those presented in this thesis, formed by bilayers as vesicles or cubosomes. Vesicles of various kinds and in different stages (open bilayers, fusion phenomena, etc.) of transformation can be investigated, it is possible see the rounded shape and the inner aqueous compartment, so it can for example distinguish between a multilamellar and a unilamellar vesicle, and estimate also the radius of the aggregates.

REFERENCES

[1] Duncan, R., *Nature Rev. Drug Discov.* 2003, 2, 347.

[2] Langer, R., *Nature* 1998, 392, 5.

[3] Allen, T. M., *Nature Rev. Drug Discov.* 2002, 2, 750.

[4] Jain, R. K., *Nature Med.* 1998, 4, 655.

[5] Srinivas, P. R.; Barker, P.; Srivastava, S., *Lab.Invest.* 2002, 82, 657.

[6] Jonsson, B.; Lindman, B.; Holmberg, K.; Kronberg, B., *Surfactants and Polymers in Aqueous Solution.*; ed. John Wiley & Sons Ltd: West Sussex., 1998.

[7] Israelchvili, J., *Intermolecular and surface Forces*. second edition; ed. Academic Press: London, 1992.

[8] Evans, D. F.; Wennerstrom, H., *The colloidal domain: where physics, chemistry, biology and technology meet.*; ed. Wiley-VCH: New York, 1999.

[9] Malmsten, M., *Surfactants and Polymers in Drug Delivery*; ed. Marcel Dekker, Inc.: New York, 2002.

[10] Fendler, J. H., *Membrane Mimetic Chemistry.*; ed. Wiley-Interscience: New York, 1982.

[11] Ostro, M., *J.Sci.Am.* 1987, 256, 102.

[12] Caria, A.; Khan, A., *Langmuir* 1996, 12, 6282.

[13] Marques, E.; Regev, O.; Khan, A.; Miguel, M.; Lindaman, B., *J.Phys.Chem.B* 1999, 103, 8353-8363.

[14] Johnsson, M.; Wagenaar, A.; Engberts, J., *J.Am.Soc.* 2003, 125, 757.

[15] Johnsson, M.; Wagenaar, A.; Engberts, J., *Langmuir* 2003, 19, 4609.

[16] Lichtenberg, D., *Biochim. Biophys. Acta* 1985, 821, 740.

[17] Lichtenberg, D.; Robson, R. J.; Dennis, E. A., *Biochim. Biophys. Acta* 1983, 285, 7377.

[18] Ni, S., *Anticancer Res*. 2002, 22, 2131.

[19] Pan, X. Q., *Pharm. Res*. 2003, 20, 417.

[20] Pan, X. Q., *Blood* 2002, 100, 594.

[21] Kwekkeboom, D.; Krenning, E. P.; De Jong, M., *Journal of Nuclear Medicine* 2000, 41, 1704.

[22] Lamberts, S. W.; Krenning, E. P.; Reubi, J. C., *Endocr.Rev*. 1991, 12, 450.

[23] Aime, S.; Botta, M.; Fasano, M.; Terreno, E., *Chem Rev*. 1998, 27, 19.

[24] Lauffer, R. B., *Chem. Rev*. 1987, 87, 901.

[25] Mettler, F. A.; Muroff, L. R.; Kulkarm, M. V.,; ed. Churchill Livingstone: New York, 1986.

[26] Friebolin, H., *Basic One- and Two-Dimensional NMR spectroscopy*.; ed. VCH: Germany, 1993.

[27] Koening, S. H.; Brown III, R. D., *Prog. NMR Spectrosc*. 1990, 22, 487.

[28] Banci, L.; Bertini, I.; Luchinat, C., *Nuclear and Electronic Relaxation*.; ed. VCH: Weinheim, 1991.

[29] Glogard, C.; Stensrud, G.; Hovland, R.; Fossheim, S. L.; Klaveness, J., *International Journal of Pharmaceutics* 2002, 233, 131.

[30] Morel, S.; Terreno, E.; Ugazio, E.; Aime, S.; Gasco, M. R., *European Journal of Pharmaceutics and Biopharmaceutics* 1998, 45, 157.

[31] Anelli, P. L.; Lattuada, L.; Lorusso, V.; Schneider, M.; Tournier, H.; Uggeri, F., *Magnetic Resonance Materials in Physics, Biology and Medicine* 2001, 12, 114.

[32] Wiener, E. C.; Brechbiel, M. W.; Brothers, H.; Magin, R. L.; Gansow, O. A.; Tomalia, D. A.; Lauterbur, P. C., *Magn. Res. Med.* 1994, 3, 1.

[33] Aime, S.; Botta, M.; Garino, E.; Geninatti Crich, S.; Giovenzana, G.; Pagliarin, R.; Palmisano, G.; Sisti, M., *Chem. Eur. J.* 2000, 6, 2609.

[34] Schmiedl, U.; Ogan, M.; Paajanen, H.; Marotti, M.; Crooks, L.; Brito, E.; Brasch, R. C., *Radiology* 1987, 162, 205.

[35] Liu, S.; Edward, D. S., *Chem. Rev.* 1999, 99, 2235.

[36] Rosenberg, B.; Kamp;, L. V.; Trosko;, J. E.; Mansour., V. H., *Nature* 1969, 222, 385.

[37] Weiss, R. B.; Christian, M. C., *Drugs* 1993, 46, 360.

[38] Williams, S. D., *Platinum and other metal coordination compounds in Cancer Chemotherapy 2.*; ed. Plenum Press: New York and London, 1996.

[39] Y. Kidani; R. Kizu; M. Miyazaki; M. Noji; A. Matsuzawa; Y. Takeda; N. Akiyama; Eriguchi, M., *Platinum and other metal coordination compounds in Cancer Chemotherapy 2.*; ed. Plenum Press: New York and London, 1996.

[40] A. F. Marcelis; G. W. Conters; Reedijk, J., *Recl. Trav. Chim. Pays-Bas* 1981, 100, 391.

[41] M. J. Cleare; complexes., P. C. H. A. p. o. m., *Met. Ions. Biol. Syst.* 1980, 11, 2.

[42] P. Kopf-Maior; Kopf., H., *Chem. Rev.* 1987, 87, 1137.

[43] G. Sava; S. Zorzet; G. Mestroni; Zassinovich, G., *Anticancer Res.* 1985, 5, 249.

[44] G. M. Kolodny; Rose, C., *Cancer Res.* 1983, 43, 3101.

[45] B. K. Keppler; D. Wehw; H. Endres; Rupp., W., *Inorg.Chem.* 1987, 26, 844.

[46] M. J. Clarke; F. Zhu; Frasca, D. R., *Chem.Rev* 1999, 99, 2511.

[47] V. M. Bailey; K. J. LaChance-Galang; P. E. Doan; Clarke, M. J., *Inorg.Chem.* 1997, 36, 1873.

[48] M. J. Clarke; S. Bitler; D. Rennert; M. Buchbinder; Kelman, A. D., *J. Inorg. Biochem.* 1980, 12, 79.

[49] B. D. Palmer; W. R. Wilson; Pullen, S. M., *J.Med.Chem.* 1990, 33, 112.

[50] J. L. Wike-Hooley; J. Haveman; Reinhold., H. S., *Radiother. Oncol.* 1984, 2, 343.

[51] D. Frasca; J. Ciampa; J. Emerson; R. S. Umans; Clarke, M. J., *Met.-Based Drugs* 1996, 3, 197.

[52] N. Farrel; Y. Qu; Roberts., J. D., *Inorg. Chem.* 1999, 1, 99.

[53] Scolaro, C.; Chaplin, A., B.;; Hartinger, C. G.; Bergamo, A.; Cocchietto, M.; Keppler, B. K.; Sava, G.; Dyson, P. J., *Dalton Transactions* 2007, 5065.

[54] Reubi, J. C.; Schaer, J. C.; Waser, B., *Cancer Res.* 1997, 57, 1377.

[55] Johnsson, M.; Hansson, P.; Edwards, K., *J.Phys.Chem.B* 2001, 105, 8420.

[56] Stejskal, E. O.; Tanner, J. E., *J.Chem.Phys.* 1965, 42, 288.

[57] Jonstromer, M.; Johnsson, B.; Lindman, B., *J. Phys. Chem* 1991, 95, 3293.

[58] Durham, E. J.; Ryskiewich, D. P., *J. Am. Chem. Soc.* 1958, 80, 4812.

[59] Berne, B.J.; Pecora, R. Dynamic Light Scattering: with Applications to Chemistry, Biology, and Physics, 2nd; 2000, ed. Dover publications, Inc.: New York.

[60] Pusey, P.N. In Neutrons, X-Ray and Light Scattering; Lindener, P.; Zemb, T.; Eds. Elsevier: Amsterdam, 2002; pp 203.

[61] Pusey, P.N. In Neutrons, X-Ray and Light: Scattering Methods Applied to Soft Condensed Matter; Lindener, P.; Zemb, T.; Eds. Elsevier: Amsterdam, 2002; pp 203-220.

[62] Brown, W. Scattering Methods: A brief Introduction. Lecture notes; 1994, Uppsala University, Sweden.

[63] Stepanek, P.; In Dynamic Light Scattering; Brown, W.; 1993; Ed. Oxford University Press: Oxford, UK, p 177.

[64] Johnsen, R..M.; Brown, W. In Laser Light Scattering in Biochemistry; Harding, S. E., Sattelle, D.B., Bloomfield, V.A.; Eds. The Royal Society of Chemistry: Cambridge, UK, 1992; p 177.

[65] Schillen, K.; Brown, W.; Johnsen, R. Macromolecules 1994, 27, 4825.

[66] Cussler, E.L.; Diffusion Mass Transfer in Fluid Systems, 2; 1997, ed. Cambridge University Press: Cambridge, UK.

[67] Kotlarchyk, M.; Chen, S. H. Journal of Chemical Physics 1983, 79, 2461.

[68] Triolo, R.; Magid, L. J.; Johnson, J. S., Jr.; Child, H. R. Journal of Physical Chemistry 1982, 86, 3689.

[69] Ma, G.; Barlow, D. J.; Lawrence, M. J.; Heenan, R. K.; Timmins, P. J. Phys. Chem. B. 2000, 104, 9081.

[70] Dubochet, J., Adrian, J.J. ; Chang, J.C. ;Homo, J. Rev. Biophys. 1988, 21, 129.

[71] Bellare, J.W.; Davies, H.T.; Scriven, L.E.; Talmon, J. Electron. Micros. Tech. 1988, 10, 87.

[72] Talmon, Y.; Ber. Bunsenges. Phys. Chem. 1996, 100, 364.

[73] Almgren, M.; Edwards, K.; Gustafsson, J. Curr .Op. Colloid Interface Sci. 1996, 1, 270.